# FORM FACTORS AND TRANSITION CHARGE DENSITIES FOR THE MULTIPOLE ELECTROEXCITATION OF SOME NUCLEI IN THE MASS 40 TO 70 REGION.

by

**PRABHU KRISHAN RAINA**



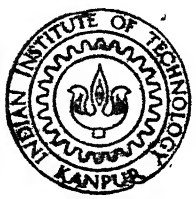


**DEPARTMENT OF PHYSICS**

INDIAN INSTITUTE OF TECHNOLOGY, KANPUR

**JUNE, 1987**

# FORM FACTORS AND TRANSITION CHARGE DENSITIES FOR THE MULTIPOLE ELECTROEXCITATION OF SOME NUCLEI IN THE MASS 40 TO 70 REGION.

A Thesis Submitted
in Partial Fulfilment of the Requirements
for the Degree of

**DOCTOR OF PHILOSOPHY**

by

**PRABHU KRISHAN RAINA**

*to the*

**DEPARTMENT OF PHYSICS**
INDIAN INSTITUTE OF TECHNOLOGY, KANPUR
**JUNE, 1987**

To

MY PARENTS

# CERTIFICATE

Certified that the work presented in this thesis entitled, "Form Factors and Transition Charge Densities for the Multipole Electroexcitation of some Nuclei in the Mass 40 to 70 Region", by Mr. Prabhu Krishan Raina has been carried out under my supervision and that this has not been submitted elsewhere for a degree.

June, 1987.

S.K. Sharma

(S.K. SHARMA)
Assistant Professor
Indian Institute of Technology
KANPUR-208016
(INDIA)

## ACKNOWLEDGEMENTS

It is my greatest pleasure to express the deepest sense of gratitude to my supervisor, Dr. Satish Kumar Sharma for his invaluable guidance during the course of my research work. It was a great experience for me to learn microscopic many-body physics from him. I shall ever be grateful to him for his untiring help, personal interest, helpful discussions and affectionate behavior throughout the span of this work.

I am also thankful to several faculty members of the Department of Physics, Indian Institute of Technology, Kanpur, for their help and suggestions from time to time.

I am very thankful to my senior colleagues Dr.Prakash Narayan Tripathi, Dr. P.K. Rath, Dr. G. Mukherjee, Dr. B. Ghosh as well as members of theory group — Mr. S. Godre, Mr.M. Nandy and Ms. Supreeti — for their help at different stages of the work.

The calculations reported in this thesis have been carried out at the DEC-1090 time sharing computer, IIT Kanpur. The Help and assistance given by the staff members of the Computer Centre, IIT Kanpur is gratefully acknowledged.

I thank Mr. U.S. Misra for typing out the thesis skilfully and accurately, Mr. R.K. Bajpai for tracing out the figures beautifully. Mr. Hrishikesh Panda alongwith Mr. L.S. Rathore for neat and efficient cyclostyling.

Last but not least, I am grateful to my family members for warm and untiring encouragements.

TABLE OF CONTENTS

## LIST OF TABLES

# LIST OF FIGURES

SYNOPSIS

P.K. RAINA

Ph.D. (Physics)
Indian Institute of Technology Kanpur

FEBRUARY 1987

# FORM FACTORS AND TRANSITION CHARGE DENSITIES FOR THE MULTIPOLE ELECTROEXCITATION OF SOME NUCLEI IN THE MASS 40 TO 70 REGION

Inelastic electron scattering has proved to be an excellent method for exploring nuclear structure. A measurement of the electroexcitation cross section permits one to obtain nuclear dynamical properties such as the transition charge and current densities. The calculation of these transition densities in terms of the nuclear wavefunctions provides a sensitive test of the latter.

Recent inelastic electron scattering experiments involving a number of doubly even 2p-1f shell nuclei have provided valuable data for the quadrupole and hexadecupole electroexcitation of the yrast levels with $J^{\pi} = 2^{+}$ and $4^{+}$ in these nuclei. Within a measured momentum-transfer range upto 3 $fm^{-1}$ the quadrupole form factors display two distinct maxima appearing at $q \sim 0.7$ and 1.6 $fm^{-1}$. The hexadecupole form factors, on the other hand, are characterized by maxima occurring at $q \sim 1.2$ and 2.2 $fm^{-1}$. The relative magnitude of

the form factors at the two maxima is expected to provide a sensitive test of the nuclear microscopic models involved in the calculations.

In recent years considerable attention has also been devoted to the coordinate-space reconstruction of the transition charge densities associated with the electroexcitation of nuclear levels; this has been achieved by employing the Fourier Bessel transforms in conjunction with the distorted-wave Born-approximation. The empirical transition charge densities acquire additional significance vis-à-vis the test of the model wave functions since they contain structural information unaffected by the accuracy of the usual plane-wave Born-approximation for large momentum transfers.

In a recent shell-model study the quadrupole electroexcitation form factors as well as the transition charge densities for some doubly even Ni isotopes were calculated in terms of the shell model wave functions resulting from semi-empirical effective interactions operating in the restricted valence spaces involving the $[(2p_{3/2}, 1f_{5/2}, 2p_{1/2})^{n} + (1f_{7/2})^{-1} (2p_{3/2}, 1f_{5/2}, 2p_{1/2})^{n+1}]$ configurations. The use of the shell model wave functions involving limited number of configurations, however, resulted in a highly mass-dependent set of proton and neutron effective charges.

The available form factor data in doubly even Zn isotopes (with $A \sim 66$) has not been analysed in a microscopic

framework thus far. A conventional shell model description of these isotopes in terms of just one $(1f_{7/2})_\pi$ hole is expected to be quite inadequate if one considers the fact that the available data on the reduced E2 transition probabilities suggests enhanced rotational collectivity compared to that in the Ni isotopes. In view of the intractability of a realistic shell model calculations it is desirable to have an approximate yet reliable ansatz for the multiparticle wave functions generated within the full 2p-1f valence space.

In the present work we show that the yrast wave functions for the $J^\pi = 0^+, 2^+$ levels projected from the Hartree-Fock-Bogoliubov (HFB) intrinsic states resulting from realistic effective interactions operating in the full 2p-1f shell permit a fairly satisfactory description of the $2^+$ form factors in some doubly even Ni and Zn isotopes (with $58 \leq A \leq 68$). In this context we also discuss the calculation of the transition charge densities in terms of the self-consistent HFB states. The calculations demonstrate that the use of the projected HFB wave functions obviate the necessity of employing widely different effective charges for various nuclei.

In Chapter I we briefly outline the overall perspective of the calculations presented in the thesis.

In Chapter II we discuss in some detail the use of the projected HFB wave functions vis-à-vis the calculation of the form factors as well as transition charge densities associated

with the electroexcitation of yrast levels.

We next discuss in Chapter III the results for the form factors, transition densities as well as the E2 transition strengths for the $0^+ \rightarrow 2^+$ transition in some doubly even Ni and Zn isotopes. It is seen that a comparison of the projected HFB transition densities with the ones extracted from the observed form factor data (via the Fourier-Bessel analyses) offers important guidelines vis-à-vis the choice of a model of the $^{40}Ca$ core-polarization contributions.

In Chapter IV we have tested the efficacy of the projected HFB description vis-à-vis the recently-measured data for the electroexcitation of $J^\pi = 4^+$ levels in a number of doubly-even isotopes of Ti,Cr,Fe and Ni. Some recent shell model calculations involving restricted configuration mixing have required highly mass-dependent effective charges (for the $4^+$ electroexcitation) which are also drastically different from the set employed for a reasonable quantitative agreement with the observed ($0^+ \rightarrow 2^+$) form factors in these nuclei. In contrast to this, our calculations provide a satisfactory quantitative discussion of the ($0^+ \rightarrow 4^+$) form factors in terms of the effective charges quite close to the ones required for a comparable fit to the ($0^+ \rightarrow 2^+$) data in these nuclei.

The recent measurements of the form factors involving the $0^+ \rightarrow 4^+$ transitions has also provided reasonably accurate

estimates of the heretofore unmeasured E4 transition probabilities, B (E4; $0^+ \rightarrow 4^+$) via an extension of the data into the momentum-transfer of the photon point. In this context we demonstrate in Chapter IV the quantitative as well as qualitative unreliability of the Bohr and Mottelson prescriptions for relating the E4 transition matrix elements with the hexadecupole intrinsic moments.

Finally in Chapter V we summarize the results and discuss some possible extensions of the present work.

# CHAPTER I

## INTRODUCTION

The elastic as well as inelastic electron-nucleus scattering turns out to be an excellent tool for studying nuclear structure for a number of reasons[1,2].

One of the important features that characterizes the choice of the electron as a probe is the weakness of the electromagnetic force responsible for the electron-nucleus interaction. Since the coupling constant for the electromagnetic interaction is much smaller than the strength of the nuclear interaction, the electron hardly perturbs the nucleus. The usefulness of the electron as a probe is also augmented by the fact that the interaction between the electron and the nucleus is the well-understood electromagnetic interaction that is described by an exact theory — quantum electrodynamics. The nuclear properties can therefore be extracted from the observed data in an unambiguous, quantitative manner.

An important consequence of the weakness of the electromagnetic interaction is the possibility of providing an adequate quantitative discussion of the electron-nucleus scattering in terms of the first Born approximation (involving only the one-photon exchange graphs) in conjunction with the description of both the incoming and outgoing electrons as plane waves. The single-step nature of the

scattering process underlying this approximation implies that a given momentum transfer is a direct measure of the spatial resolution of the probe.

In the context of the excitation of nuclear levels, the inelastic electron scattering has advantages over the processes involving real photons : for a fixed energy loss of the electron one can vary the momentum $\vec{q}$ transferred to the nucleus. This contrasts keenly with the situation in the case of the real photons where one has only a single possible momentum transfer for a given energy transfer. Thus inelastic electron scattering facilitates the study of the complete $q^2$ behaviour of the matrix elements involved in the transition.

In the framework of some phenomenological models for inelastic electron scattering, the differential cross-section can be characterized approximately by $[j_L(qR)]^2$, where $j_L$ is the spherical Bessel function, L is the multipolarity of the transition and R the nuclear dimensions. As one increases q, by either raising the incident energy or by considering large-angle scattering, the factor $j_L(qR)$ approaches its first diffraction minimum located, say, around $q_1$. However, higher multipoles (L+1) are expected to rise up to their first maximum for $q \sim q_1$. One may thus maximize a certain multipole while suppressing the strength of lower multipoles. This raises the possibility of exciting strongly new levels which would not be excited by other means.

We must also mention here some of the inherent drawbacks associated with the electro-excitation experiments. The significant distortion of the electron wavefunction by the Coulomb interaction necessitates the use of distorted wave functions for interpreting experiments involving heavy nuclei ($Z > 20$). Further, due to their small mass, the electrons are easily deflected. The resulting radiation provides strong background to the scattering cross sections.

In the case of nuclear electro-excitations, one can extract the Fourier transforms of the charge and current densities associated with the transition from a measurement of the cross section by invoking the plane wave Born approximation. The momentum-transfer dependence of the nuclear matrix elements contains information about the spatial structure of the nuclear states. A comparison of the observed momentum-transfer dependence with the one resulting from model wavefunctions is expected to provide significant test of the latter.

A number of recent inelastic electron scattering experiments have provided valuable data on the $0^+ \rightarrow 2^+_{1,2}$ as well as $0^+ \rightarrow 4^+_1$ transitions in several 2p-1f shell nuclei[3-12]. The available form factor data covering the range $q = 0.1 - 3.0$ fm$^{-1}$ is characterized by the following salient features:

(i) The observed form factors for the transition $0^+ \rightarrow 2^+_{1,2}$ display two distinct maxima appearing at $q \sim 0.7$ and $1.6$ fm$^{-1}$.

The minima of the form factors appear at $q \sim 1.3$ fm$^{-1}$.

(ii) The maxima of the form factors associated with the $0^+ \rightarrow 4_1^+$ transition occur at $q \sim 1.2$ and $2.2$ fm$^{-1}$.

(iii) Although the qualitative features of the form factors associated with the $0^+ \rightarrow 2_2^+$ transition are quite similar to those of the observed form factors for the $0^+ \rightarrow 2_1^+$ transition, the magnitudes in the case of former transitions are smaller by an order of magnitude.

(iv) In the case of the $0^+ \rightarrow 2_1^+$ transitions, the magnitude of the form factors at the second maxima are usually 10 to 15 times smaller compared to the values at the first maxima. In the case of the $0^+ \rightarrow 4_1^+$ transition, on the other hand, the ratio of the form factors at the first and the second maxima ranges between 50 and 100. The ratio of the form factors at the first and second maxima is expected to depend sensitively on the nuclear microscopic model involved in the calculations.

The topic of the coordinate space reconstruction of the transition charge densities associated with the electro-excitation of nuclear levels has received a lot of attention in recent years[12]. The transition charge densities have been deduced from the available inelastic scattering data in a nearly model-independent way by employing the technique of the Fourier-Bessel transforms in conjunction with the distorted-wave Born approximation. If one considers a simple

single-particle transition — an excitation of a nucleon from state a to state b — the transition charge density is essentially the product of the radial wavefunctions of the initial orbit a and the final orbit b times the charge of the nucleon. The empirical transition charge densities thus provide a detailed picture of the underlying nuclear wavefunctions. Further, they acquire additional significance vis-à-vis the test of the model wavefunctions since they provide structural details unaffected by the accuracy of the usual plane-wave Born approximation for large momentum transfers.

In this thesis we attempt a consistent microscopic description of the available experimental data on the form factors as well as transition charge densities for the 2p-1f shell nuclei in terms of the angular momentum projected Hartree-Fock-Bogoliubov (HFB) wave functions[13-15] resulting from the realistic effective interaction[16] obtained by Kuo and Brown for the valence space spanned by the ($1f_{7/2}$, $2p_{3/2}$, $2p_{1/2}$, $1f_{5/2}$) orbits. In view of the intractability of the unrestricted shell model calculations involving the $(1f_{7/2}, 2p_{3/2}, 2p_{1/2}, 1f_{5/2})^{\pi,\nu}$ space for the nuclei with $40 < A < 80$ — and this is because the dimensionalities of the relevant shell model matrices are prohibitively large — the approach discussed in the present work is expected to provide an approximate yet reliable ansatz for the multiparticle wave functions generated within the <u>full</u> 2p-1f valence space.

In Chapter II we describe the calculational framework involving the use of the projected HFB wave functions for interpreting the recent data on the form factors as well as transition charge densities associated with the electro-excitation of the $2_1^+$ and $4_1^+$ levels.

We next discuss in Chapter III the results for the form factors, transition charge densities as well as the E2 transition probabilities for the $0^+ \rightarrow 2_1^+$ transition in a number of doubly even Ni and Zn isotopes in the second half of the 2p-1f shell.

In a recent study[17], the shell model wave functions resulting from semi-empirical effective interactions operating in the restricted valence spaces involving the $[(2p_{3/2}, 1f_{5/2}, 2p_{1/2})^n + (1f_{7/2})^{-1}(2p_{3/2}, 1f_{5/2}, 2p_{1/2})^{n+1}]$ configurations have been employed for calculating the $0^+ \rightarrow 2_1^+$ form factors as well as the relevant transition charge densities for some doubly even Ni isotopes. The inadequacy of these shell model wave functions for interpreting and correlating the available data is reflected in the use of significantly mass-dependent proton and neutron effective charges that are required for optimizing the agreement with the experiments.

In the case of the doubly even Zn isotopes, the inappropriateness of the shell model descriptions involving just one $(1f_{7/2})^{\pi,\nu}$ hole is emphasized by the fact that the

available data on the reduced E2 transition probabilities indicates considerably enhanced rotational collectivity compared to that in the Ni isotopes[18,19]. Because of these considerations, the available form factor data in doubly even Zn isotopes (with A ~ 66) has not been interpreted in a microscopic framework thus far.

The calculations presented in Chapter III demonstrate that the yrast wave functions with $J^{\pi} = 0^+, 2^+$ projected from the HFB intrinsic states resulting from realistic two-body effective interactions operating in the full 2p-1f shell yield a reasonably satisfactory unified description of the available form factor data for the $0^+ \rightarrow 2_1^+$ transition in the nuclei $^{58,60,62}$Ni and $^{64,66,68}$Zn. It turns out that the use of the projected HFB wave functions obviates the necessity of employing widely different effective charges for various nuclei. We have also discussed the calculation of the transition charge densities in terms of the self-consistent projected HFB wave functions. It is seen that a comparison of the model space transition densities with the empirical ones extracted from the data via the Fourier-Bessel analyses supports unambiguously one of the two existing models for the $^{40}$Ca core-polarization transition density.

The calculations presented in Chapter IV examine the efficacy of the projected HFB wave functions vis-à-vis the recently-measured data involving the hexadecupole

electroexcitation in a number of doubly even isotopes of Ti, Cr, Fe and Ni. It is encouraging to note that, in the framework of the projected HFB method, the effective charges required for a satisfactory quantitative discussion of the $0^+ \rightarrow 4_1^+$ form factors are quite close to the ones required for a comparable fit to the quadrupole electroexcitation data in these nuclei. This again contrasts keenly with the results obtained in some recent shell model calculations[17] involving restricted configuration mixing in which the optimization of the agreement with the observed $|F|^2 (0^+ \rightarrow 4^+)$ data has required highly mass-dependent effective charges which are also drastically different from the values employed in the (shell model) studies of the $0^+ \rightarrow 2_1^+$ form factors.

An important implication of the recent measurements of the form factors associated with the $0^+ \rightarrow 4_1^+$ transitions is the availability of the heretofore unmeasured E4 transition probabilities, $B(E4; 0^+ \rightarrow 4^+)$, via an extension of the data into the momentum-transfer of the photon point. In view of this, we digress a little in Chapter IV to demonstrate the quantitative as well as qualitative unreliability of the usual Bohr and Mottelson prescriptions for relating the E4 matrix elements and the intrinsic hexadecupole moments. It turns out that the relative efficacy of the rotor model predictions for the quadrupole and hexadecupole operators is mostly dictated by the degree of closeness between the

eigenfunctions of these operators and the ones resulting from the two-body interactions via the HF/HFB prescription.

Finally in Chapter V we summarize the main results and discuss some possible extensions of the present work.

## REFERENCES


1. T. De Forest and J. Walecka, Advances in Physics 15, 1 (1966).

2. H. Überall, Electron Scattering From Complex Nuclei (Academic, New York, 1971).

3. Y. Torizuka et al., Phys. Rev. 185, 1499 (1969).

4. J. Heisenberg, J.S. McCarthy and I. Sick, Nucl. Phys. A164, 353 (1971).

5. K. Hosoyama et al., Res. Rep. Nucl. Sc. (Tohoku University), 7, 279 (1974); 8, 55 (1975).

6. J.W. Lightbody, Jr. et al., Bull. Am. Phys. Soc. 20, 568 (1975).

7. R. Neuhausen, Nucl. Phys. A282, 125 (1977).

8. K. Hosoyama et al., Res. Rep. Nucl. Sc. (Tohoku University) 11, 1 (1978).

9. J. Heisenberg, in Advances in Nuclear Physics, edited by J.W. Negele and E. Vogt (Plenum, New York, 1981), Vol. 12.

10. T. Iwamoto, H. Horie and A. Yokoyama, Phys. Rev. C25, 658 (1982).

11. J.W. Lightbody, Jr. et al., Phys. Rev. C27, 113 (1983).

12. B. Dreher et al., Nucl. Phys. A235, 219 (1974); H. Rothaas, J. Friedrich, K. Merle and B. Dreher, Phys. Lett. 51B, 23 (1974).

13. A.L. Goodman, in Advances in Nuclear Physics, edited by J.W. Negele and E. Vogt (Plenum, New York, 1979), Vol. 11.

14. N. Onishi and S. Yoshida, Nucl. Physics 80, 367 (1966).

15. G. Mukherjee and S.K. Sharma, Phys. Rev. C29, 2101 (1984); C31, 689 (1985).

16. T.T.S. Kuo and G.E. Brown, Nucl. Phys. A114, 241 (1968).

17. R.B.M. Mooy and P.W.M. Glaudemans, Nucl. Phys. A438, 461 (1985).

18. P.M. Endt, Atomic and Nuclear Data Tables 23, 547 (1979).

19. J.F. Bruandet et al., in Proceedings of the EPS International Conference, Florence (Italy) 1977, edited by P. Blasi and R.A. Ricci (Editrice Compositori, Bologna, 1978), p. 535.

# CHAPTER II

## MICROSCOPIC DESCRIPTION OF THE ELECTROEXCITATION FORM FACTORS AS WELL AS TRANSITION CHARGE DENSITIES IN TERMS OF THE PROJECTED HARTREE-FOCK-BOGOLIUBOV METHOD

### II.1 Introduction

In this chapter we shall first present in Section II.2 the theoretical framework relevant for a general discussion of the nuclear electroexcitation in the context of the plane-wave-Born-approximation (PWBA). The information about the nuclear wave function is contained in the (nuclear) form factors, which are determined by the appropriate nuclear charge and current densities. These form factors are in fact the Fourier-Bessel transforms into momentum-transfer space of the nuclear densities. Stated differently, the charge and current densities are the Fourier-Bessel transforms of the form factors into the co-ordinate space. In Section II.3 we discuss the outline of the procedure involved in the reconstruction of the densities (from the available experimental data) in terms of their Fourier-Bessel parameterization. We next discuss in Section II.4 and II.5 the use of projected HFB intrinsic states for the calculation of the electroexcitation form factors. Although the projected HFB method has been extensively used in the past for the calculation of sub-shell occupation numbers, level energies, static quadrupole

moments and reduced E2 transition probabilities, its use vis-à-vis the calculation of the electroexcitation form factors as well as transition densities has not been reported in the literature.

## II.2 Electroexcitation Form Factors for Nuclear Levels

We shall be working in the perturbation theoretical framework of scattering[1,2]. The electron-nucleus interaction may be considered as an exchange of virtual photons and can be represented by the Feynman graphs given in Figure II.1. Here Figure II.1(a) shows one-photon exchange, where photon is coupled to the electron by the coupling constant e and to the nucleus by the constant Ze. So the expansion parameter of the series is $Z\alpha = Ze^2$. This graph gives the first Born amplitude contribution. Graph of Figure II.1(b) gives the second-order Born amplitude where two photons have been exchanged and the contribution is of the order of $(Z\alpha)^2$. The perturbation series is a power series in powers of $(Z\alpha)$ for the amplitude. In general the cross section involves square of the amplitude. The lowest term in cross section is proportional to the square of graph of Figure II.1(a) and is known as the "first Born approximation" of the cross section [having order $(Z\alpha)^2$]. Next highest term contributing to cross-section is of order $(Z\alpha)^3$ coming from the cross product of Figure II.1(a) and Figure II.1(b) which is called the second Born

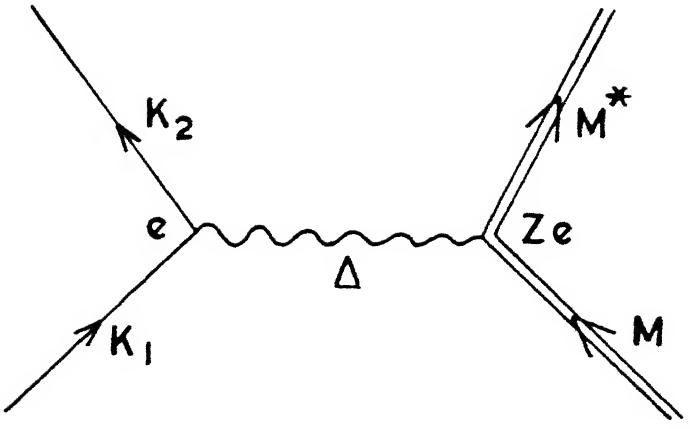


(a)

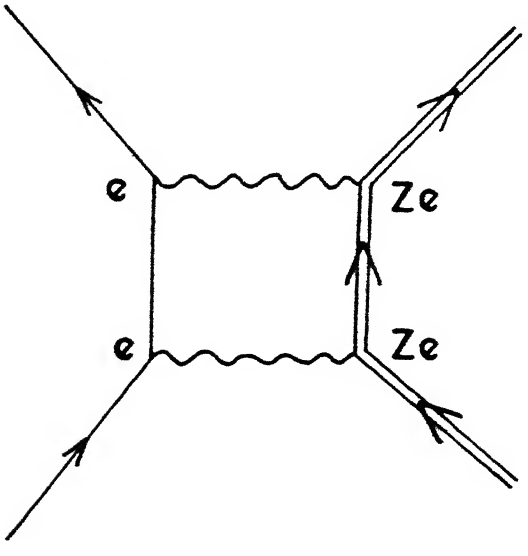


(b)

FIG.II.1 (a) ONE-PHOTON (b) TWO-PHOTON EXCHANGE IN ELECTRON-NUCLEUS SCATTERING.

approximation. Square of Figure II.1(b) and the other graphs contribute to higher power of $(Z\alpha)$. In all these cases initial and final particles are considered free. In the 2p-1f shell nuclei, with $Z\alpha \sim 0.14$-$0.21$, the contribution of graphs other than the one-photon exchange ones are expected to be small. In what follows, we discuss nuclear electroexcitation in the one-photon exchange approximation.

Consider an electron with four-momentum $k_{1\mu} = (k_1, iE_1)$ incident on a nucleus of mass M. After exchange of virtual photon with four-momentum $\Delta = (\vec{q}, iE)$ the electron gets scattered carrying four-momentum $k_{2\mu} = (\vec{k}_2, iE_2)$. For electrons with the energy of the order of a few hundred MeV, we can take $E_1 \simeq k_1$ and $E_2 \simeq k_2$. The different kinematical relations satisfied by these quantities are

$$\vec{k}_1 - \vec{k}_2 = \vec{q}; \quad q = (k_1^2 + k_2^2 - 2k_1 k_2 \cos\Theta)^{1/2} ; \qquad (II.1)$$

$$k_1 + M = k_2 + E' , \qquad (II.2)$$

where $$E' = (q^2 + M'^2)^{1/2} . \qquad (II.3)$$

Here M' is the mass of the excited nucleus.

Let the quantities $(\vec{A}_e, i\Phi_e)$ characterize the electromagnetic field of the passing electron. The quantities summarizing the electromagnetic properties of the nucleus are: the nuclear charge density $e\rho(\vec{r})$ normalized to

$$\int \rho(\vec{r}) \, d^3r = Z , \qquad (II.4)$$

the nuclear current density, $e\vec{j}_c(\vec{r})$ and the nuclear magnetization density $e\vec{\mu}_s(\vec{r})$. The interaction Hamiltonian which completely describes the electroexcitation process is given by

$$H_I = H_c + H_T \quad . \tag{II.5}$$

where the Coulomb part is

$$H_c = e \int \rho_N(\vec{r}) \; \Phi_e(\vec{r}) \; d^3r \; , \tag{II.6}$$

and the transverse part is given by

$$H_T = -e \int [\, \vec{j}_c(\vec{r}) . \vec{A}_e(\vec{r}) + \vec{\mu}_s(\vec{r}) . \vec{\nabla} \times \vec{A}_e(\vec{r}) \,] d^3r . \tag{II.7}$$

The transverse interaction plays role mainly for large angle scatterings. From now onwards we shall be concentrating here on the Coulomb part only.

The Coulomb potential of electron is given by

$$\Phi_e(\vec{r}) = \int [\, \rho_e(\vec{r}') / |\vec{r} - \vec{r}'| \,] d^3r' \quad . \tag{II.8}$$

So we have

$$H_c = e \int [\, \rho_N(\vec{r}) \; \rho_e(\vec{r}') / |\vec{r} - \vec{r}'| \,] \; d^3r \; d^3r' \; . \tag{II.9}$$

We write $R^{-1} = 1/|\vec{r} - \vec{r}'|$ in terms of its Fourier transform:

$$R^{-1} = 2\pi^{-3} \int \exp(i\vec{q}.\vec{R}) \; [\, \exp(-i\vec{q}.\vec{R}')/R' \,] \; d^3R' d^3q . \tag{II.10}$$

After integration w.r.t. $R'$, we get

$$|\vec{r} - \vec{r}'|^{-1} = (2\pi^2)^{-1} \int \exp[i\vec{q}.(\vec{r} - \vec{r}')]\, q^{-2} d^3q \ . \quad (II.11)$$

Now we make use of Rayleigh expansion, i.e. multipole expansion of a plane wave

$$\exp(i\vec{q}.\vec{r}) = \sum_L i^L (2L+1)\, j_L(qr)\, P_L(\text{Cos}\ \theta_{12}); \theta_{12} = \text{Cos}^{-1}(\hat{q}.\hat{r}). \quad (II.12)$$

Using

$$P_L\ (\text{Cos}\ \theta_{12}) = \sum_M \left(\frac{4\pi}{2L+1}\right) Y^*_{LM}(\hat{q})\, Y_{LM}(\hat{r}), \quad (II.13)$$

we obtain

$$\exp(i\vec{q}.\vec{r}) = 4\pi \sum_{LM} i^L\, j_L(qr)\, Y^*_{LM}(\hat{q})\, Y_{LM}(\hat{r}) \ . \quad (II.14)$$

Now Coulomb interaction can be written as

$$H_c = \frac{2e}{\pi} \sum_{LM} \int (d^3q/q^2)\, Y^*_{LM}(\hat{q})\, f_{LM}(q)\, X(\vec{q}) \ , \quad (II.15)$$

where the nuclear Coulomb matrix element is given by

$$f_{LM}(q) = i^L \int \rho_N(\vec{r})\, j_L(qr)\, Y_{LM}(\hat{r})\, d^3r, \quad (II.16)$$

and $X(\vec{q})$ is the Fourier transform of electron charge density,

$$X(\vec{q}) = \int \rho_e(\vec{r}')\, \exp(-i\, \vec{q}.\vec{r}')\, d^3r' \ . \quad (II.17)$$

Here we shall be making use of the plane wave solution of Dirac equation for initial and final states of the electron, or in other words we shall be working in the framework of the plane wave Born approximation.

Initial and final states of the electron are

$$\Psi_i = u(\vec{k}_1)\ \exp i(\vec{k}_i.\vec{r} - \omega t),\ \Psi_f = u(\vec{k}_2)\exp i(\vec{k}_2.\vec{r}-\omega t) \qquad (II.18)$$

and the expression for transition charge density is

$$\rho_e = -e\ \bar{\Psi}_f \gamma_o \Psi_i \qquad (II.19)$$

Then expression (II.17) reduces to

$$X(\vec{q}) = -e \int \bar{u}(\vec{k}_2)\gamma_o\, u(\vec{k}_1)\ \exp i(-\vec{k}_2.\vec{r}' + \omega t)\exp i(\vec{k}_1.\vec{r}'-\omega t)$$
$$\times\ \exp(-i\,\vec{q}.\,\vec{r}')\ d^3r'$$
$$= -e\,(2\pi)^3\,\delta(\vec{k}_1 - \vec{k}_2 - \vec{q})\ (\bar{u}(\vec{k}_2)\gamma_o\, u(\vec{k}_1)) \ . \qquad (II.20)$$

Substituting this in (II.15) we have

$$H_c = -\frac{16\pi^2}{q^2}\, e\,(\bar{u}(\vec{k}_2)\,\gamma_o\, u(\vec{k}_1))\ \sum_{LM} Y^*_{LM}(\hat{q})\ f_{LM}(q) . \qquad (II.21)$$

The differential scattering cross section is obtained by multiplying $|H_c|^2$ by $2\pi$ times the phase space factors. The phase space factor is given by

$$(2\pi)^{-3}\ d^3k_2\ \delta(k_1 + M - k_2 + E') \ , \qquad (II.22)$$

where normalizing volume ($\Omega$) has been taken to be equal to 1. Überall[2] has pointed out that the phase space factors are not affected by dynamic (nuclear) recoil effects involving free motion of nuclear centre of mass. Making use of invariant normalization ($m_e/E$) for spinors $u(\vec{k}_{1,2})$ and dividing

by the incident flux $k_1/E_1$, the cross section in the laboratory frame is given by

$$d\sigma = (2\pi E_1/k_1)\,\delta(k_1+M-k_2-E')(m_e^2/E_1E_2)\,|H_c|^2\,d^3k_2(2\pi)^{-3}. \qquad (II.23)$$

If we consider the scattering of the outgoing electron in the solid angle $d\Omega$, then

$$\int \delta(k_1+M-k_2-E'(k_2))\,d^3k_2 = k_2^2\,d\Omega\,|1 + dE'(k_2)/dk_2|^{-1}$$
$$= k_2^2\,d\Omega[1 + (2k_1/M)\sin^2(\theta/2)]. \qquad (II.24)$$

$$\text{Since } dE'(k_2)/dk_2 = (dE'/dq)(dq/dk_2)$$
$$= (q/E')\,(dq/dk_2)\,, \qquad (II.25)$$

where we have used the equations (II.3) and (II.1) and the approximation $E' \simeq M$, $k_2 = k_1$.

The actual cross section involves a factor $|H_c|^2$ and hence the expression $|\bar{u}(\vec{k}_2)\gamma_o\,u(\vec{k}_1)|^2$. For unpolarized beam this has to be summed over final states and averaged over initial states. We need to evaluate

$$\frac{1}{2}\sum_{S_1,S_2} |\bar{u}(\vec{k}_2, S_2)\gamma_o\,u(\vec{k}_1, S_1)|^2\,, \qquad (II.26)$$

Making use of the following relation[3]

$$\sum_{S_1,S_2} u_\beta(\vec{k}, S_2)\bar{u}_\delta(\vec{k}, S_1) = [(\not{k} + m_e)/2m_e]_{\beta\delta}\,, \qquad (II.27)$$

and the trace identities for even number of matrices

$$Tr(\not{a}_1\not{a}_2 \ldots\ldots \not{a}_{2n}) = a_1 \cdot a_2 \, tr(\not{a}_3 \ldots \not{a}_{2n}) - a_1 \cdot a_3 \, tr(\not{a}_2 \not{a}_4 \ldots) + \ldots\ldots\ldots, \qquad (II.28)$$

$$tr\, \gamma^0 \gamma^0 = 4 \ ,$$

the expression (II.26) simplifies to

$$Tr[(\gamma^0(\not{k}_2 + m_e)/2m_e)(\gamma_0(\not{k}_1 + m_e)/2m_e)]$$

$$= (E_1 E_2 + \vec{k}_1 \cdot \vec{k}_2 + m_e^2)/m_e^2 \ . \qquad (II.29)$$

Next we make an extension of the formalism with a view to incorporate the possibility of nuclear electro-excitation. We replace the nuclear matrix element $f_{LM}(q)$ by its operator definition

$$f_{LM}^{op}(q) = i^L \int \rho^{op}(\vec{r})\ j_L(qr)\ Y_{LM}(\hat{r})\ d^3r \qquad (II.30a)$$

$$= i^L \sum_k e_k\ j_L(qr_k)\ Y_{LM}(\hat{r}_k), \qquad (II.30b)$$

where $\rho^{op}(\vec{r}) = \sum_k e_k \delta(\vec{r} - \vec{r}_k)$ .

Let us denote initial and final states of the nucleus by $|J_i M_i>$ and $|J_f M_f>$ respectively. Then the reduced matrix elements of $f_{LM}$ are

$$<J_f M_f | f_{LM}^{op} | J_i M_i> = [J_f]^{-1} <J_i\ M_i,\ LM | J_f M_f> <J_f || f_{LM}^{op} || J_i> . \qquad (II.31)$$

where we have made use of Wigner-Eckart theorem. Here

$$[a]^{-1} = (2a + 1)^{1/2} \quad . \qquad (II.32)$$

To obtain the differential cross Section (II.23), we collect the terms involved in it and substitute from (II.21), (II.24), (II.29) and (II.30). Starting with ground state $|J_i M_i>$, the operators $H_c^\dagger$ and $H_c$ occurring in $|H_c|^2$ can take it to final states $|J_f M_f>$ and $|J_f' M_f'>$ respectively. Then the differential cross section comes in the form of "density matrix" with indices $(J_f M_f)$ and $(J_f' M_f')$:

$$\left(\frac{d\sigma}{d\Omega}\right)^{J_i \to J_f, J_f'}_{M_i \to M_f, M_f'} = (4\pi)^2 (2e^2 k_2/k_1 \Delta^4 [J_f][J_f'])$$

$$\sum_{LM, L'M'} (J_i M_i, LM | J_f M_f)(J_i M_i, L'M' | J_f M_f)$$

$$\times \quad R_{LL'}^{MM'} \quad , \qquad (II.33)$$

where

$$R_{LL'}^{MM'} = V_c(\Theta)\, Y^*_{L'M'}(\hat{q})\, Y_{LM}(\hat{q})\, (f_L^{if})^*\, f_{L'}^{if} \quad , \qquad (II.34)$$

$$V_c(\Theta) = (\Delta^2/q^2)^2 (E_1 E_2 + \vec{k}_1 . \vec{k}_2 + m_e^2), \qquad (II.35)$$

and

$$f_L^{if}(q) = <J_f || f_L(q) || J_i> \quad . \qquad (II.36)$$

Finally, the differential cross section for electron scattering with simultaneous nuclear transition $J_i \to J_f$ is obtained from the density matrix by putting $J_f' = J_f$,

$M_f' = M_f$ and summing over final projection $M_f$ and averaging over initial ones $M_i$. Carrying out these operations, we get

$$\left(\frac{d\sigma}{d\Omega}^{J_i \to J_f}\right)_{\text{Coulomb}} = [J_i]^{-2} \sum_{M_i M_f} \left(\frac{d\sigma}{d\Omega}\right)^{J_i \to J_f, J_f}_{M_i \to M_f, M_f} . \qquad (II.37)$$

This can be simplified by using orthogonality of Clebsch-Gordan coefficients

$$\sum_{M_i, M_f} (J_i\, M_i,\, LM | J_f M_f)(J_i M_i, L'M' | J_f M_f) = [J_f]^2 [L]^{-1} [L']^{-1} \delta_{LL'} \delta_{MM'}$$

and

$$\sum_{M} Y^*_{LM}(\hat{q})\; Y_{LM}(\hat{q}) = [L]^2 / 4\pi .$$

We finally get the expression

$$\left(\frac{d\sigma}{d\Omega}\right)^{J_i \to J_f} = (2Z^2 e^2 K_2 / K_1 \Delta^4)\, V_c(\theta) |F(q)|^2 \cdot f_{\text{recoil}} , \qquad (II.38)$$

where the recoil factor is added for the sake of completeness and is given by

$$f_{\text{recoil}} = [1 + (2k_1/M)\, \text{Sin}^2 \tfrac{\theta}{2}]^{-1} , \qquad (II.39a)$$

and the form factor is given by

$$|F(q)\ (J_i^+ \to J_f^+)|^2 = (4\pi/Z^2)(2J_i+1)^{-1} \sum_L |\langle J_f \| f_L^{op} \| J_i \rangle|^2 . \qquad (II.39b)$$

Further, in order to compare the form factors calculated by the PWBA with the experiments, the experimental data is plotted at the effective momentum transfer $q_{eff}$ instead of the kinematic q.

$$q_{eff} = q \left[1 + \frac{3Z\alpha\hbar}{2E_i R_{eq}}\right] \qquad (II.40)$$

where $R_{eq}$ is the radius of the equivalent uniform charge distribution of the ground state and $E_i$ is the energy of the incident electrons.

Sometimes the cross sections are given as a function of scattering angle. In these cases the momentum transfer is calculated using the relation

$$q = 2(E_1 E_2)^{1/2} \, \mathrm{Sin}(\theta/2) \, . \qquad (II.41)$$

For the evaluation of the single particle matrix elements we have employed the oscillator wave functions with the length parameter given by $b = 1.01\ A^{1/6}$. The centre-of-mass correction[2] has been taken into account by multiplying a factor $\exp(b^2q^2/4A)$. The correction[4] due to the finite size of proton has been incorporated by multiplying with the proton form factor $f_p(q)$:

$$f_p(q) = 1/(1 + q^2a_p^2/12)^2 \, , \qquad (II.42)$$

where $a_p = 0.84$ fm.

## II.3 Nuclear Transition Charge Density

The nuclear charge density operator $\rho(\vec{r})$ appearing in equation (II.30a) can be expanded in multipoles:

$$\rho^{op}(\vec{r}) = \sum_{LM} \rho^{op}_{LM}(r) \; Y^{*}_{LM}(\theta,\phi) \qquad (II.43)$$

The charge density can be characterized in terms of its reduced matrix elements between the initial and final nuclear states of spins $J_i$ and $J_f$ (refs. 5-7)

$$\langle J_f M_f | \rho^{op} | J_i M_i \rangle = \sum_{LM} \langle J_i M_i LM | J_f M_f \rangle \langle J_f || \rho^{op}_{L}(r) || J_i \rangle \times Y^{*}_{LM}(\theta, \phi) \; . \qquad (II.44)$$

The nuclear electroexcitation form factor is related to the transition charge density by the relation

$$F_L(q)\,(J_i \to J_f) = [(2J_f+1)/(2J_i+1)] \int_0^{\infty} \langle J_f || \rho^{op}_{L} || J_i \rangle \times j_L(qr)\, r^2\, dr \; . \qquad (II.45)$$

The form factors are thus the Fourier-Bessel transforms into momentum-transfer space of the nuclear transition charge densities. In other words, the densities are the Fourier-Bessel transforms of the form factors into coordinate space.

In view of the relation (II.44) it is clear that the nuclear transition charge densities and the form factors are

equivalent quantities. However, the form factor acquires significance — and can be considered more basic — in the case of the light nuclei (with small Z) because the reliability of the PWBA in these nuclei permits one to relate it directly to the experimentally measured cross sections (see Eq. II.41). On the other hand, for nuclei with large Z, distorted wave Born approximation (DWBA) calculations become necessary since the Coulomb distortion of the electron wave function is expected to be significant. In the framework of the DWBA calculations, the experimentally measured cross section can be related to the nuclear transition charge densities in a form that cannot be presented through the form factors given by Eq. (II.44). The simple relationship between the cross section and the charge densities (via the form factor) is no longer present. In such cases the transition charge densities play a more basic role since they summarize the nuclear structure information independent of the precision of the PWBA.

## Fourier-Bessel Parametrization of Transition Charge Densities

The basic assumption underlying the Fourier-Bessel parametrization[7] is that the transition charge density is restricted to a region $r < R_c$, and may be expanded into a Fourier-Bessel series with the spherical Bessel function $j_L$ of order L:

$$\rho_L(r) = \begin{cases} \sum_{\mu=1}^{\infty} A_\mu \, j_L(q_\mu r) & \text{for } r \leq R_c \\ 0 & \text{for } r > R_c \end{cases} \quad . \tag{II.46}$$

Here the $q_\mu$'s are given by the condition

$$j_L(q_\mu R_c) = 0 \quad .$$

In the PWBA framework, the coefficients $A_\mu$ are easily expressed in terms of the form factors $F_L(q_\mu)$ [i.e. $(d\sigma/d\Omega)^{1/2}$] measured at the momentum transfer $q_\mu$ :

$$A_\mu = \frac{2(2J_i+1)}{(2J_f+1)} \frac{1}{R_c^3 \, j_{L+1}^2(q_\mu R_c)} F_L(q_\mu) \quad . \tag{II.47}$$

Equation (II.47) has been derived by using the expression (II.45) in conjunction with the following relation:

$$\int_0^{R_c} r^2 \, [j_l(q_\mu r)]^2 \, dr = \frac{R_c^3}{2} [j_{l+1}(q_\mu R)]^2 \quad . \tag{II.48}$$

In view of the non-availability of the form factors for momentum-transfers $q > q_{max}$, the Eq. (II.47) permits the determination of only a certain number of the coefficients $A_\mu$.

Considering the $0^+ \rightarrow 2^+$ transition and taking $R_c = 10$ fm, it is seen that the usual data (covering the range $q = 0 - 2.5$ fm$^{-1}$) permits the determination of seven coefficients, $A_\mu (\mu = 1,2.....7)$, corresponding to the zeros of $j_2(q_\mu R_c)$ occurring at $qR_c = 5.76, 9.10, 12.4, 15.5, 18.7, 21.85$ and $25.0$. In the case of the $0^+ \rightarrow 4^+$ transition, an identical range of the available experimental data facilitates the evaluation of six coefficients corresponding to the zeros of $j_4(q_\mu R_c)$ at $qR_c = 8.18, 11.7, 15.0, 18.3, 21.5$ and $24.7$.

For the unknown large-q behaviour of the form factor for $q > q_{max}$ ($\sim 3$ fm$^{-1}$) one usually makes the following choices dictated by general physical arguments:

(a) The relation

$$F_L(q) < c \; q^{-4} \; f_p(q) \qquad \text{(II.49)}$$

is considered as the upper limit for the large-q form factors. Here $f_p(q)$ is the form factor of the proton (eq. II.42). The constant c is adjusted by matching the observed form factor at the second or the third maximum.

(b) The upper limit

$$F_L(q) < c \; f_p(q)$$

is also sometimes employed in the Fourier-Bessel analysis.

Outline of the procedure employed for extracting the transition charge densities from the measured form factors

The procedure involves the use of the PWBA as well as the DWBA methods in the following manner:

(i) One first chooses a cut-off radius $R_c$ = 10 fm. This value is expected to be reasonable for the 2p-1f shell nuclei. The zeroth-order values of about 15-20 coefficients are calculated using phenomenological form factors (such as the Tassie form factors[8]).

(ii) One next determines the first 5-6 coefficients corresponding to those $q_\mu$ lying inside the experimentally observed momentum-transfer range by invoking the DWBA framework.

(iii) The next step involves the use of the transition charge densities obtained in the step (ii) to transform the experimental cross sections to "experimental" form factors $F_{L,exp}$. One employs the relation

$$F_{L,exp} = F_{L,Calc.} \left[1 + 0.5 \left( \left( d\sigma/d\Omega \right)_{exp} - \left( d\sigma/d\Omega \right)_{Calc} \right) / \left( d\sigma/d\Omega \right)_{Calc} \right] \qquad (II.50)$$

where $(d\sigma/d\Omega)_{Calc.}$ is obtained via the DWBA framework using the Fourier-Bessel expansion of $\rho(r)$ obtained in the step (ii). Eq. (II.50) is easily derived by considering that the value of $(d\sigma/d\Omega)_{Calc.}$ is simply the square of $F_{L,Calc.}$, and by assuming that the fractional difference between the experimental and the calculated PWBA cross sections

is the same as the fractional difference between the experimental and the calculated DWBA cross sections.

(iv) The "experimental" form factors are next employed for carrying out an optimization of the complete set of expansion coefficients involved in the step (i). This is again performed in the PWBA framework. One also considers here the variation of the cut-off radius $R_c$ as well as the effects due to different choices for the large-q behaviour of the form factor. The optimized set of parameters is employed in repeating the procedure from step (ii) onwards.

The influences of the cut-off radius and of the large-q behaviour has been examined by Neuhausen[6] by considering, as an illustrative example, the case of the $2_1^+$ state of $^{64}Zn$.

## II.4 The Projected Hartree-Fock-Bogoliubov Method

In this section we discuss the calculation of the nuclear matrix element appearing in eq. (II.39b) in terms of the states $|J_i>$ and $|J_f>$ obtained via an explicit projection from the HFB intrinsic states. In this connection we first discuss the basic elements of the HFB theory.

### II.4.1 The HFB Method

The many-body Hamiltonian of the nucleus can be written as

$$H = \sum_{\alpha} \langle \alpha | \varepsilon | \alpha \rangle a^{\dagger}_{\alpha} a_{\alpha} + \frac{1}{4} \sum_{\alpha\beta\gamma\delta} \langle \alpha\beta | V_A | \gamma\delta \rangle a^{\dagger}_{\alpha} a^{\dagger}_{\beta} a_{\delta} a_{\gamma} \qquad (II.51)$$

with summation indices running over the orbits constituting the valence space. Here $a^{\dagger}_{\alpha}$ and $a_{\alpha}$ are particle creation and annihilation operators, respectively. The single particle energies, $\langle \alpha | \varepsilon | \alpha \rangle$, include the contribution due to the spherical single-particle field of the $^{40}$Ca core. Further, $\langle \alpha\beta | V_A | \gamma\delta \rangle$ is the antisymmetrized two-body matrix element. In the HFB procedure, the first step is to go to the quasiparticle bases by applying unitary transformation on the particle bases and finally assuming that the interaction between quasiparticles is relatively weak[9].

We can write the Hamiltonian in terms of quasiparticles as

$$H = E_o + H_{qp} + H_{qp-int}\,, \qquad (II.52)$$

where $E_o$ is the energy of the quasiparticle vacuum, $H_{qp}$ describes the elementary quasiparticle excitations and $H_{qp-int}$ is the (relatively) weak interaction between quasiparticles.

The Hamiltonian (II.52) has many symmetries associated with it and correspondingly we have conserved quantum numbers. But the part $(E_o + H_{qp})$ of Hamiltonian may not, in general, preserve all the symmetries of H. In HFB one imposes the constraints by introducing Lagrange multipliers

in such a way that atleast the observables corresponding to the violated symmetries have the desired expectation values. More specifically, in the HFB framework one includes pairing correlations by introducing number non-conserving wave functions. The Hamiltonian H is replaced by

$$H' = H - \lambda_\pi N_\pi - \lambda_\nu N_\nu \ , \qquad (II.53)$$

where the Lagrange multipliers $\lambda_\pi$ and $\lambda_\nu$ are chosen in such a way that the number operators

$$N_\pi = \sum_\alpha a^\dagger_{\alpha\pi} a_{\alpha\pi} \quad \text{and} \quad N_\nu = \sum_\alpha a^\dagger_{\alpha\nu} a_{\alpha\nu}$$

have the expectation values

$$\langle \Phi_o | N_\pi | \Phi_o \rangle = Z \quad \text{and} \quad \langle \Phi_o | N_\nu | \Phi_o \rangle = A-Z \ . \qquad (II.54)$$

The general Bogoliubov transformation employed in the HFB method is

$$q^\dagger_\alpha = \sum_\beta (U_{\alpha\beta} a^\dagger_\beta + V_{\alpha\beta} a_\beta) \ . \qquad (II.55)$$

So each quasiparticle is a linear combination of all particle creation and annhilation operators. U and V are NxN complex matrices for N single particle basis states. Then 2Nx2N linear transformation

$$\begin{bmatrix} q^{\dagger} \\ q \end{bmatrix} = \begin{bmatrix} U & V \\ V^{*} & U^{*} \end{bmatrix} \begin{bmatrix} a^{\dagger} \\ a \end{bmatrix} \qquad \text{(II.56)}$$

is required to be unitary. The unitarity of the transformation matrix

$$M = \begin{bmatrix} U & V \\ V^{*} & U^{*} \end{bmatrix} , \qquad \text{(II.57)}$$

i.e. $MM^{\dagger} = M^{\dagger}M = I$, implies the relations

$$UU^{\dagger} + VV^{\dagger} = U^{\dagger}U + \tilde{V}V^{*} = I \qquad \text{(II.58)}$$

and

$$U\tilde{V} + V\tilde{U} = U^{\dagger}V + \tilde{V}U^{*} = 0 \qquad \text{(II.59)}$$

where $U^{\dagger}$, $\tilde{U}$ and $U^{*}$ stand for the adjoint, transpose and complex conjugate of the matrix U. These relations can also be satisfied by requiring that the particles and quasiparticles obey the fermion anticommutation relations

$$[a_{\alpha}^{\dagger}, a_{\beta}] = \delta_{\alpha\beta} \quad , \quad [a_{\alpha}^{\dagger}, a_{\beta}^{\dagger}] = [a_{\alpha}, a_{\beta}] = 0 \qquad \text{(II.60)}$$

$$[q_{\alpha}^{\dagger}, q_{\beta}] = \delta_{\alpha\beta} \quad , \quad [q_{\alpha}^{\dagger}, q_{\beta}^{\dagger}] = [q_{\alpha}, q_{\beta}] = 0 \qquad \text{(II.61)}$$

Since $M^{-1} = M^{\dagger}$, we can invert (II.55) to express particle operators in terms of the quasiparticle operators

$$a_{\alpha}^{\dagger} = \sum_{\beta} (U_{\beta\alpha}^{*} q_{\beta}^{\dagger} + V_{\beta\alpha} q_{\beta}) \quad . \qquad \text{(II.62)}$$

The quasiparticle vacuum is defined through the relation

$$q_\alpha |\Phi_o\rangle = 0 \quad \text{for all } \alpha \qquad \text{(II.63)}$$

which has a solution

$$|\Phi_o\rangle = N \prod_\alpha q_\alpha |0\rangle$$

where N is a normalization constant and $|0\rangle$ is the particle vacuum.

Derivation of the HFB Equations

In the derivation of HFB equations we shall be making use of the expectation values of the operators $a^\dagger_\alpha a_\beta$ and $a_\alpha a_\beta$. We define density matrix $\rho$ and the pairing tensor t by

$$\rho_{\alpha\beta} = \langle \Phi_o | a^\dagger_\beta a_\alpha | \Phi_o \rangle \qquad \text{(II.64)}$$

$$t_{\alpha\beta} = \langle \Phi_o | a_\beta a_\alpha | \Phi_o \rangle \qquad \text{(II.65)}$$

Using equations (II.61) and (II.62) we can write

$$\rho_{\alpha\beta} = \langle \Phi_o | [\sum_\nu (U^*_{\nu\beta} q^\dagger_\nu + V_{\nu\beta} q_\nu)] [\sum_\delta (V^*_{\delta\alpha} q^\dagger_\delta + U_{\delta\alpha} q_\delta)] | \Phi_o \rangle$$

$$= \sum_\nu \sum_\delta V_{\nu\beta} V^*_{\delta\alpha} \delta_{\nu\delta} = \sum_\delta V_{\delta\beta} V^*_{\delta\alpha} = (V^\dagger V)_{\alpha\beta} .$$

i.e. $\rho = V^\dagger V$ , $\qquad \text{(II.66)}$

and

$$t_{\alpha\beta} = \langle \Phi_o | [ \sum_\delta ( V^*_{\delta\beta} q^\dagger_\delta + U_{\delta\beta} q_\delta )] [ \sum_\gamma ( V^*_{\gamma\alpha} q^\dagger_\gamma + U_{\gamma\alpha} q_\gamma )] | \Phi_o \rangle$$

$$= \sum_\delta \sum_\gamma U_{\delta\beta} V^*_{\gamma\alpha} \delta_{\delta\gamma} = \sum_\delta V^*_{\delta\alpha} U_{\delta\beta} = (V^\dagger U)_{\alpha\beta}$$

$$\text{or } t = V^\dagger U \ . \qquad \text{(II.67)}$$

Using equation (II.59) we can write

$$t = (U^\dagger V)^\dagger = -(\tilde{V}\, U^*)^\dagger = -\tilde{U}\, V^* = -\tilde{t} \ . \qquad \text{(II.68)}$$

It follows from equations (II.66) and (II.68) that $\rho$ is hermitian and t is antisymmetric.

As a next step, we are interested in the expansion of operators appearing in $H'$ in terms of normal ordered products. Normal product of an operator (made up of products of annihilation and creation operators) is obtained by expressing the particle operators in terms of the quasi-particle operators and then rearranging them in such a way that creation operators are to the left of the annihilation operators. A minus sign is included for an odd number of operator permutations. The contraction $\langle O \rangle$ of an operator is defined as the expectation value of O with respect to quasiparticle vacuum.

The expansion of operators in terms of normal products is given by Wick's theorem which states that any product of operators O is equivalent to the sum of normal products :O: which contains all possible contractions. The Hamiltonian $H'$

involves operator products of the type $a^{\dagger}_{\alpha}a_{\beta}$ and $a^{\dagger}_{\alpha}a^{\dagger}_{\beta}a_{\gamma}a_{\delta}$. From Wick's theorem we can expand these operators as

$$a^{\dagger}_{\alpha}a_{\beta} = \langle a^{\dagger}_{\alpha} a_{\beta}\rangle + :a^{\dagger}_{\alpha}\ a_{\beta}: \qquad \text{(II.69)}$$

and

$$\begin{aligned} a^{\dagger}_{\alpha}a^{\dagger}_{\beta}a_{\gamma}a_{\delta} = {} & \langle a^{\dagger}_{\alpha} a_{\delta}\rangle\langle a^{\dagger}_{\beta} a_{\gamma}\rangle - \langle a^{\dagger}_{\alpha}\ a_{\gamma}\rangle \langle a^{\dagger}_{\beta}\ a_{\delta}\rangle + \langle a^{\dagger}_{\alpha}\ a^{\dagger}_{\beta}\rangle \\ & \langle a_{\gamma}\ a_{\delta}\rangle \\ & + \langle a^{\dagger}_{\alpha}\ a_{\delta}\rangle\ :a^{\dagger}_{\beta}\ a_{\gamma}: + a^{\dagger}_{\beta}a_{\gamma}\ :a^{\dagger}_{\alpha}a_{\delta}: - \langle a^{\dagger}_{\alpha}\ a_{\gamma}\rangle \\ & :a^{\dagger}_{\beta}\ a_{\delta}: \\ & - \langle a^{\dagger}_{\beta}\ a_{\delta}\rangle\ :a^{\dagger}_{\alpha}a_{\gamma}: + \langle a^{\dagger}_{\alpha}\ a^{\dagger}_{\beta}\rangle\ :a_{\gamma}\ a_{\delta}: + \langle a_{\gamma}\ a_{\delta}\rangle \\ & :a^{\dagger}_{\alpha}\ a^{\dagger}_{\beta}: \\ & + :a^{\dagger}_{\alpha}a^{\dagger}_{\beta}\ a_{\gamma}\ a_{\delta}: \qquad \text{(II.70)} \end{aligned}$$

Substituting (II.69) and (II.70) into the equation (II.53) and using definitions (II.64) and (II.65) we can write H' as

$$H' = H'_{o} + H'_{2} + H'_{4} \qquad \text{(II.71)}$$

where $H'_{n}$ has n uncontracted operators:

$$H'_{o} = \mathrm{tr}\left[(\varepsilon - \lambda_{\pi} - \lambda_{\nu} + (1/2)\Gamma)\rho + (1/2)\Delta t^{\dagger}\right], \qquad \text{(II.72)}$$

$$\begin{aligned} H'_{2} = {} & \sum_{\alpha\beta}(h - \lambda_{\pi} - \lambda_{\nu})_{\alpha\beta}\ :a^{\dagger}_{\alpha}\ a_{\beta}: \\ & + (1/2)\sum_{\alpha\beta}\Delta_{\alpha\beta}\ :a^{\dagger}_{\alpha}\ a^{\dagger}_{\beta}: + (1/2)\sum_{\alpha\beta}\Delta^{\dagger}_{\alpha\beta}\ :a_{\alpha}\ a_{\beta}: \end{aligned} \qquad \text{(II.73)}$$

$$H_4' = (1/4) \sum_{\alpha\beta\gamma\delta} \langle\alpha\beta | V_A | \gamma\delta\rangle \quad : a_\alpha^\dagger a_\beta^\dagger a_\delta a_\gamma : \tag{II.74}$$

Here the HF Hamiltonian h, the HF potential $\Gamma$ and the pair potential $\Delta$ are given by

$$h = \varepsilon + \Gamma \ , \ \Gamma_{\alpha\beta} = \sum_{\gamma\delta} \langle\alpha\gamma | V_A | \beta\delta\rangle \rho_{\delta\gamma} \tag{II.75}$$

and $$\Delta_{\alpha\beta} = \frac{1}{2} \sum_{\gamma\delta} \langle\alpha\beta | V_A | \gamma\delta\rangle t_{\gamma\delta} \tag{II.76}$$

By invoking the properties of $\langle | V_A | \rangle$:

$\langle\alpha\beta | V_A | \gamma\delta\rangle = - \langle\beta\alpha | V_A | \gamma\delta\rangle$ ; $\langle\alpha\gamma | V_A | \beta\delta\rangle = \langle\beta\delta | V_A | \alpha\gamma\rangle$,

and using the hermiticity of $\rho$ and antisymmetry of t, it follows that h and $\Gamma$ are hermitian and $\Delta$ is antisymmetric.

Since the expectation values of all normal order products involved in H' vanish, we have

$$\langle \Phi_o | H | \Phi_o \rangle = \mathrm{tr}\left[ \left( \varepsilon - \lambda_\pi - \lambda_\nu + \frac{1}{2}\Gamma \right) \rho + \frac{1}{2} \Delta t^\dagger \right] \tag{II.77}$$

The $H_2'$ part of the Hamiltonian describes quasiparticle excitations and the remaining $H_4'$ contains quasiparticle interactions.

In HFB approximation, H' should acquire the form

$$H' = H_o' + \sum_\alpha E_\alpha q_\alpha^\dagger q_\alpha + H_{qp-int} \ . \tag{II.78}$$

This can be achieved if we assume that the "independent quasiparticle" Hamiltonian has the form

$$H_2' = \sum_\alpha E_\alpha q_\alpha^\dagger q_\alpha \qquad (II.79)$$

The commutator $[H_2', q_\alpha^\dagger]$ is given by

$$[H_2', q_\alpha^\dagger] = E_\alpha q_\alpha^\dagger = E_\alpha \sum_\beta (U_{\alpha\beta} a_\beta^\dagger + V_{\alpha\beta} a_\beta) \quad . \qquad (II.80)$$

This commutator evaluated by using equations (II.73) yields

$$[H_2', q_\alpha^\dagger] = \sum_{\beta\gamma} [h'_{\beta\gamma} U_{\alpha\gamma} + \Delta_{\beta\gamma} V_{\alpha\gamma}] a_\beta^\dagger + \sum_{\beta\gamma} [-\Delta^*_{\beta\gamma} U_{\alpha\gamma} - h'^*_{\beta\gamma} V_{\alpha\gamma}] a_\beta \quad . \qquad (II.81)$$

where $h' = \varepsilon - \lambda_\pi - \lambda_\nu$ .

On comparison of the equations (II.80) and (II.81) we get the general HFB equations:

$$\begin{bmatrix} h' & \Delta \\ -\Delta^* & -h'^* \end{bmatrix} \begin{bmatrix} \vec{U}_i \\ \vec{V}_i \end{bmatrix} = E_i \begin{bmatrix} \vec{U}_i \\ \vec{V}_i \end{bmatrix} \qquad (II.82)$$

where $\vec{U}_i = (U_{i1}, U_{i2}, \ldots\ldots, U_{iN})$.

Time-reversal Symmetry

We have assumed time-reversal symmetry in our calculations in the 2p-1f shell nuclei. All the basis states in the configuration space spanned by the orbits $1f_{7/2}$, $2p_{3/2}$, $2p_{1/2}$ and $1f_{5/2}$ are divided into two sets. The first set containing states $|k>$ is characterized by an

even value for $(m + 1/2)$. The set of time-reversed states $|\bar{k}> = T|k>$ has $(m + 1/2)$ = odd integer. The phase convention is: $T|nljm> = (-1)^{l+j-m}|n\ lj-m>$.

The states $|k>$ are taken to be:

$(1f_{7/2\ 7/2})$, $(1f_{7/2\ 3/2}, 1f_{5/2\ 3/2}, 2p_{3/2\ 3/2})$

$(1f_{7/2-1/2}, 1f_{5/2-1/2}, 2p_{3/2-1/2}, 2p_{1/2-1/2})$

and $(1f_{7/2-5/2}, 1f_{5/2-5/2})$.

For quasiparticle transformations

$$q^{\dagger}_{\alpha} = \sum_{\beta} (U_{\alpha\beta}\, a^{\dagger}_{\beta} + V_{\alpha\beta}\, a_{\bar{\beta}}) \qquad (II.83)$$

$$q^{\dagger}_{\bar{\alpha}} = \sum_{\beta} (\bar{U}_{\alpha\beta}\, a^{\dagger}_{\bar{\beta}} + \bar{V}_{\alpha\beta}\, a_{\beta}) \qquad (II.84)$$

we immediately notice that $\rho$ cannot connect $|k>$ and $|\bar{k}>$ states and t has non-zero contribution only for elements connecting $|k>$ and $|\bar{k}>$ so we can partition $\rho$ and t as

$$= \begin{bmatrix} \rho_1 & 0 \\ 0 & \rho_2 \end{bmatrix}, \quad t = \begin{bmatrix} 0 & t_1 \\ t_2 & 0 \end{bmatrix} \qquad (II.85)$$

Since the interaction V conserves the magnetic projections the potentials $(r, \Delta)$ can also be partitioned as

$$h = \begin{bmatrix} h_1 & 0 \\ 0 & h_2 \end{bmatrix}, \quad \Delta = \begin{bmatrix} 0 & \Delta_1 \\ \Delta_2 & 0 \end{bmatrix} \qquad (II.86)$$

Time-reversal symmetry is imposed by requiring

$$q_{\bar{\alpha}}^{\dagger} = T\, q_{\alpha}^{\dagger}\, T^{-1} \quad , \tag{II.87}$$

so that $$\bar{U}_{\alpha\beta} = U_{\alpha\beta}^{*} \quad , \quad \bar{V}_{\alpha\beta} = -V_{\alpha\beta}^{*} \tag{II.88}$$

The quasiparticle vacuum is now invariant under time-reversal.

Canonical Representation for the Time-reversally Symmetric HFB Wavefunction

Next we are interested in the simultaneous diagonalization[10] of $\rho$ and $t$. Creation and annihilation operators can be treated simultaneously by defining

$$A^{\dagger} = \begin{bmatrix} q_{\alpha}^{\dagger} \\ q_{\alpha} \end{bmatrix}, \quad B^{\dagger} = \begin{bmatrix} a_{\alpha}^{\dagger} \\ a_{\alpha} \end{bmatrix} \tag{II.89}$$

Here $A^{\dagger}$ contains quasiparticle operators and $B^{\dagger}$ has only particle operators. Then the general quasiparticle transformation is given by

$$A^{\dagger} = M\, B^{\dagger} \quad . \tag{II.90}$$

We can now define the generalized quasiparticle density matrix Q by

$$Q_{\alpha\beta} = \langle \Phi_o \mid A_{\beta}^{\dagger} A_{\alpha} \mid \Phi_o \rangle \quad . \tag{II.91}$$

From the commutation relations of quasiparticles (II.61) we have

$$\langle q_{\alpha}^{\dagger} q_{\beta} \rangle = \langle q_{\alpha}^{\dagger} q_{\beta}^{\dagger} \rangle = \langle q_{\alpha} \; q_{\beta} \rangle = 0, \langle q_{\alpha} \; q_{\beta}^{\dagger} \rangle = \delta_{\alpha\beta} \quad . \tag{II.92}$$

Substitution of (II.89) and (II.92) into (II.91) yields

$$Q = \begin{bmatrix} 0 & 0 \\ 0 & 1 \end{bmatrix} \qquad \text{(II.93)}$$

where '0' here is NxN null matrix and '1' stands for NxN unit matrix.

Similarly we define the generalized particle density matrix R by

$$R_{\alpha\beta} = \langle \Phi_o \mid B_\beta^\dagger \; B_\alpha \mid \Phi_o \rangle \qquad \text{(II.94)}$$

Substitution of (II.89), (II.64) and (II.65) into (II.94) leads to

$$R = \begin{bmatrix} \rho & t \\ t^\dagger & 1-\tilde{\rho} \end{bmatrix} . \qquad \text{(II.95)}$$

By looking at the inverted relation corresponding to (II.90) and comparing (II.91) and (II.94) we find that the generalized particle and quasiparticle matrices are related by a unitary transformation

$$R = M^+ Q M . \qquad \text{(II.96)}$$

Since $M^+M = 1$ and $Q^2 = Q$, it follows that

$$R^2 = (M^\dagger Q M)^2 = M^\dagger Q (M M^\dagger) Q M = M^\dagger Q^2 M = M^\dagger Q M . \qquad \text{(II.97)}$$

The relation $R^2 = R$ yields from (II.95)

$$\rho^2 + t\, t^\dagger = \rho \qquad \text{(II.98)}$$

and $$\rho t + t - t\tilde{\rho} = t \quad \text{or} \quad \rho t = t\tilde{\rho} \qquad \text{(II.99)}$$

Thus $\rho_1 t_1 = t_1 \rho_1$. This ensures us that $\rho_1$ and $t_1$ can be diagonalized simultaneously.

We can now have a basis spanned by $[\,|k_1\rangle, |k_2\rangle, \ldots\ldots; |\bar{k}_1\rangle, |\bar{k}_2\rangle \ldots\ldots\,]$ such that $\rho$ and t are in the canonical forms

$$\rho = \left[\begin{array}{cc|cc} \rho_1 & 0 & & \\ 0 & \rho_{\bar{1}} & & \\ \hline & & \rho_2 & 0 \\ & & 0 & \rho_{\bar{2}} \end{array}\right], \quad t = \left[\begin{array}{cc|cc} 0 & t_{1\bar{1}} & & \\ -t_{1\bar{1}} & 0 & & \\ \hline & & 0 & t_{2\bar{2}} \\ & & -t_{2\bar{2}} & 0 \end{array}\right] \qquad \text{(II.100)}$$

where the basis states are taken to be $|k\rangle = b_k^\dagger |0\rangle$

$$b_k^\dagger = \sum_\alpha C_{k,\alpha}\, a_\alpha^\dagger ; \quad b_{\bar{k}}^\dagger = \sum_\alpha C_{k,\alpha}^*\, a_{\bar{\alpha}}^\dagger \qquad \text{(II.101)}$$

Let $\rho_1$ and $t_1$ have the eigenvalues $\rho_k$ and $t_{k\bar{k}}$ respectively then from (II.98) we obtain

$$|t_{k\bar{k}}| = [\rho_k (1 - \rho_k)]^{1/2} \qquad \text{(II.102)}$$

putting $\rho_k = V_k^2$, $(U_k^2 + V_k^2 = 1)$ we get

$$|t_{k\bar{k}}| = U_k V_k \,. \qquad \text{(II.103)}$$

To satisfy the equations (II.102) and (II.103), the

quasiparticle vacuum can be expressed as

$$| \Phi_o > = \prod_k (U_k + V_k\, b_k^\dagger\, b_{\bar{k}}^\dagger) | 0 > \qquad (II.104)$$

Approximations employed in the present set of calculations

We recall the special quasiparticle transformations

$$q_k^\dagger = U_k^* b_k^\dagger - V_k^* b_{\bar{k}} \qquad (II.105)$$

and

$$q_{\bar{k}}^\dagger = U_k^* b_{\bar{k}}^\dagger + V_k^* b_k \qquad (II.106)$$

After inversion of this transformation and substitution into two-operator part of H' we can expand $H_2'$ as

$$H_2' = H_{11}' + H_{20}' \qquad (II.107)$$

with $H_{11}' = \sum_{kk'} (H_{11}')_{kk'}\, q_k^\dagger\, q_{k'}$ and

$$H_{20}' = \sum_{kk'} [(H_{20}')_{kk'}\, q_k^\dagger\, q_{k'}^\dagger + (H_{20}')^*_{kk'}\, q_{k'}\, q_k] \qquad (II.108)$$

In order to realize the free quasiparticle approximation, as we have seen earlier, the Hamiltonian (II.107) must satisfy the condition $H_{20}' = 0$, and $H_{11}'$ must be diagonal. The condition $(H_{20})_{k\bar{k}} = 0$ leads to the BCS equations and the requirements $(H_{20}')_{k\bar{k}} = 0$, $(H_{11}')_{kk'} = 0$ $(k \neq k')$ gives HF - like equations provided $h'_{kk'} = 0$ and $\Delta_{\bar{k}k'} = 0$ (with $k \neq k'$). We have considered here the latter approximation, viz. $\Delta_{k\bar{k}'} = 0$. The

coefficients $C_{k,\alpha}$ appearing in eq. (II.101) result from a diagonalization of the HF - like potential h' (which includes the relevant density $\rho_k = V_k^2$) :

$$(h'_{\alpha\beta})_{\pi/\nu} = < \alpha \mid \varepsilon - \lambda_{\pi/\nu} \mid \beta > + \sum_k < \alpha k \mid V_A \mid \beta k > V_k^2 \qquad (II.109)$$

The occupation probabilities are obtained from BCS equations:

$$\Delta_{k\bar{k}} = \frac{1}{2} \sum_{k'} < k\bar{k} \mid V_A \mid k' \bar{k}' > U_{k'} V_{k'} . \qquad (II.110)$$

Let $\Theta_k$ be the eigenvalues of (II.109). Then the condition $(H'_{20})_{k\bar{k}} = 0$ leads to

$$2\Theta_k U_k V_k - \Delta_{k\bar{k}} (U_k^2 - V_k^2) = 0 \qquad (II.111)$$

where

$$U_k^2 + V_k^2 = 1 \qquad (II.112)$$

The set of equations (II.111) and (II.112) can be solved easily by making substitution

$$V_k = \text{Cos}\,\varphi \text{ and } U_k = \text{Sin}\,\varphi \qquad (II.113)$$

From (II.111) we have

$$\Theta_k \text{Sin}2\varphi = - \Delta \text{Cos}\, 2\varphi$$

or $\tan 2\varphi = -\Delta/\Theta_k$ , (II.114)

or $\text{Cos}\, 2\varphi = U_k^2 - V_k^2 = \Theta_k / [\Theta_k^2 + \Delta_{k\bar{k}}^2]^{1/2}$ (II.115)

This equation together with (II.112) yields

$$U_k^2 = \frac{1}{2}\left[1 + \theta_k/(\theta_k^2 + \Delta^2_{k\bar{k}})^{1/2}\right] \qquad \text{(II.116)}$$

and

$$V_k^2 = \frac{1}{2}\left[1 - \theta_k/(\theta_k^2 + \Delta^2_{k\bar{k}})^{1/2}\right] \qquad \text{(II.117)}$$

Substitution of equations (II.116) and (II.117) into (II.120) gives

$$\Delta_{k\bar{k}} = \frac{1}{2}\sum_{k'} \langle k\bar{k} \mid V_A \mid k'\bar{k}' \rangle \left[\Delta_{k'\bar{k}'}/(\theta^2_{k'} + \Delta^2_{k'\bar{k}'})^{1/2}\right] \qquad \text{(II.118)}$$

The condition $2\sum_k V^2_{k,\pi(\nu)} = N_{\pi(\nu)}$ yields

$$\sum_{k\,\pi(\nu)} \left[1 - \theta_k/(\theta_k^2 + \Delta^2_{k\bar{k}})^{1/2}\right] = N_{\pi(\nu)} \qquad \text{(II.119)}$$

To discuss the iterative procedure used in the calculations we define the quantities

$$P[\mu, (\Delta_{1\bar{1}}, \Delta_{2\bar{2}}, \ldots \Delta_{10\,\overline{10}}) = \sum_{k=1}^{10} (\varepsilon_k/[(\varepsilon_k - \mu)^2 + \Delta^2_{k\bar{k}}]^{1/2}) \qquad \text{(II.120)}$$

$$Q[\mu, (\Delta_{1\bar{1}}, \Delta_{2\bar{2}}, \ldots \Delta_{10\,\overline{10}})] = \sum_{k=1}^{10} (1/[(\varepsilon_k - \mu)^2 + \Delta^2_{k\bar{k}}]^{1/2}) \qquad \text{(II.121)}$$

Here $\mu = \lambda_{\pi/\nu}$ and $\theta_k = \varepsilon_k - \mu$. (II.122)

Summing both sides of eq. (II.117) over k, we have

$$N_{\pi/\nu} = 10.0 - P + \mu Q \qquad \text{(II.123)}$$

We thus obtain a convenient expression for $\mu$ :

$$\mu = (P - 10.0 + N_{\pi/\nu})/Q \ . \qquad \text{(II.124)}$$

We have followed the following iteration procedure in our work:

a. We first carry out the usual HF calculation. This provides an "educated" initial guess for the set of values of $\varepsilon_k$'s ($k = 1,10$), $\mu$ as well as the expansion coefficients defining the orbits $|k>$ ($k = 1,10$).

b. We next assign a constant non-zero value (say 0.5) to all $\Delta_{k\bar{k}}$'s. The equations (II.120), (II.121) and (II.124) are iterated until one obtains a "self-consistent" value for $\mu$ .

c. This value of $\mu$ is next employed to obtain a set of self-consistent values of $\Delta_{k\bar{k}}$'s by using repeatedly the equation (II.118).

d. The $\Delta_{k\bar{k}}$ values resulting from the preceding step are next employed to obtain an improved self-consistent value of $\mu$ by again using the equations (II.120) and (II.121) and (II.124).

e. One obtains finally a mutually consistent set of values of $\mu$ as well as $\Delta_{k\bar{k}}$'s by repeating the preceding steps (c) and (d).

f. We next solve the equation (II.109) to obtain a new set of $\epsilon_k$'s and $\lambda$. The procedure just discussed is then repeated from the step c onwards until successive iteration cycles produce nearly the same set of numbers for various parameters.

In the HF-BCS procedure one simply terminates the calculations at the step e.

## II.4.2 The Technique of Angular Momentum Projection

We discuss in this section the general technique[11] of projecting the intrinsic deformed wave function (of the HF or the HFB type) on the subspace of angular momentum J. The intrinsic state involving axially symmetric deformed single-particle orbitals is characterized by the eigenvalue of $J_z$ operator. We denote the intrinsic state by $|\Phi_K\rangle$ ($K = \langle J_z \rangle$) and expand it in terms of states of good angular momentum:

$$|\Phi_K\rangle = \sum_J a_J |\Psi_K^J\rangle \qquad \text{(II.125)}$$

Applying the rotation operator

$$R(\Omega) = e^{-i\alpha J_z} e^{-i\theta J_y} e^{-i\gamma J_z}, \qquad \text{(II.126)}$$

we obtain

$$\hat{R}(\Omega) \mid \Phi_K > = \sum_{JM} a_J \; D^J_{MK}(\Omega) \mid \Psi^J_M > \qquad (II.127)$$

where $D^J_{MK}$ are the matrix elements of the rotation operator in the basis $\mid \Psi^J_K >$. $\Omega$ stands for Eulerian angles $\alpha$, $\theta$ and $\gamma$.

Multiplying (II.128) by $D^{J'*}_{M'K}$ and integrating over $\Omega$, we have

$$\mid \Psi^J_M > \; = \; \frac{2J+1}{8\pi^2 a_J} \int d\Omega \, D^{J*}_{MK}(\Omega) \, \hat{R}(\Omega) \mid \Phi_K > \qquad (II.128)$$

where we have used

$$\int d\Omega = \int_0^{2\pi} d\alpha \int_0^{\pi} d\theta \; \sin\theta \int_0^{2\pi} d\gamma \qquad (II.129)$$

and the orthogonality of the D-matrices:

$$\int d\Omega \; D^{J*}_{MK}(\Omega) \; D^{J'}_{M'K}(\Omega) \; = \; \frac{8\pi^2}{2J+1} \, \delta_{JJ'} \delta_{MM'} \qquad (II.130)$$

In view of the equation (II.128), we can say that the state of angular momentum J with projection M in the laboratory frame is projected out from the deformed intrinsic HF/HFB state $\mid \Phi_K >$ possessing projection K of $J_z$ on the Z-axis of the intrinsic frame.

Equation (II.128) can be written as

$$\mid \Psi^J_K > \; = \; P^J_{KK} \mid \Phi_K > \qquad (II.131)$$

where

$$P^J_{KK} = \frac{2J+1}{8\pi^2 a_J} \int d\Omega D^{J*}_{KK}(\Omega) \quad R(\Omega) \ . \tag{II.132}$$

The projection operator $P^J_{KK}$ satisfies the following properties:

$$(i) \quad (P^J_{KK})^\dagger = P^J_{KK} \tag{II.133}$$

$$(ii) \quad (P^J_{KK})^2 = P^J_{KK} \tag{II.134}$$

$$(iii) \quad [H, P^J_{KK}] = 0 \tag{II.135}$$

Making use of these properties of the projection operator along with (II.131), the energy of the projected state $|\Psi^J_K>$

$$E_J = \frac{<\Psi^J_K | H | \Psi^J_K>}{<\Psi^J_K | \Psi^J_K>} \tag{II.136}$$

can be expressed as

$$E_J = \frac{<\Phi_K | H P^J_{KK} | \Phi_K>}{<\Phi_K | P^J_{KK} | \Phi_K>} \tag{II.137}$$

Using the expression for $P^J_{KK}$ and $\hat{R}(\Omega)$ given by equations (II.132) and (II.126), respectively, we have

$$E_J = \frac{\int_0^\pi d\theta \ \mathrm{Sin}\theta \ d^J_{KK}(\theta) <\Phi_K | H \ e^{-i\theta J_y} | \Phi_K>}{\int_0^\pi d\theta \ \mathrm{Sin}\theta \ d^J_{KK}(\theta) <\Phi_K | \ e^{-i\theta J_y} | \Phi_K>} \ , \tag{II.138}$$

where we have used the property that $\exp(-i\alpha J_z)$ and $\exp(-i\gamma J_z)$ operating on $<\Phi_K|$ and $|\Phi_K>$ states produce

$\exp(-i\alpha K)$ and $(-i\gamma K)$, respectively. $d^J_{KK}(\Theta)$ are related to $D^J_{KK}(\Omega)$ by

$$D^J_{KK}(\Omega) = e^{-i\alpha K} \; d^J_{KK}(\Theta) \; e^{-i\gamma K} \qquad \text{(II.139)}$$

## II.5 Electroexcitation Form Factors and Transition Charge Densities in Terms of Projected HFB Wavefunctions

The axially symmetric intrinsic deformed HFB state with K=0 can be written as[12]

$$|\Phi_o\rangle = \prod_{im} (U^m_i + V^m_i \; b^\dagger_{im} \; b^\dagger_{i\bar{m}}) \; |0\rangle, \qquad \text{(II.140)}$$

where

$$b^\dagger_{im} = \sum_j C^m_{ji} \; a^\dagger_{jm} \text{ and } b^\dagger_{i\bar{m}} = \sum_j (-1)^{j-m} C^m_{ji} \; a_{j-m} \; . \qquad \text{(II.141)}$$

The index i distinguishes the states with same m value and j labels the spherical single particle orbitals $2p_{1/2}$, $2p_{3/2}$, $1f_{5/2}$ and $1f_{7/2}$.

We can rewrite $|\Phi_o\rangle$ in the form

$$|\Phi_o\rangle = N \; \exp\left(\frac{1}{2} \sum_{\alpha\beta} f_{\alpha\beta} \; a^\dagger_\alpha \; a^\dagger_\beta\right) \; |0\rangle \qquad \text{(II.142)}$$

with

$$f_{\alpha\beta} = \sum_i C^{m_\alpha}_{j_\alpha i} \; C^{m_\beta}_{j_\beta i} \; \frac{V^{m_\alpha}_i}{U^{m_\alpha}_i} \; \delta_{m_\alpha, -m_\beta} \; . \qquad \text{(II.143)}$$

Here $\alpha$ stands for quantum numbers ( $j_\alpha$, $m_\alpha$) and N is a normalisation constant.

The state with angular momentum J is given by

$$|\Psi^J_K> = P^J_{KK} |\Phi_K> = \frac{2J+1}{8\pi^2} \int D^J_{KK}(\Omega)\, R(\Omega) |\Phi_K> d\Omega . \qquad (II.144)$$

Making use of equation (II.127) for $R(\Omega)$ ,

$$|\Psi^J_{K=0}> = N \int d\Omega\, D^J_{KO} \exp\left(\sum_{\alpha\beta} F_{\alpha\beta}(\Theta)\ a^\dagger_\alpha a^\dagger_\beta\right) |0> \qquad (II.145)$$

where

$$F_{\alpha\beta} = \sum_{m'_\alpha} \sum_{m'_\beta} d^{j_\alpha}_{m_\alpha m'_\alpha}(\Theta)\, d^{j_\beta}_{m_\beta m'_\beta}(\Theta)\, f_{j_\alpha m'_\alpha\, ,\, j_\beta m'_\beta} \qquad (II.146)$$

Expression for overlap $<\Psi^J_o |\Psi^J_o>$ is given by (apart from normalizations N)

$$<\Psi^J_o |\Psi^J_o> = \int_o^\pi \mathrm{Sin}\Theta\, d\Theta\, d^J_{oo}(\Theta) <0| \exp\left(\frac{1}{2}\sum_{\alpha\beta} f^*_{\alpha\beta} a_\beta a_\alpha\right)$$

$$\times \exp\left(\frac{1}{2} \sum_{\alpha'\beta'} F_{\alpha'\beta'}(\Theta)\, a^\dagger_{\alpha'}, a^\dagger_{\beta'},\right) |0> \qquad (II.147)$$

$$= \exp\left(\frac{1}{2}\, \mathrm{Tr}\,[\ln(1 + M(\Theta))]\right.$$

$$= [\det\,(1 + M(\Theta))]^{1/2} \qquad (II.148)$$

where

$$M(\Theta) = F(\Theta)\, f^\dagger \qquad (II.149)$$

The general expression for the matrix elements of an irreducible tensor is given by[13]

$$\langle \Psi_o^{J'} | T_o^L | \Psi_o^J \rangle = [n^J n^{J'}]^{-1/2} [(2J+1)/8\pi^2] \begin{bmatrix} J & L & J' \\ 0 & 0 & 0 \end{bmatrix}$$

$$\times \sum_\mu \begin{bmatrix} J & L & J' \\ 0 & \mu & \mu \end{bmatrix} \int d\Omega D^{J*}_{o\mu}(\Omega) \langle \Phi_o | R(\Omega)\, T^L_\mu | \Phi_o \rangle \qquad (II.150)$$

Any matrix element can be derived[14] from equation (II.148) by differentiating with respect to $f^*$ and F. The expression

$$\langle \Phi_o | R(\Omega)\, T^L_\mu | \Phi_o \rangle = \langle 0 | \exp(\tfrac{1}{2} \sum_{\alpha\beta} F_{\alpha\beta}\, a_\beta\, a_\alpha) T^L_\mu \exp(\tfrac{1}{2} \sum_{\gamma\delta} f_{\gamma\delta}\, a^\dagger_\gamma\, a^\dagger_\delta) | 0 \rangle \qquad (II.151)$$

where

$$T^L_\mu \equiv \sum_{pq} \langle p | T^L_\mu | q \rangle a^\dagger_p\, a_q$$

then leads to the following final expression for the matrix elements of $f^{op}_{LM=0}$ :

$$\langle \Psi_o^{J_f} | f^{op}_{LM=0} | \Psi_o^{J_i} \rangle = [n^{J_f}\, n^{J_i}]^{-1/2} \int_o^{\pi/2} \sum_\mu \begin{bmatrix} J_i & L & J_f \\ -\mu & \mu & 0 \end{bmatrix} d^{J_i}_{-\mu o}(\theta) n($$

$$\{ \sum_{\tau_3} \sum_{\alpha\beta} e_{\tau_3} \langle n_\alpha l_\alpha | j_L(qr) | n_\beta l_\beta \rangle \langle \alpha | Y^L_{M'} | \beta \rangle \rho^{\tau_3}_{\alpha\beta}(\theta) \} \sin\theta\, d\theta \qquad (II.152)$$

where the density matrix is given by

$$\rho(\theta) = \frac{M(\theta)}{1 + M(\theta)} \qquad (II.153)$$

and the normalizationsare given by

$$n^J = \int_0^{\pi/2} n(\theta)\, d^J_{00}(\theta)\, \sin\theta\, d\theta; \quad n(\theta) = [\det(1+M(\theta))]^{1/2} \tag{II.154}$$

The matrix elements of the Bessel function in the oscillator basis are given by[1]

$$\langle n'l'|j_L(qr)|nl\rangle = \frac{2^L}{(2L+1)!!}\, y^{L/2} \exp(-y)((n'-1)!(n-1)!)^{1/2}$$

$$\times (\Gamma(n'+l'+\tfrac{1}{2})\,\Gamma(n+l+\tfrac{1}{2}))^{1/2}$$

$$\times \sum_{m'=0}^{n'-1} \sum_{m=0}^{n-1} \frac{(-1)^{m'+m}}{m'!m!(n'-m'-1)!(n-m-1)!}$$

$$\times \frac{\Gamma(\frac{1}{2}(l'+l+2m'+2m+L+3))}{\Gamma(m'+l'+\frac{3}{2})\Gamma(m+l+\frac{3}{2})}$$

$$\times F(\tfrac{1}{2}(L-l'-l-2m'-2m; L+\tfrac{3}{2}; y) \tag{II.155}$$

where $y = (bq/2)^2$ and F is the confluent hypergeometric function.

The expression for the reduced transition probability for electric $2^L$-pole transition, $B(EL, 0^+ \to 2^+)$, and the static quadrupole moments for the $L^+$ state, $Q_{L^+}$, are given by

$$B(EL, 0^+ \to L^+) = \frac{1}{16\pi} |\langle \Psi^L_o || Q^L || \Psi^o_o \rangle|^2 \tag{II.156}$$

and

$$Q_{L+} = \langle \Psi^{L}_{L} \mid Q^{L}_{o} \mid \Psi^{L}_{L} \rangle \qquad (II.157)$$

where

$$Q^{L}_{\mu} = \sqrt{\left[\frac{16\pi}{2L+1}\right]}\, r^{L}\, Y^{L}_{\mu}(\Omega) \qquad (II.158)$$

The expression for the reduced matrix element appearing in equation (II.156) can be obtained by replacing $j_L(qr)$ by $r^L$ in the equation (II.152).

The steps involved in the calculations are as follows: First the wave functions $\mid \Phi_o \rangle$ are obtained by carrying out the HFB (or HF-BCS) calculations. The amplitudes, $(U^m_i, V^m_i)$, and the expansion coefficients, $C^m_{ji}$, resulting from self-consistent calculations are used for computing the f matrices defined by equation (II.143). One next evaluates the matrices F, (1+M) and $M(1+M)^{-1}$ appearing in equations (II.146), (II.149) and (II.153), respectively, for twenty values of the Gaussian quadrature points in the range $(0,\pi/2)$. Finally one computes the matrix element (II.152) in terms of these quantities.

The transition charge density $\rho_L(r)$ is the reduced matrix element of $\rho^{op}_L$:

$$\rho_L(r) = \langle J_f \| \rho^{op}_L \| J_i \rangle \qquad (II.159)$$

Making use of the equations (II.44) and (II.45) and the projected HFB wave functions (II.145), we obtain the

following expression for the transition charge density:

$$\rho_L(J_i \rightarrow J_f) = (n^{J_f}\, n^{J_i})^{-1/2}\,(2J_i+1)^{-1/2} \int_0^{\pi/2} \sum_{\mu} \begin{bmatrix} J_i & L & J_f \\ -\mu & \mu & 0 \end{bmatrix} d^{J_i}_{-\mu 0}(\theta$$

$$\times\, n(\theta)\Big[ \sum_{k,\alpha,\beta} e_k\, R_{n_\alpha l_\alpha}(r)\, R_{n_\beta l_\beta}(r) \langle \alpha \,|\, Y^L_{M'} \,|\, \beta \rangle$$

$$\times [M(\theta)\,(1 + M(\theta))^{-1}]\, \sin\theta \; d\theta \qquad \text{(II.160)}$$

where $R_{nl}(r)$ is the radial part of the harmonic oscillator states $|nl\rangle$.

## REFERENCES


1. T. de Forest and Walecka, Adv. Phys. 15, 1 (1966).

2. H. Uberall, Electron Scattering From Complex Nuclei, (Academic, New York 1971).

3. C. Itzykson and J.B. Zuber, Quantum Field Theory (McGraw Hill, New York, 1980).

4. J.W. Lightbody, Jr. et al, Phys. Rev. C27, 113 (1983).

5. J. Heisenberg, in Advances in Nuclear Physics, edited by J.W. Negele and E. Vogt (Plenum, New York, 1981), Vol. 12.

6. R. Neuhausen, Nucl. Phys. A282, 125 (1977).

7. B. Dreher, et al., Nucl. Phys. A235 , 219 (1974).

8. L.J. Tassie, Austral. J. Phys. 9 (1956) 407.

9. A.L. Goodman, in Advances in Nuclear Physics, edited by J.W. Negele and E. Vogt (Plenum, New York, 1979), Vol. 11.

10. C. Bloch and A. Messiah, Nucl. Phys. 39, 95 (1962). S.B. Khadkikar and M.R. Gunye, ibid A144, 289 (1970).

11. F. Villars, in Proceedings of International School of Physics "Enrico Fermi", Course 36, edited by C. Bloch (Academic, New York, 1966).

12. N. Onishi and S. Yoshida, Nucl. Phys. A260, 226 (1966).

13. G. Ripka, in Advances in Nuclear Physics, edited by M. Baranger and E. Vogt (Plenum, New York, 1968) Vol.1.

14. J.M. Blatt, Theory of Superconductivity (Academic Press, New York, 1964).

# CHAPTER III

## FORM FACTORS AND TRANSITION CHARGE DENSITIES FOR THE QUADRUPOLE ELECTROEXCITATION OF SOME DOUBLY EVEN NUCLEI IN THE SECOND HALF OF THE 2p-1f SHELL

### III.1 Introduction

Recent inelastic electron scattering experiments have provided valuable data on the $0^+ \rightarrow 2_1^+$ as well as $0^+ \rightarrow 4_1^+$ transitions in a number of doubly even 2p-1f shell nuclei[1-5]. Within a measured momentum-transfer range upto 3 $fm^{-1}$ the observed C2 form factors are characterized by two distinct maxima appearing at $q_{eff} \sim 0.7$ and 1.6 $fm^{-1}$. The maxima of the C4 form factors occur at $q \sim 1.2$ and 2.2 $fm^{-1}$. The relative magnitude of the form factors at the two maxima is expected to provide a sensitive test of the nuclear microscopic models involved in the calculations.

In this Chapter we demonstrate that the yrast wave-functions with $J^\pi = 0^+, 2^+$ projected from the HFB intrinsic states resulting from realistic effective interactions operating in the 2p-1f shell permit a fairly satisfactory interpretation of the available data on the $2_1^+$ form factors in some doubly even Ni and Zn isotopes (with $58 \leq A \leq 68$) in the second half of the 2p-1f shell. In this context we also discuss the microscopic prescription for

calculating the transition charge densities in terms of the self-consistent projected HFB wavefunctions.

Recently Mooy and Glaudemans[6] have calculated the form factors as well as the transition charge densities for the $0^+ \rightarrow 2_1^+$ transitions in the nuclei $^{58,60,62}$Ni in terms of shell model wave functions[7] resulting from semi-empirical effective interactions operating in the restricted valence spaces involving the $[(2p_{3/2}, 1f_{5/2}, 2p_{1/2})^n + (1f_{7/2})^{-1} \ldots (2p_{3/2}, 1f_{5/2}, 2p_{1/2})^{n+1}]$ configurations. The calculations involved an independent variation of the effective charges for protons and neutrons so as to fit the $B(E2; 0^+ \rightarrow 2_1^+)$ values as well as the ratio of the form factor at the first and the second maxima for each isotope. The procedure yielded significantly mass-dependent effective charges; the values for the proton effective charge, $e_\pi$, turned out to be (2.60, 3.30, 1.85) for the nuclei $^{58,60,62}$Ni, respectively.

The available data on the reduced E2 transition probabilities in the Zn isotopes suggests enhanced rotational collectivity in these isotopes compared to that in the Ni isotopes[8,9]. It is thus desirable to have an extended shell model description of these isotopes involving more than just one $(1f_{7/2})$ hole. In view of the near-intractability of such a description – the dimensionalities of the matrices involved in the earlier shell model calculations[6] with smaller number of valence particles are already above 1000 — the available form factor data in doubly even Zn isotopes

has not been analyzed in a microscopic framework thus far.

In the present work we show that the use of $J^{\pi} = 0^{+}, 2^{+}$ states projected from the HFB wave functions generated in the full 2p-1f space leads to a fairly satisfactory unified interpretation of the available $|F|^2$ $(0^+ \rightarrow 2_1^+)$ in the nuclei $^{58,60,62}$Ni and $^{64,66,68}$Zn in terms of reasonable value of nearly mass-independent effective charges. This set of effective charges is also shown to yield excellent quantitative agreement between the calculated and the observed values of the reduced E2 transition probabilities in these nuclei.

In recent years considerable attention has been devoted to the coordinate-space reconstruction of the transition charge densities associated with the electroexcitation of nuclear levels in the framework of the Fourier-Bessel method of Dreher et al.[10]; these analyses have been carried out by Heisenberg[1] for the Ni isotopes and by Neuhausen[2] for the Zn isotopes. The empirical transition densities acquire significance vis-à-vis the test of model wave functions since they contain structural information unaffected by the accuracy of the usual plane-wave Born approximation (PWBA) for large momentum transfers. We have calculated here the transition charge densities for various Ni and Zn isotopes in terms of the projected HFB wave functions. By combining the model space transition densities resulting from the self-consistent wave functions with each of the two existing models for the core-polarization transition density we have

attempted to examine whether the empirical values point towards a preferred choice.

In Section III.2 we present some details of the calculational framework. In Section III.3 we discuss some general qualitative aspects of the electroexcitation form factors associated with the $2^+$ levels in the 2p-1f shell nuclei. In Section III.4 we discuss the form factors, transition densities as well as the E2 transition strengths for the $0^+ \rightarrow 2_1^+$ transition in some doubly even Ni and Zn isotopes. Finally Section III.5 contains some concluding remarks.

## III.2 Calculational Details

### III.2.1 Effective Interaction

In the calculations presented here we have employed as an effective interaction for the $(1f_{7/2}, 2p_{3/2}, 2p_{1/2}, 1f_{5/2})$ space a slightly modified version of the Kuo-Brown (KB) interaction[11] suggested by McGrory, Wildenthal and Halbert[12]. The KB interaction consists of the bare matrix elements derived from the phenomenological Hamada-Johnston potential and the renormalization due to the three-particle one-hole (3p-1h) excitation in the $^{40}$Ca core. Mc Grory, Wildenthal and Halbert[12] found it necessary to modify the T=1 part of the KB interaction for optimizing the agreement between the shell model and the observed spectra for the $^{42-50}$Ca nuclei. The modifications consisted of lowering the

centre-of-gravity of the $\langle(1f_{7/2})^2|V|(1f_{7/2})^2\rangle_{J,T=1}$ matrix elements by nearly 0.3 MeV, as well as raising the centre-of-gravity of the $\langle(1f_{7/2})(\ j\ )|V|(1f_{7/2})(\ j\ )\rangle_{J,T=1}$ $(j=1f_{5/2}, 2p_{3/2}, 2p_{1/2})$ matrix elements by nearly the same amount. This modified version of the KB interaction is hereafter labelled as the MWH interaction. In Appendix A we have tabulated the two-body matrix elements of the MWH interaction.

The single-particle energies characterizing the one-body part of the Hamiltonian employed in the present calculation are (in MeV) : $\varepsilon(1f_{7/2}) = 0.0$, $\varepsilon(2p_{3/2}) = 2.1$, $\varepsilon(2p_{1/2}) = 3.9$ and $\varepsilon(1f_{5/2}) = 6.5$.

III.2.2 The Choice of Intrinsic States

For calculating $0^+ \rightarrow 2_1^+$ form factors in various 2p-1f shell nuclei, we have obtained the axially symmetric intrinsic states by following three different methods — the HFB method for the nuclei $^{58,60}$Ni, the deformed HF-BCS method for the nuclei $^{62}$Ni and $^{64}$Zn and the usual deformed HF method for the nuclei $^{66,68}$Zn. The HFB and HF-BCS methods are discussed in Section II.4. Pairing correlations between only the like particles are allowed in our HFB and HF-BCS calculations. The choice of the intrinsic state for a particular nucleus has been dictated by the following considerations. It is seen that the inclusion of pairing correlations (in the HFB framework) results in nearly spherical

intrinsic states in nuclei having either N=28 or N $\geq$ 34. This is related to the fact that the usual HFB method does not permit a treatment of the deformation and pairing degrees of freedom on the same footing because of the subshell closure at N=28 and the approaching shell closure at N=40; it tends to emphasize the latter degree of freedom. The HFB intrinsic states for the nuclei with N=28 or N $\geq$ 34 therefore yield vanishingly small ( < 10%) amplitudes for the yrast states with J $\geq$ 2. These HFB intrinsic states are inappropriate vis-à-vis the present calculation which requires, as an essential prerequisite, a reasonably satisfactory simultaneous description of the $J^{\pi} = 0^{+}$, $2^{+}$ and $4^{+}$ states. The HF-BCS intrinsic states for the nuclei $^{62}$Ni and $^{64}$Zn, and the HF intrinsic states for the nuclei $^{66,68}$Zn contain $J^{\pi} = 2^{+},4^{+}$ states with sizable ( > 10%) amplitudes.

## III.3 Qualitative Features Associated with the Form Factors for the $0^{+} \rightarrow 2_{1}^{+}$ Transitions in the 2p-1f Shell Nuclei

In view of the relation (II.152) we expect the matrix elements $< f|j_2(qr)|f >$ and $< f|j_2(qr)|p >$ to play important roles vis-à-vis the observed squared form factors. The gross qualitative features of the appearance of two maxima at $q \sim 0.7$ fm$^{-1}$ and $q \sim 1.7$ fm$^{-1}$ can be understood in terms of the q-dependence of these matrix elements. We assume here that the effective charges do not have significant effect

on the q-dependence of these matrix elements. Figure III.1 shows that the matrix element $|\langle f|j_2(qr)|f\rangle|$ possesses maxima at $q \sim 0.8$ fm$^{-1}$ and $q \sim 1.9$ fm$^{-1}$, and the maxima of the matrix elements $|\langle f|j_2(qr)|p\rangle|$ occur at $q \sim 0.7$ fm$^{-1}$ and $q \sim 1.6$ fm$^{-1}$. The zeros of the matrix elements $\langle f|j_2(qr)|f\rangle$ and $\langle f|j_2(qr)|p\rangle$ are at $q \sim 1.6$ fm$^{-1}$ and $q \sim 1.2$ fm$^{-1}$, respectively. Since the expression for form factors involves a linear combination of the matrix elements $\langle f|j_2(qr)|f\rangle$ and $\langle f|j_2(qr)|p\rangle$, we expect the maxima of the form factor to occur in the ranges $q = (0.7, 0.8)$ fm$^{-1}$ and $q = (1.6, 1.9)$ fm$^{-1}$. Similarly, we also expect the form factors to display a zero in the range $q = (1.2, 1.6)$ fm$^{-1}$. These qualitative features of the form factors are consistent with the characteristics of the observed form factors in various 2p-1f shell nuclei.

## III.4 The $0^+ \rightarrow 2_1^+$ Transition in the Nuclei $^{58,60,62}$Ni and $^{64,66,68}$Zn

### III.4.1 Form Factors

We first discuss here the Ni isotopes. The squared form factors $|F(q)|^2$ $(0^+ \rightarrow 2_1^+)$ in these isotopes are calculated and compared with the experiments[1] in Figure III.2. The form factors have been computed with the effective charges $e_\pi = 1.8$ for protons and $e_\nu = 0.8$ for neutrons. As discussed later, it is seen that this set of effective charges is quite consistent with the available $B(E2; 0^+ \rightarrow 2_1^+)$

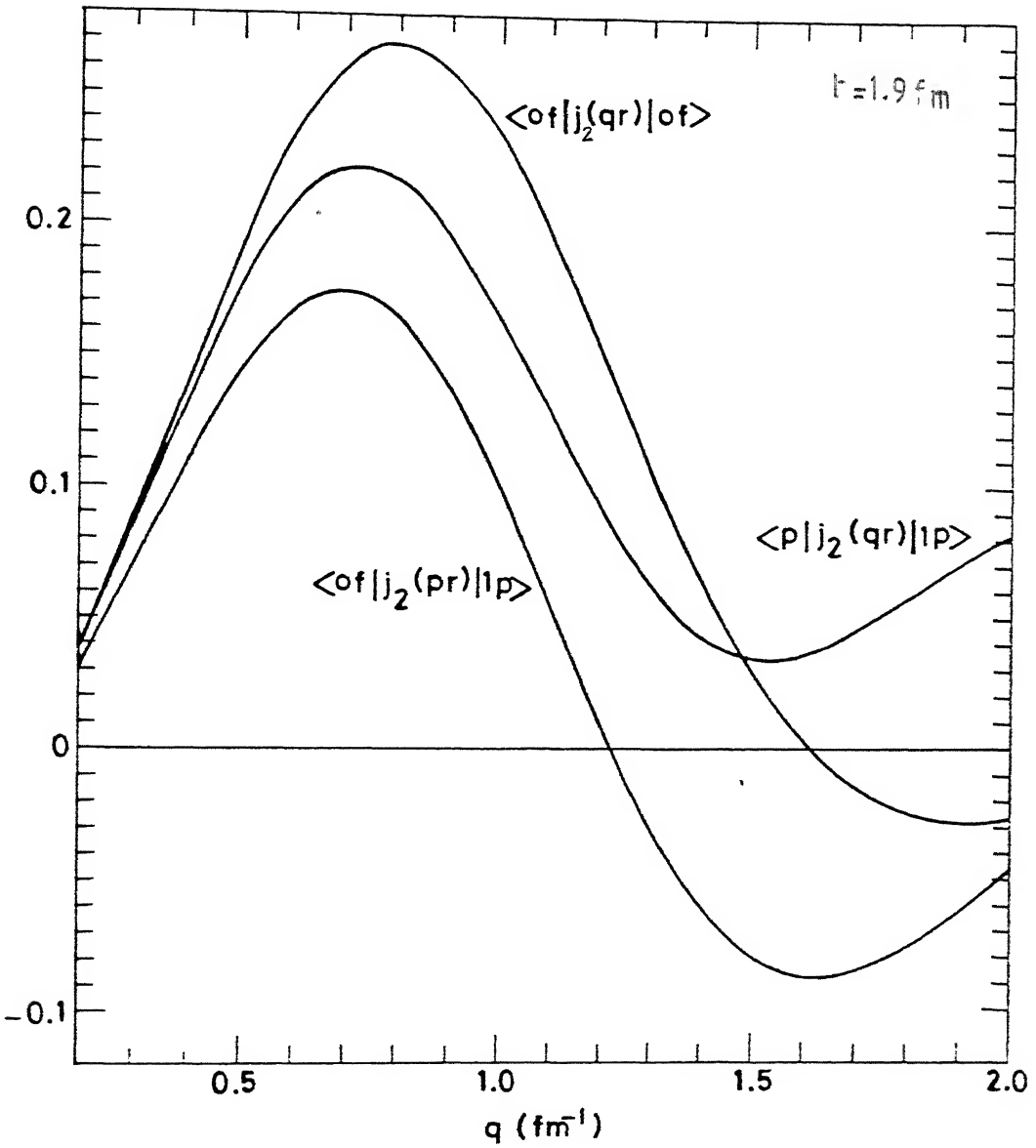


FIG.III.1 THE MOMENTUM-TRANSFER DEPENDENCE OF THE MATRIX ELEMENTS OF $j_2(qr)$ IN THE OSCILLATOR BASIS.

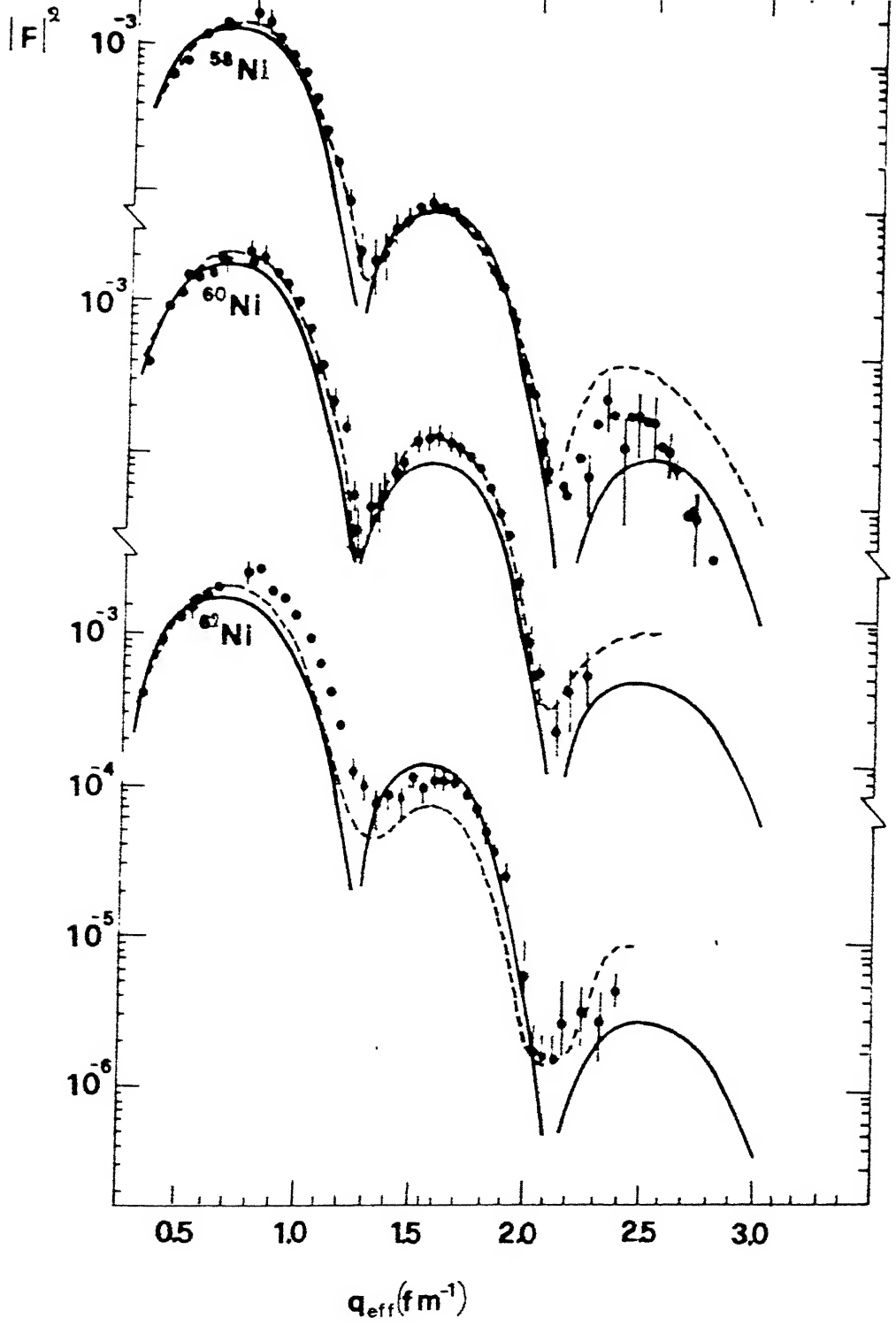


FIG. III.2 EXPERIMENTAL AND CALCULATED SQUARED FORM FACTORS $|F|^2$ FOR THE $0^+ \rightarrow 2^+$ TRANSITIONS IN THE NUCLEI $^{58,60,62}$Ni. THE SOLID CURVES SHOW THE RESULTS OBTAINED WITH THE SELF-CONSISTENT WAVE FUNCTIONS. THE BROKEN CURVES DISPLAY THE RESULTS OBTAINED IN THE RECENT SHELL MODEL CALCULATION INVOLVING RESTRICTED CONFIGURATION MIXING.

values in these isotopes.

Overall, it is seen that the agreement between the calculated and the observed form factors is remarkably good throughout the momentum-transfer range q = 0.5-2.8 $fm^{-1}$. The degree of quantitative agreement in the nuclei $^{58,60}Ni$ is quite satisfying, particularly in view of the fact that the effective charges were not fine-tuned for each isotope.

A significant discrepancy occurs in the case of the nucleus $^{62}Ni$ where the present calculation underestimates the form factors for the range q = 0.8 - 1.2 $fm^{-1}$ by about 30 percent. This may be due to the non-inclusion of the $1g_{9/2}$ orbit in the valence space. As pointed out by Delphini and Glaudemans[13] as well as Potbhare et al.[14], the $1g_{9/2}$ orbit is expected to play an important role vis-à-vis the structure of the yrast levels in Ni isotopes with A $\geq$ 60. However, the non-availability of the core-renormalized effective interactions for the ($1f_{7/2}$, $2p_{3/2}$, $2p_{1/2}$, $1f_{5/2}$, $1g_{9/2}$) space has prevented us from examining here the explicit role of the $1g_{9/2}$ orbit.

We have also presented in Figure III.2 the results obtained by Mooy and Glaudemans[6] in the framework of the shell model involving the $[(2p_{3/2}, 2p_{1/2}, 1f_{5/2})^{n} + (1f_{7/2})^{-1} (2p_{3/2}, 2p_{1/2}, 1f_{5/2})^{n+1}]$ configurations. These calculations employed the effective charges ($e_{\pi}$, $e_{\nu}$) = (2.60, 0.72), (3.30, 0.50) and (1.85, 0.82) for the nuclei $^{58,60,62}Ni$, respectively.

Considering first the momentum-transfer range $0.5 < q < 2.1$ fm$^{-1}$, we find that the projected HFB and the shell model estimates are quite close except around the second maximum ($q \sim 1.6$ fm$^{-1}$) in the nucleus $^{62}$Ni, where the latter are smaller by roughly a factor of two. For larger momentum-transfers the shell model estimates are an order of magnitude larger — a feature that emphasizes the desirability of precise form factor data for $q > 2.1$ fm$^{-1}$ in the nuclei $^{60,62}$Ni.

It is interesting to note that the proton effective charges employed in the shell model calculations in the nuclei $^{58,60}$Ni are considerably larger than the A-independent value ($e_\pi = 1.8$) employed in the present work. This can be qualitatively understood in the following manner. The shell model value of the proton effective charge simulates partly the effects due to the excitations involving two or more $1f_{7/2}$ -protons. Since the proton-neutron interactions are strongest for orbits with large spatial overlap, such processes are expected to be favoured in the nuclei $^{58,60}$Ni, where the energy-difference between the proton and neutron Fermi surfaces is not very large[15]. In heavier nuclei ($A \geq 62$) with larger neutron-excess, the amplitude of proton excitations leading to correlated proton-neutron configurations is expected to decrease due to larger gap between the proton and neutron Fermi surfaces.

Figure III.3 presents a comparison of the calculated and the experimental[2] $|F(q)|^2$ values for the $0^+ \rightarrow 2_1^+$ transitions in the nuclei $^{64,66,68}Zn$. These form factors have earlier been analyzed with phenomenological models — the modified Tassie model[16] and the Gaussian model[17]. The best-fit calculations carried out in the framework of the latter model have also been shown here.

As in the case of the Ni isotopes, the present form factor calculations for the Zn isotopes also employ effective charges such that the isovector effective charge, defined by $(e_\pi - e_\nu)$, is always 1e. However, it turns out that a reasonable variation of the isoscalar effective charge — with $e_\nu = (0.75, 0.55, 0.75)$ for the nuclei $^{64,66,68}Zn$ respectively — is required for optimizing the agreement with the available $B(E2; 0^+ \rightarrow 2_1^+)$ values. With these effective charges, the form factors for $q < 1.2$ fm$^{-1}$ computed with the self-consistent wave functions are also in excellent agreement with the experiments[2]. We notice, however, systematic discrepancies between the calculated and observed form factors for $q > 1.2$ fm$^{-1}$. The calculated form factors for $q \sim 1.5$ fm$^{-1}$ are smaller by about 40 percent than the observed ones, and the second maxima of the theoretical form factors display small but noticeable shift towards higher momentum-transfer. These discrepancies may again be reflecting the necessity of explicit involvement of $^{40}Ca$ core-excitations as well as the $1g_{9/2}$ -excited configurations.

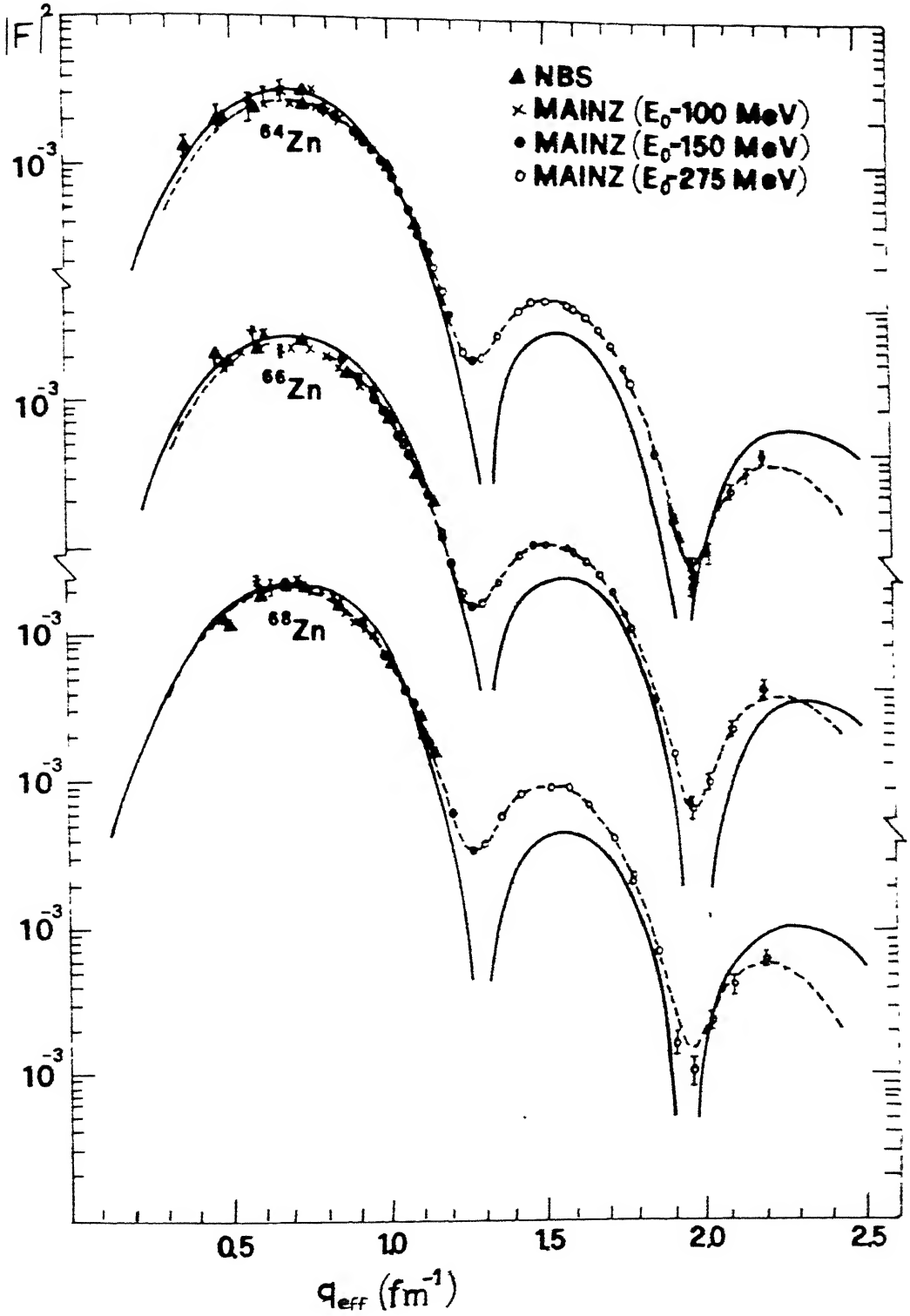


FIG.III.3 EXPERIMENTAL AND CALCULATED FORM FACTORS FOR THE $0^+ \rightarrow 2^+$ TRANSITIONS IN THE NUCLEI $^{64,66,68}Zn$. THE BROKEN CURVES REPRESENT THE BEST-FIT CALCULATIONS WITH THE FOURIER-BESSEL EXPANSION OF THE TRANSITION CHARGE DENSITIES.

Present calculations reveal (see the second column of Table III.1) that the total intrinsic quadrupole moments for the Zn isotopes are substantially larger than the ones obtained for the lighter Ni isotopes. This onset of sizable oblate deformation may signal enhanced $1g_{9/2}$ occupation via a lowering of the (downsloping) Nilsson orbitals with $k = \pm 9/2$.

As discussed later, the apparent inadequacy of the effective charges to simulate the excitations from the core into model space - or out of model space into higher orbits - in the context of large momentum-transfer data manifests itself in the form of discrepancies between the calculated and the empirical transition densities in the interior region ($r < 3$ fm).

### III.4.2 The Reduced Transition Probabilities, $B(E2; 0^+ \rightarrow 2_1^+)$ and the Static Quadrupole Moments, $Q(2_1^+)$

In Table III.1 and Figure III.4 we have presented the results for the static quadrupole moments, $Q(2_1^+)$, as well as the reduced transition probabilities, $B(E2; 0^+ \rightarrow 2_1^+)$ in the nuclei $^{58,60,62}$Ni and $^{64,66,68}$Zn. The $Q(2_1^+)$ and the $B(E2)$ values have been computed with the effective charges employed in the calculation of the form factors for various isotopes discussed in the preceding section. The calculated $B(E2; 0^+ \rightarrow 2_1^+)$ values are seen to be in excellent agreement

## TABLE III.1

The $Q(2_1^+)$ and $B(E2;\ 0^+ \rightarrow 2_1^+)$ values (labelled PHFB) in the nuclei $^{58,60,62}Ni$ and $^{64,66,68}Zn$ calculated with the set of effective charges employed in the form factor calculations. The $B(E2;\ 0^+ \rightarrow 2_1^+)$ values are in units of $(e^2.fm^4)$ and the $Q(2_1^+)$ values have been given in units of $(e.fm^2)$. Here $<Q_o^2>_\pi$ ($<Q_o^2>_\nu$) gives the contribution of the valence protons (neutrons) to the intrinsic state

| Nucleus | $<Q_o^2>$ $[<Q_o^2>_\pi, <Q_o^2>_\nu]$ | $(e_\pi, e_\nu)$ | $B(E2;\ 0^+ \rightarrow 2_1^+)$ | | $Q(2_1^+)$ | |
|---|---|---|---|---|---|---|
| | | | PHFB | EXP | PHFB | EXP |
| $^{58}Ni$ | $-3.4$ $[-1.1, -2.3]$ | (1.80,0.80) | 647 | $668\pm70$[a] | 2.8 | $-15\pm8$[c] |
| $^{60}Ni$ | $-12.5$ $[-3.9, -8.6]$ | (1.80,0.80) | 846 | $909\pm70$[a] | 16.1 | $3\pm7$[c] |
| $^{62}Ni$ | $-13.1$ $[-5.3, -7.8]$ | (1.80,0.80) | 970 | $876\pm75$[a] | 21.3 | $5\pm12$[c] |
| $^{64}Zn$ | $-20.3$ $[-10.1, -10.2]$ | (1.75,0.75) | 1610 | $1580\pm50$[b] | 31.8 | - |
| $^{66}Zn$ | $-24.6$ $[-13.5, -11.1]$ | (1.55, 0.55) | 1457 | $1370\pm50$[b] | 34.3 | - |
| $^{68}Zn$ | $-18.2$ $[-9.8, -8.4]$ | (1.75,0.75) | 1210 | $1360\pm60$[b] | 29.9 | - |

[a]Reference 8 ; [b]Reference 9; [c]Reference 18.

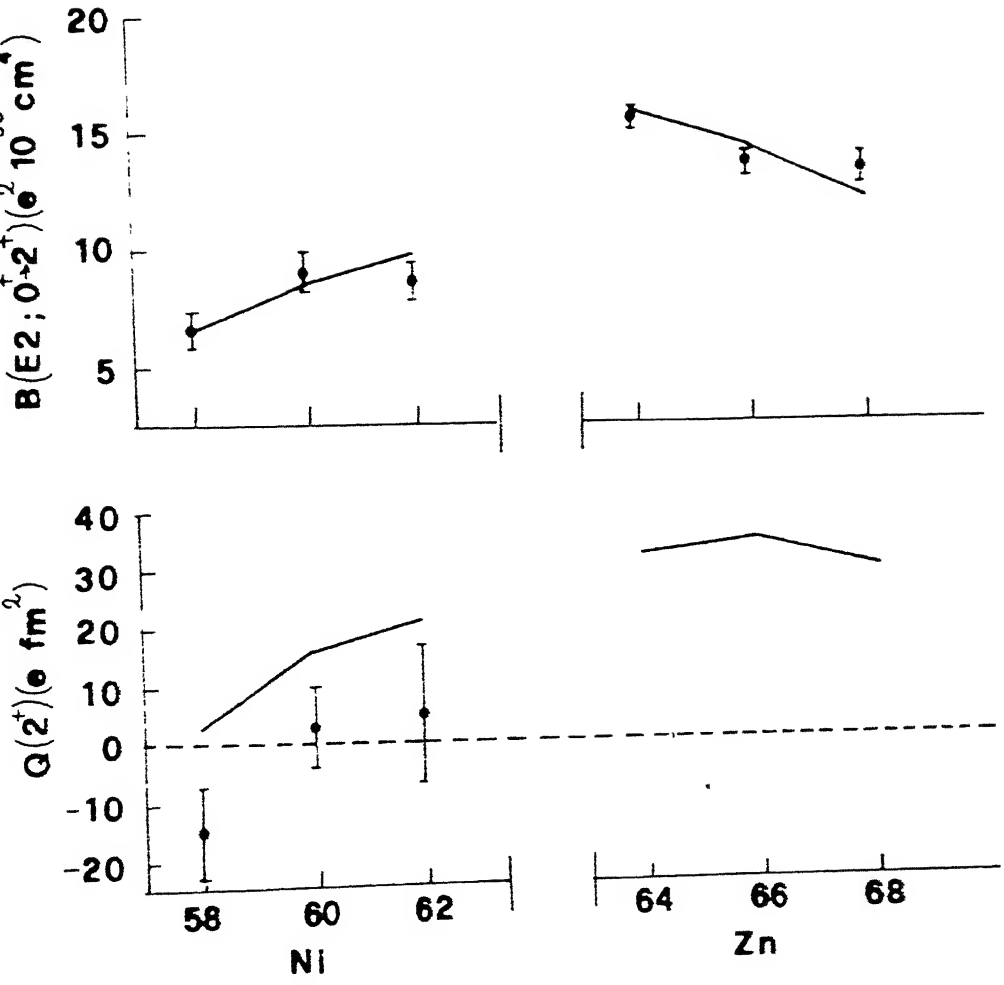


FIG.III.4 GRAPHICAL PRESENTATION OF THE RESULTS FOR ELECTRIC QUADRUPOLE TRANSITION PROBABILITIES AND STATIC QUADRUPOLE MOMENTS IN SOME DOUBLY EVEN Ni AND Zn ISOTOPES. THE STRAIGHT LINES JOIN THE POINTS CALCULATED WITH THE EFFECTIVE CHARGES EMPLOYED IN THE FORM FACTOR CALCULATIONS.

with the experiments[18]; the only noticeable discrepancy occurs in the case of the nucleus $^{68}$Zn where the present calculation underestimates the lower bound of the observed value by about 6.6 percent.

The usefulness of the available $Q(2_1^+)$ values - and these are just three in number - vis-à-vis a test of the present microscopic description is severely constrained by the large error bars arising due to the uncertainties associated with the effects of higher excited states in the Coulomb excitation processes. The calculated values are, however, qualitatively consistent with the available data; in particular, the latter seem to support our prediction of oblate intrinsic shapes in the nuclei $^{60,62}$Ni.

### III.4.3 Transition Charge Densities

In the preceding sections we have seen that the introduction of the state- and (nearly) mass-independent effective charges for the valence particles is on the whole quite adequate in most of the cases for describing the observed B(E2) values and the form factors. The effective charge model implicitly assumes that the contributions arising from the core-polarizations or the extra-model-space components are proportional to the valence space contributions. A more realistic model involves the mixing of the zeroth-order valence wave function with the $2^L$-pole, $n\hbar\omega$ giant resonances; this description is consistent with the use of

the separable, multipole-multipole interaction in conjunction with the first-order perturbation theory. In view of the expected sensitivity of the transition densities towards the details of the radial characteristics of various parts of wave functions, we have also considered here this prescription for invoking core-polarization by assuming the Tassie model[16] for the $2^L$-pole excitations. The total transition density is constructed as the sum of two terms - the valence-space term A(r) with isoscalar effective charge set to zero, and the Tassie core-polarization transition density term B(r) (Ref. 19):

$$\rho(r) = A(r) + N\ B(r) \qquad \text{(III.1)}$$

when B(r) is related to the ground state charge densities $\rho_{gs}(r)$ by the relation[2,6]

$$B(r) = r^{L-1}\ \frac{d}{dr}\rho_{gs}(r) \qquad \text{(III.2)}$$

The normalization constant N is obtained by requiring overall consistency with the usual effective charge model; we adjust N so that the total charge resulting from an integration of $\rho(r)$ is just $e_\pi$ .

In Figure III.5 we present the transition charge densities for Ni isotopes calculated by combining the projected HFB predictions with one or the other of the two models for the core-polarization component. We have compared our results with the empirical transition densities extracted from the

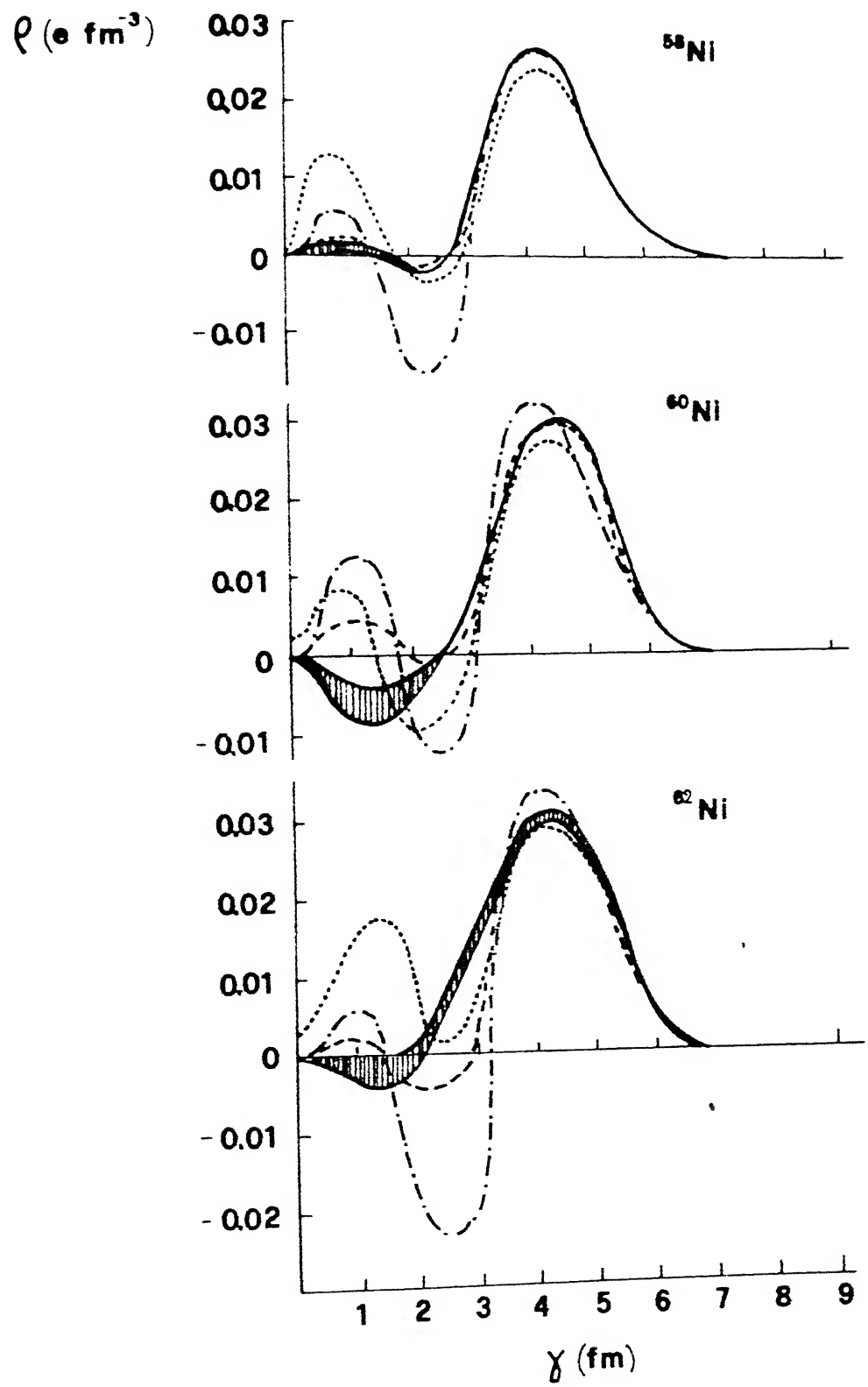


FIG.III.5 TRANSITION CHARGE DENSITIES FOR THE FIRST $2^+$ STATE IN $^{58,60,62}Ni$ CALCULATED WITH THE EFFECTIVE CHARGE MODEL (DOT-DASHED LINE) AND WITH THE TASSIE MODEL (DASHED LINE). THE EMPIRICAL CHARGE DENSITIES HAVE BEEN SHOWN IN THE FORM OF AN ERROR BAND. THE DOTTED CURVE REPRESENTS THE SHELL MODEL RESULTS.

available form factor data in the framework of Fourier-Bessel method by Heisenberg[1]. It is seen that in the region 3 fm < r < 8 fm the predictions of the effective charge ( dot-dashed line) and the Tassie prescriptions ( dashed line) do not differ significantly. Whereas the latter prescription yields transition densities in excellent agreement with the empirical ones, the estimates involving the A-independent effective charges display only, minor discrepancies in $^{60,62}$Ni. In the interior region ( 0 < r < 3 fm), however, the Tassie model for core-polarization provides vastly improved description of the transition densities, in keen contrast with the effective charge model estimates which show large oscillations. The effective charge model emphasizes the role of the underlying valence orbits. On the other hand, the collective contributions inherent in the Tassie model reduce considerably the single-particle features of the valence part.

We have also displayed in Figure III.5 the shell model results for transition densities obtained by Mooy and Glaudemans[6] with the effective charge prescription for the core-polarization. The results are in qualitative agreement with the projected HFB estimates involving the effective charges. The quantitative differences arise from the enhanced $(1f_{7/2} \rightarrow 1f_{5/2})^{\nu}$ and $(1f_{7/2} \rightarrow 2p_{3/2})^{\pi}$ transitions allowed in the present calculations. As pointed out by Mooy and Glaudemans[6], these transitions govern to a large extent the

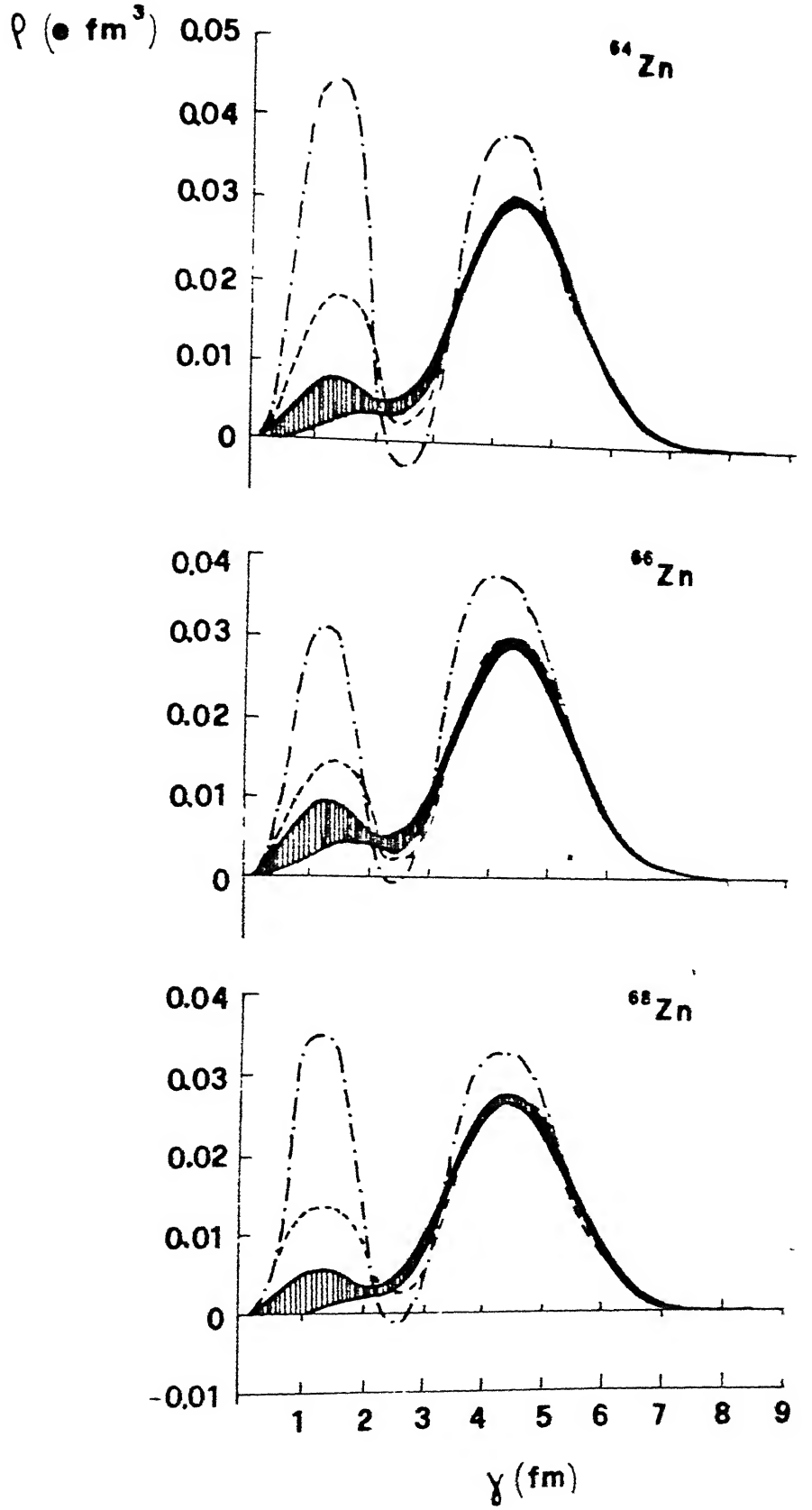


FIG. III.6 THE EMPIRICAL TRANSITION DENSITIES (ERROR BAND) AND THE THEORETICAL PREDICTIONS INVOLVING THE EFFECTIVE CHARGE MODEL (DOT-DASHED LINES) AS WELL AS THE TASSIE MODEL (DOTTED LINES).

first maximum at r ~ 1 fm and the first minimum at r ~ 2.5 fm in the valence part of the transition densities.

In Figure III.6 we have presented a comparison of the projected HFB results for the transition densities in the nuclei $^{64,66,68}$Zn with the empirical values extracted from the form factor data by Neuhausen[2]. Here again we find that the Tassie prescription for the core participation permits a significantly improved description of the empirical transition densities.

## III.5 Conclusions

We have discussed here the calculation of the form factors associated with the electroexcitation of the $2_1^+$ levels in some doubly even Ni and Zn isotopes. The B(E2) values as well as the transition charge densities for the $0^+ \rightarrow 2_1^+$ transition have also been calculated. It turns out that the projected HFB ansatz for the wave functions in conjunction with the realistic 2p-1f shell effective interactions provides a nearly parameter-free framework for interpreting and correlating the available data in a microscopic perspective. The calculations discussed here also demonstrate that the projected HFB technique is equally efficacious for the nuclei in the first- as well as the second-half of the 2p-1f shell[20].

Present calculations have revealed significant discrepancies vis-à-vis the large momentum-transfer ($q > 2.0$ fm$^{-1}$) form factor data — and the related transition densities data for the interior region ($r < 3$) — in some cases. An explicit inclusion of the $^{40}$Ca core-excitations as well as $(1g_{9/2})^{\nu}$ configurations may lead to an improved description of the form factors and the transition densities, apart from reducing considerably the quantitative significance of the choice of a model for "effective charge" contributions.

## REFERENCES


1. J. Heisenberg, in Advances in Nuclear Physics, edited by J.W. Negele and E. Vogt (Plenum, New York, 1981), Vol. 12.

2. R. Neuhausen, Nucl. Phys. A282, 125 (1977).

3. K. Hayakawa et al., Res. Rep. Nucl. Sc. (Tohoku University) 11, 1 (1978).

4. J.W. Lightbody, Jr. et al., Phys. Rev. C27, 113 (1983).

5. Y. Torizuka et al., Phys. Rev. 185, 1499 (1969).

6. R.B.M. Mooy and P.W.M. Glaudemans, Nucl. Phys. A438, 461 (1985).

7. R.B.M. Mooy and P.W.M. Glaudemans, Z. Phys. A312, 59 (1983).

8. P.M. Endt, Atomic and Nuclear Data Tables 23, 547 (1979).

9. J.F. Bruandet et al., in Proceedings of the EPS International Conference, Florence (Italy) 1977, edited by P. Blasi and R.A. Ricci (Editrice Compositori, Bologna, 1978), p. 535.

10. B. Dreher et al., Nucl. Phys. A235, 219 (1974); H. Rothaas, J. Friedrich, K. Merle and B. Dreher, Phys. Lett. 51B, 23 (1974).

11. T.T.S. Kuo and G.E. Brown, Nucl. Phys. A114, 241 (1968).

12. J.B. McGrory, B.H. Wildenthal and E.C. Halbert, Phys. Rev. C2, 186 (1970).

13. M.G. Delphini and P.W.M. Glaudemans, Z. Phys. A317, 357 (1984).

14. V. Potbhare, S.K. Sharma and S.P. Pandya, Phys. Rev. C24, 2355 (1981).

15. B. Ghosh and S.K. Sharma, Phys. Rev. C29, 648 (1984).

16. L.J. Tassie, Australian J. Phys. 9, 407 (1956).

17. H. Überall, Electron Scattering From Complex Nuclei (Academic, New York, 1971).

18. A. Christy and O. Häusser, Nucl. Data Tables 11, 281 (1972).

19. B.A. Brown, R. Radhi and B.H. Wildenthal, Phys. Rep. 101, 313 (1983).

20. G. Mukherjee and S.K. Sharma, Phys. Rev. C29, 2101 (1984); C31, 689 (1985).

# CHAPTER IV

## FORM FACTORS AND TRANSITION CHARGE DENSITIES ASSOCIATED WITH THE ELECTROEXCITATION OF THE YRAST LEVELS WITH $J^{\pi} = 4^{+}$ IN SOME 2p-1f SHELL NUCLEI

### IV.1 Introduction

In the context of a general discussion of the shape-collective aspects of nuclear dynamics, a study of the electric hexadecupole matrix elements is a logical extension of the studies involving the electric quadrupole operator. The non-availability of the $B(E4; 0^{+} \rightarrow 4^{+})$ values has, however, hindered progress on this topic in light- and medium-mass nuclei; the E4 decay branches are unmeasurably small with respect to the competing E2 branches.

A number of recent experiments[1-3] have yielded important information involving electroexcitation form factors covering a broad momentum-transfer range, with $q = 0.5\text{-}3.0\ fm^{-1}$, for the $0^{+} \rightarrow 4^{+}$ transitions. Apart from providing an estimate of the heretofore unmeasured E4 transition probabilities via an extension of the data into the momentum-transfer of the photon point, $q = E_{4^{+}} - E_{0^{+}}$, the measured form factors are also expected to be extremely useful in the context of the test of various microscopic models of the yrast $J^{\pi} = 4^{+}$ state.

In this chapter we discuss the calculation of the $|F|^2$ $(0^+ \rightarrow 4^+)$ values in the nuclei $^{48,50}Ti$, $^{50,52,54}Cr$, $^{54}Fe$ and $^{60}Ni$ with a view to test the efficacy of the projected HFB description vis-à-vis the recently-measured data. The recent work of Mooy and Glaudemans[4] has revealed that a restricted shell model description of the $(0^+ \rightarrow 4^+)$ form factors in the nuclei $^{52}Cr$, $^{54}Fe$ and $^{60}Ni$ requires highly mass-dependent effective charges which are also drastically different from the set required for a reasonable quantitative agreement with the observed $(0^+ \rightarrow 2^+)$ form factors in these nuclei; the values $[e_\pi(0^+ \rightarrow 2^+), e_\pi(0^+ \rightarrow 4^+)]$ required to optimize the fit to the observed data are [1.33, 2.06], [1.42, 1.76] and [3.33, 1.54] for the isotopes $^{52}Cr$, $^{54}Fe$ and $^{60}Ni$ respectively. In this context we find that the HFB description for the $J^\pi = 4^+$ states in the Ti, Cr, Fe and Ni isotopes not only obviates the necessity of invoking significant mass-dependence, it also permits a good quantitative discussion of the $(0^+ \rightarrow 4^+)$ form factors in terms of effective charges quite close to the ones required for a comparable fit to the $(0^+ \rightarrow 2^+)$ data in these nuclei. The calculations discussed here have also been carried out employing the MWH interaction described in the preceding Chapter.

In Section IV.2 we discuss some qualitative features associated with the $0^+ \rightarrow 4^+$ transitions in the 2p-1f shell nuclei. In Section IV.3 we discuss the $0^+ \rightarrow 4^+$ transition in

the 2p-1f shell nuclei with N or Z = 28. The hexadecupole electroexcitation of the 2p-1f shell nuclei with open proton and neutron shells is next discussed in the Section IV.4. In view of the recent revival of interest in the $B(E4; 0^+ \rightarrow 4^+)$ values due to the availability of the $|F|^2$ $(0^+ \rightarrow 4^+)$ values, one is prompted to ask if the usual Bohr and Mottelson (BM) prescription for relating the $B(E2; 0^+ \rightarrow 2^+)$ values and the intrinsic quadrupole moments could also be extended to the hexadecupole operator. In Section IV.5 we demonstrate the quantitative as well as qualitative unreliability of the BM prescription vis-à-vis the hexadecupole operator by carrying out Hartree-Fock-Bogoliubov calculations followed by explicit angular momentum projection for a number of 2p-1f shell nuclei. Section IV.6 contains some concluding remarks.

## IV.2 Qualitative Features Associated with the $0^+ \rightarrow 4^+$ Transitions in the 2p-1f Shell Nuclei

The qualitative aspects of the $0^+ \rightarrow 4^+$ form factors in the 2p-1f shell nuclei are mainly governed by the two radial matrix elements $\langle 1f|\, j_4(qr)\,|1f\rangle$ and $\langle 1f|\, j_4(qr)\,|2p\rangle$, if we assume that the q-dependence of these matrix elements is not significantly changed by the $^{40}Ca$ core-polarization processes. It turns out that (see Fig. IV.1) whereas the matrix element $\langle 1f|\, j_4(qr)\,|1f\rangle$ possesses just one maximum at $q \sim 1.2$ fm$^{-1}$, the matrix element $\langle 1f|\, j_4(qr)\,|2p\rangle$ possesses a maximum at $q \sim 1.1$ fm$^{-1}$ followed by a minimum at $q \sim 2.2$ fm$^{-1}$.

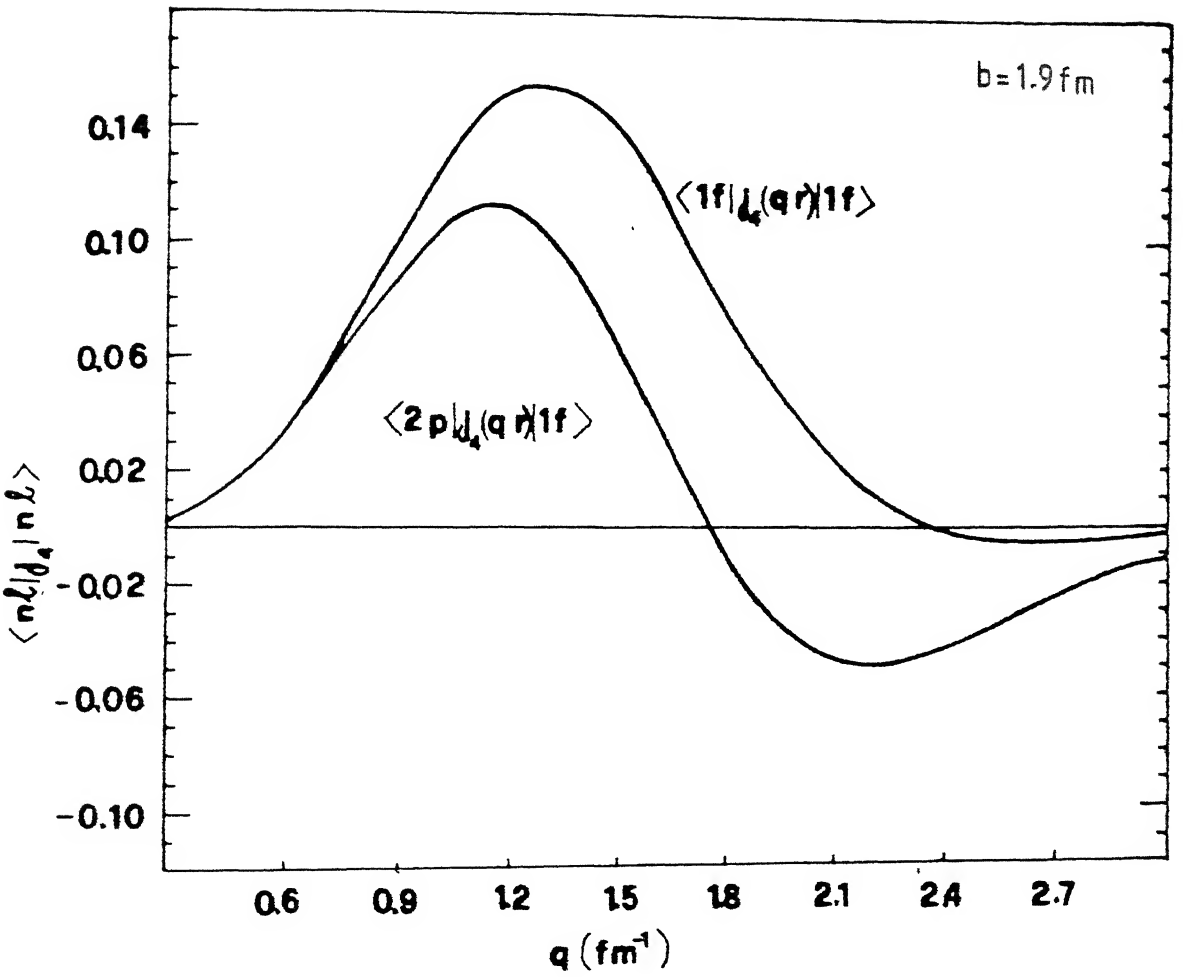


FIG. IV.1 THE MOMENTUM-TRANSFER DEPENDENCE OF THE MATRIX ELEMENTS $\langle nl|j_4(qr)|n'l'\rangle$ IN THE 2p-1f SHELL.

The zeros of the matrix elements $<1f|j_4(qr)|2p>$ and $<1f|j_4(qr)|1f>$ occur at $q \sim 1.8$ and $2.4\ fm^{-1}$, respectively. Since the description of $F(q)$ in the projected HFB framework involves a linear combination of the matrix elements $<1f|j_4(qr)|1f>$ and $<1f|j_4(qr)|2p>$, it is expected to display the following general features:

(i) In view of the proximity of the maxima of the two matrix elements, we do not expect significant A-dependence in the position of the first maximum. This feature is strikingly reflected in the observed data[1-3]; the first maximum appears at practically the same position — at $q \sim 1.2\ fm^{-1}$ — in various nuclei.

(ii) We do not anticipate the occurrence of the second maximum in nuclei with structure dominated by the $(1f_{7/2})^n$ configurations for protons as well as neutrons, since, in such cases, the form factor is governed by only the matrix element $<1f|j_4(qr)|1f>$.

(iii) In the deformed 2p-1f shell nuclei, the $2p_{3/2}$ orbit is also expected to play an important role. The magnitude of $|F(q)|^2$ at the second maximum as well as the location of this maximum is, therefore, expected to display considerable variation over the range $q = 1.8 - 2.5\ fm^{-1}$, depending on the relative importance of the matrix element $<1f|j_4(qr)|2p>$.

## IV.3 Hexadecupole Electroexcitation in the 2p-1f Shell Nuclei with N or Z = 28

### IV.3.1 Form Factors

The squared form factors for the $0^+ \rightarrow 4^+$ transitions in the nuclei $^{50}Ti$, $^{52}Cr$, $^{54}Fe$ and $^{60}Ni$ are calculated and compared with the experiments[1-3] in Fig. IV.2. In the calculations reported in this and the next section, we have employed the mass-independent set of effective charges $(e_\pi, e_\nu) = (1.5, 0.5)$ for the nuclei $^{48,50}Ti$ and $^{50,52,54}Cr$. In the case of the nuclei $^{54}Fe$ and $^{60}Ni$, the values employed are (1.7, 0.7) and (1.8, 0.8), respectively.

From the results presented in Figure IV.2 one finds that the calculated form factors are in very good quantitative agreement with the experiments[2]. In the case of the nucleus $^{52}Cr$ present calculation predicts correctly the position as well as the magnitude of the second maximum.

It is seen that a lack of enough reliable data points for $q < 1.0$ fm$^{-1}$ prevents a detailed test of the calculated results. The importance of the low-q data for the $0^+ \rightarrow 4^+$ transitions is further emphasized by the fact that the experimental values for $B(E4; 0^+ \rightarrow 4^+)$ — and these are the limits of the relevant form factors as q approaches zero — are not available for testing the microscopic description. This contrasts keenly with the situation in the case of the $0^+ \rightarrow 2^+$ transitions; in these cases the $|F(q)|^2$ estimates for $q < 1$ are usually supplemented by the $B(E2)$ values deduced from the measured $2^+$ half lives.

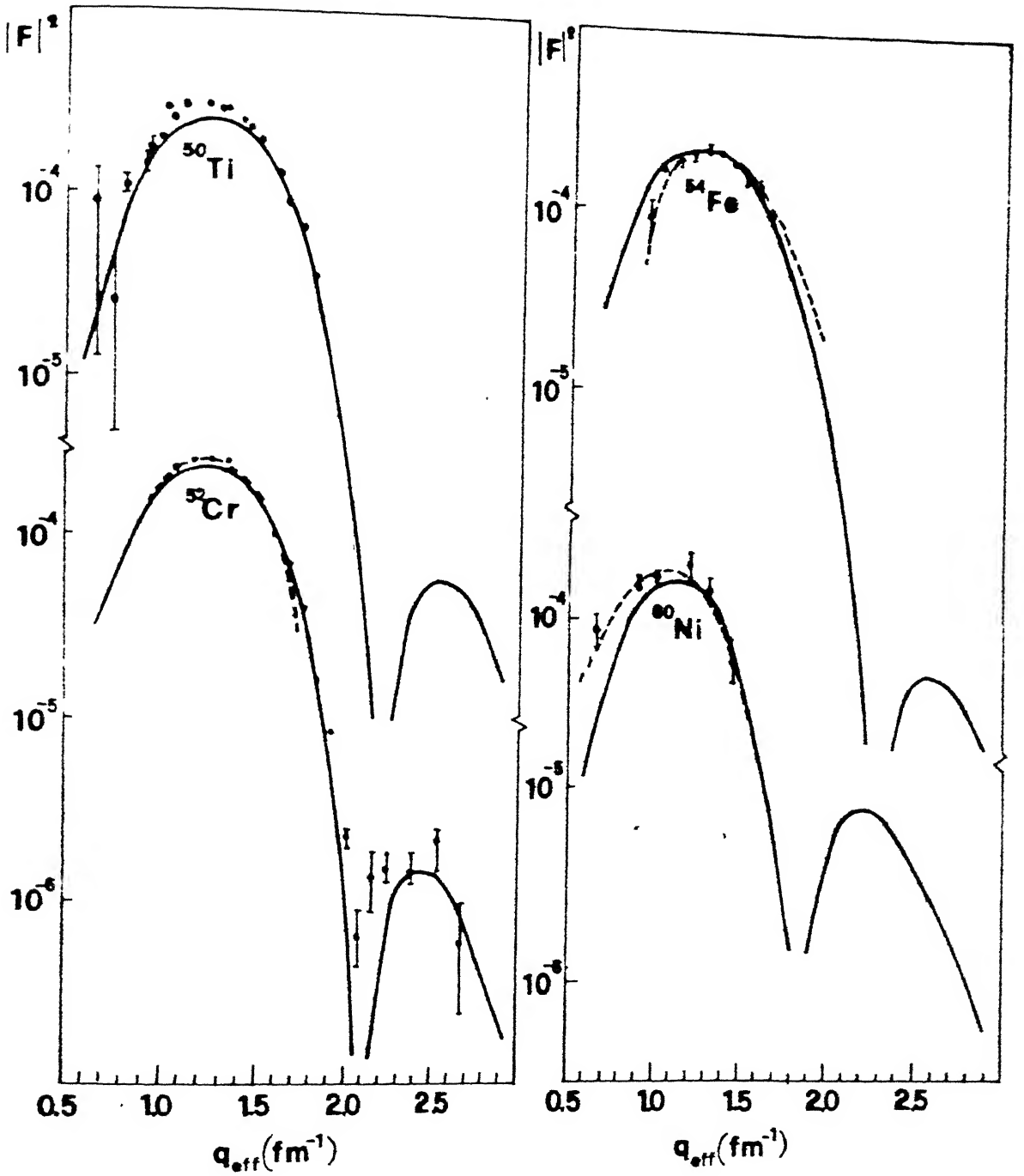


FIG.IV.2 EXPERIMENTAL AND CALCULATED SQUARED FORM FACTORS $|F|^2$ FOR THE $0^+ \rightarrow 4^+$ TRANSITIONS IN THE NUCLEI $^{50}Ti$, $^{52}Cr$, $^{54}Fe$ AND $^{60}Ni$. THE BROKEN CURVES SHOW THE SHELL MODEL RESULTS.

We find that in the nuclei considered here the magnitude of the calculated $|F(q)|^2$ at the second maximum is smaller by more than two orders of magnitude compared to the values at the first maximum. In view of the general discussion of the form factors given earlier, the result implies the dominance of the $(1f_{7/2})^n$ configurations in the yrast states with $J^\pi = 0^+, 4^+$ in these nuclei.

We have also given in Figure IV.2 the results obtained by Mooy and Glaudemans[4] in the cases of the nuclei $^{52}Cr$, $^{54}Fe$ and $^{60}Ni$. The effective charges $(e_\pi, e_\nu) = (2.06, 1.06)$, $(1.76, 0.76)$ and $(1.54, 0.54)$ were employed for the nuclei $^{52}Cr$, $^{54}Fe$ and $^{60}Ni$, respectively, in these calculations. The shell model calculations have been reported only for the range $q = 0.6 - 1.8$ fm$^{-1}$ covering just the first maxima. The calculations reproduce the observed data quite well in this momentum-transfer range. We note that in the nucleus $^{52}Cr$, the shell model $(e_\pi, e_\nu)$ values are considerably larger than the ones considered in the present calculation. Large renormalized values of the effective charge, which imply an enhanced involvement of the $2p_{3/2}$ orbit, are not unexpected in this nucleus in view of the significant non-sphericity of the zeroth-order description of the proton wave function in terms of the $(1f_{7/2})^{4\pi}$ configuration.

It may be pointed out here that the effective charges employed in the present calculation of the $0^+ \rightarrow 4^+$ form factors for various 2p-1f shell nuclei are either the same or lie within 12 percent of the values employed in our earlier calculations[5] for the $0^+ \rightarrow 2^+$ form factors in these nuclei. This feature is not shared by the shell model calculations (see columns 5 and 7, Table IV.1); the shell model results are characterized by large differences between the effective charges employed for the $0^+ \rightarrow 2^+$ transitions and those for the $0^+ \rightarrow 4^+$ transition.

IV.3.2 Transition Charge Densities

In Figure IV.3 we have displayed the calculated transition charge densities associated with the $0^+ \rightarrow 4^+$ transitions in the nuclei $^{50}Ti$, $^{52}Cr$, $^{54}Fe$ and $^{60}Ni$. The transition charge densities have been computed using the effective charges employed in the form factor calculations.

In view of the nonavailability of the empirical $0^+ \rightarrow 4^+$ transition densities extracted from the Fourier-Bessel analyses, it is not possible to assess the results obtained here. However, it is interesting to note that the present calculation does reveal significant qualitative differences between the results obtained for the traditional $(f_{7/2})^n$ nuclei — the nuclei $^{50}Ti$, $^{52}Cr$ and $^{54}Fe$ — and those for the nucleus $^{60}Ni$; the presence of the $(2p_{3/2})^{4\nu}$ configurations in the latter nucleus is signalled by the

## TABLE IV.1

The $B(E2; 0^+ \rightarrow 2^+)$ and $B(E4; 0^+ \rightarrow 4^+)$ values in the nuclei $^{48,50}Ti$, $^{50,52,54}Cr$, $^{54}Fe$ and $^{60}Ni$. The B(E4) values have been calculated with the set of effective charges employed for calculating the form factors for the $0^+ \rightarrow 4^+$ transition. The $B(EL; 0^+ \rightarrow L^+)$ values are in units of $e^2\ fm^{2L}$. Here $<Q_o^L>_\pi$ ($<Q_o^L>_\nu$) gives the contribution of the valence protons (neutrons) towards the $2^L$-pole moment of the intrinsic state. The reduced transition probabilities resulting from the present calculation have been compared with the predictions of the recent shell model calculations[4] (labelled SM) in some cases.

| $<Q_o^2>$ | $<Q_o^4>$ | $B(E2; 0^+ \rightarrow 2^+)$ | | | $B(E4; 0^+ \rightarrow 4^+)$ | |
|---|---|---|---|---|---|---|
| $[<Q_o^2>_\pi, <Q_o^2>_\nu]$ | $[<Q_o^4>_\pi, <Q_o^4>_\nu]$ | PHFB $[e_\pi, e_\nu]$ | SM[a] $[e_\pi, e_\nu]$ | EXPT[b] | PHFB $[e_\pi, e_\nu]$ | SM[a] $[e_\pi, e_\nu]$ |
| 16.4<br>[6.7, 9.7] | 21.3<br>[16.5,4.8] | 547<br>[1.7,0.7] | – | 690 ± 40<br>750 ± 50 | $1.61 \times 10^3$<br>[1.5,0.5] | – |
| -9.4<br>[-4.8,-4.6] | 14.9<br>[6.1,8.8] | 378<br>[1.7,0.7] | – | 330 ± 40<br>315 ± 30 | $2.36 \times 10^3$<br>[1.5,0.5] | – |
| 26.3<br>[13.0,13.3] | 33.2<br>[19.1,14.1] | 1302<br>[1.6,0.6] | – | 1040 ± 115<br>1135 ± 100 | $1.23 \times 10^3$<br>[1.5,0.5] | – |
| 11.4<br>[7.8,3.6] | 15.7<br>[9.7,6.0] | 727<br>[1.7,0.7] | 635<br>[1.3,1.6] | 565 ± 50<br>660 ± 30 | $2.63 \times 10^3$<br>[1.5,0.5] | $7.9 \times 10^4$<br>[2.06,1.06] |

Continued.....

TABLE IV.1 (CONTINUED):

| $\langle Q_o^2 \rangle$ [$\langle Q_o^2 \rangle_\pi, \langle Q_o^2 \rangle_\nu$] | $\langle Q_o^4 \rangle$ [$\langle Q_o^4 \rangle_\pi, \langle Q_o^4 \rangle_\nu$] | B(E2; $0^+ \rightarrow 2^+$) PHFB [$e_\pi$, $e_\nu$] | B(E2; $0^+ \rightarrow 2^+$) $SM^a$ [$e_\pi$, $e_\nu$] | B(E2; $0^+ \rightarrow 2^+$) EXPT[b] | B(E4; $0^+ \rightarrow 4^+$) PHFB [$e_\pi$, $e_\nu$] | B(E4; $0^+ \rightarrow 4^+$) $SM^a$ [$e_\pi$, $e_\nu$] |
|---|---|---|---|---|---|---|
| 26.7 [13.1, 13.6] | 33.7 [20.3, 13.4] | 1232 [1.5, 0.5] | – | $1000 \pm 70$[c] | $2.33 \times 10^3$ [1.5, 0.5] | – |
| 9.0 [6.4, 2.6] | -7.5 [-5.5, -2.0] | 600 [1.7, 0.7] | 500 [1.4, 2.3] | $535 \pm 40$[d] | $2.91 \times 10^3$ [1.7, 0.7] | $1.3 \times 10^5$ [1.76, 0.76] |
| -12.5 [-3.9, -8.6] | 17.3 [9.1, 8.2] | 846 [1.8, 0.8] | 909 [3.3, 0.5] | $675 \pm 40$ $914 \pm 20$[c] | $3.46 \times 10^3$ [1.8, 0.8] | $2.2 \times 10^5$ [1.54, 0.54] |

Reference 4

Reference 6

Reference 7

Reference 8.

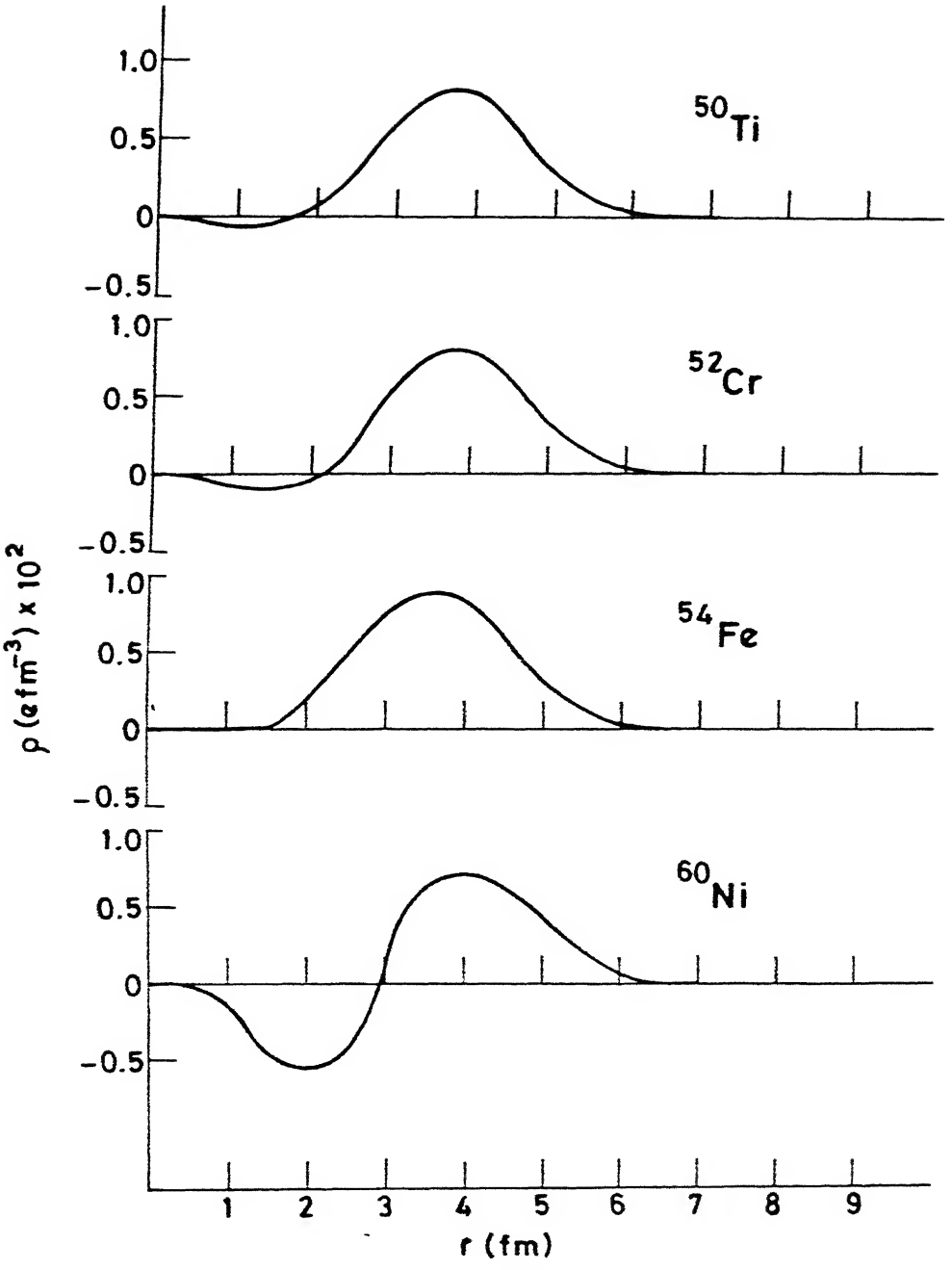


FIG. IV.3 TRANSITION CHARGE DENSITIES ASSOCIATED WITH THE $0^+ \rightarrow 4^+$ TRANSITION IN THE NUCLEI $^{50}$Ti, $^{52}$Cr, $^{54}$Fe AND $^{60}$Ni.

appearance of an oscillatory form.

## IV.4 Hexadecupole Electroexcitation in the Nuclei $^{48}Ti$, $^{50}Cr$ and $^{54}Cr$

### IV.4.1 Form Factors

Figure IV.4 compares the calculated and observed $|F|^2$ for the $0^+ \rightarrow 4^+$ transitions in the nuclei $^{48}Ti$, $^{50}Cr$ and $^{54}Cr$.

Although the $0^+ \rightarrow 2^+$ transitions in the nuclei $^{48}Ti$ and $^{50}Cr$ have earlier been discussed by Iwamoto et al.[9] in the framework of the shell model involving restricted configurations, no shell model calculation has so far been reported in these nuclei for the $0^+ \rightarrow 4^+$ form factors. Since these nuclei do not involve the $1f_{7/2}$ sub-shell closure, it is difficult to justify à priori any truncation scheme for reducing the number of shell model configurations.

As mentioned earlier, the projected HFB calculations have been carried out with a constant set of effective charges — with $e_\pi = 1.5$ and $e_\nu = 0.5$ — for the nuclei considered here. It is seen that the present calculation is quite successful in reproducing the magnitude of the form factors at the first maxima. However, one observes discrepancies in the momentum-transfer range $1.5 < q < 2.7$ fm$^{-1}$; the position of the first minimum is shifted towards higher momentum-transfers and the calculation underestimates the

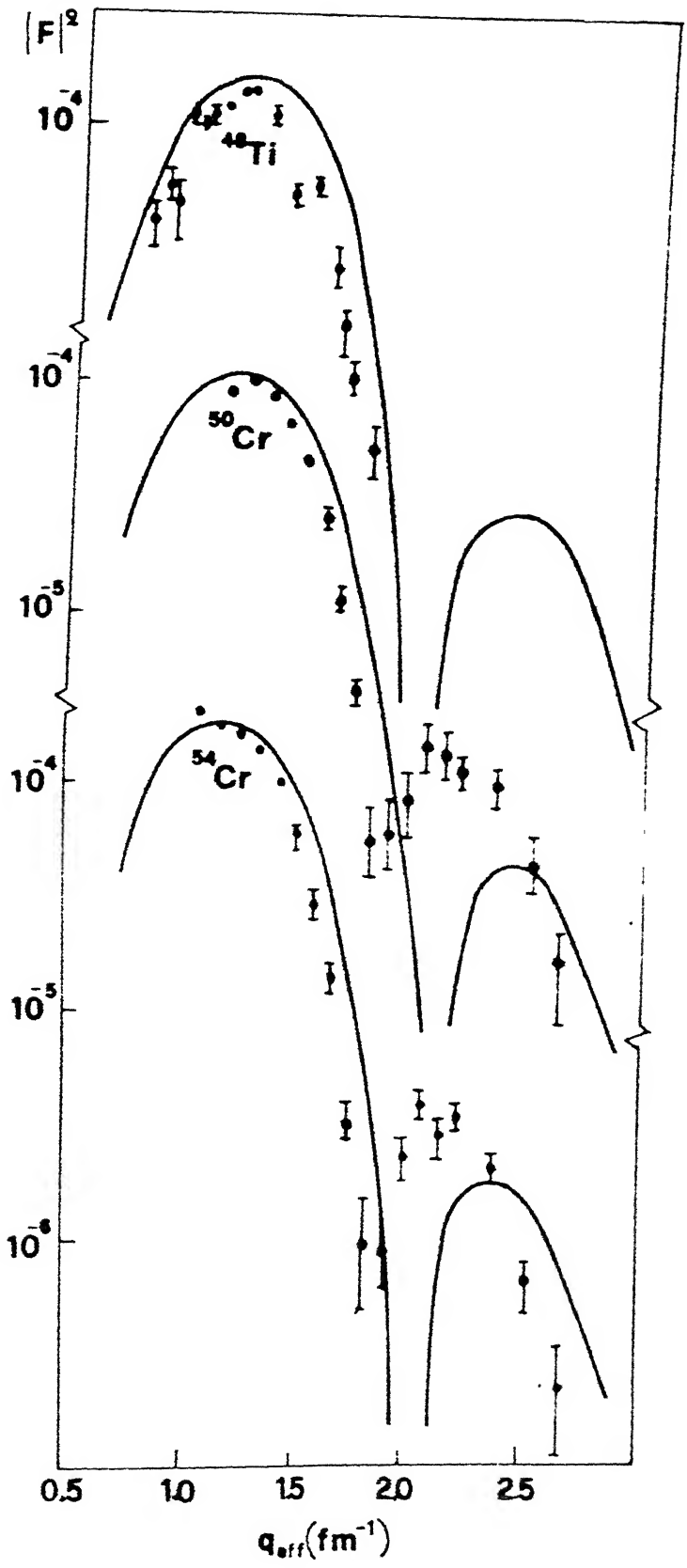


FIG. IV.4 EXPERIMENTAL AND CALCULATED SQUARED FORM FACTORS $|F|^2$ FOR THE $0^+ \rightarrow 4^+$ TRANSITION IN THE NUCLEI $^{48}Ti$, $^{50}Cr$ AND $^{54}Cr$.

magnitude of $|F|^2$ around its second maximum in the nuclei $^{50,54}Cr$. It is seen that the quadrupole moments of the intrinsic states (see column 2, Table IV.1) in the nuclei $^{48}Ti$, $^{50,54}Cr$ are significantly larger than those for the nuclei with N or Z = 28. The onset of sizable quadrupole deformations may warrant the inclusion of the $1g_{9/2}$ orbit in the configuration space. It would also be worthwhile to examine the effect of incorporating more configurational admixtures within 2p-1f shell by considering quasiparticle-excited K = 0 intrinsic states, in addition to the usual ones resulting from the HFB calculation.

IV.4.2 Transition Charge Densities

In Figure IV.5 we have displayed the calculated transition charge densities associated with the $0^+ \rightarrow 4^+$ transition in the nuclei $^{48}Ti$ and $^{50,54}Cr$.

One notices in these nuclei significant correlation between the ratio of the form factors at their first and second maxima and the size of the 'dip' in the calculated transition densities in the interior region ($0 < r < 3$ fm); the near-disappearance of the dip (at $r \sim 2$ fm) in the transition charge density in $^{50}Cr$ is seen to be associated with the significantly reduced estimates (relative to the values around first maximum) of the form factors around second maximum. The empirical transition charge densities are thus expected to provide important clues regarding the

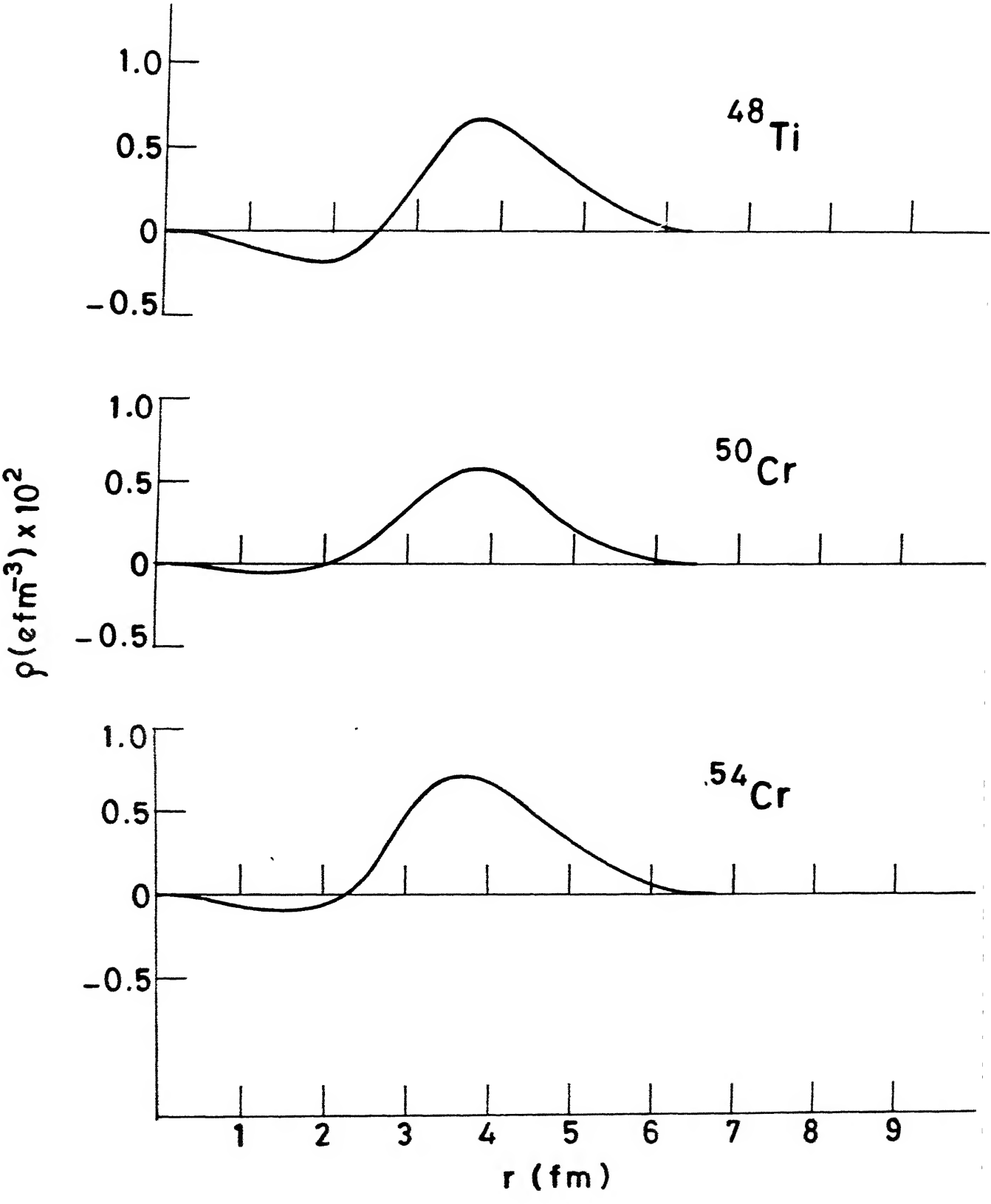


FIG. IV.5 TRANSITION CHARGE DENSITIES ASSOCIATED WITH THE $0^+ \rightarrow 4^+$ TRANSITION IN THE NUCLEI $^{48}$Ti, $^{50}$Cr AND $^{54}$Cr.

origin of the discrepancy between the calculated and the observed form factors for $q > 1.5$ fm$^{-1}$ in the nucleus $^{50}$Cr.

## IV.5 Validity of the Rotational Model Predictions vis-à-vis the Hexadecupole Operator

The rotational spectra in nuclei are usually discussed in the framework of the unified model of Bohr and Mottelson[10]. The model is characterized by the decoupling of single-particle and rotational motions; the wave function of a yrast state in quasirotational nuclei is given, for example, by the product of the symmetric top wave function and an intrinsic state describing, respectively, the collective rotation and the single-particle motion. The BM or the rotor model relates the reduced electric $2^L$-pole transition probabilities to the intrinsic $2^L$-pole moments — the expectation values of $Q_o^L$ operators with respect to the intrinsic states — in a simple manner:

$$B(EL;\ J_i^+ \to J_f^+) = (1/16\pi) \begin{bmatrix} J_i & L & J_f \\ 0 & 0 & 0 \end{bmatrix}^2 \langle Q_o^L \rangle^2 \qquad (IV.1)$$

As discussed by Villars[11], eq. (IV.1) can also be realized in a completely microscopic (quantal) perspective by considering the zeroth-order approximation to the matrix element $\langle \Phi | P^{J_f} Q_o^L P^{J_i} | \Phi \rangle$ in powers of $\langle \Phi | J^2 | \Phi \rangle^{-1}$, where $|\Phi\rangle$ is an intrinsic state and $P^J$ is the Peierls-Yoccoz

projection operator. It may be stressed here that the apparent validity of this approximation scheme depends only on the $\langle J^2 \rangle$ value and not on the multipole involved.

The relation (IV.1) has been extensively used in the past for obtaining semiquantitative estimates[12] of the reduced transition probabilities for electric quadrupole transitions, $B(E2; 0^+ \rightarrow 2^+)$, in terms of intrinsic quadrupole moments, $\langle Q_o^2 \rangle$, resulting from either phenomenological models such as the Nilsson model or microscopic, Hartree-Fock (HF) or Hartree-Fock-Bogoliubov (HFB) descriptions. The BM prescription has also often been invoked for obtaining Nilsson parameters for quadrupole deformations in different mass-regions by first extracting the $\langle \Phi | Q_o^2 | \Phi \rangle$ values from the measured transition probabilities[6].

As mentioned in the beginning of this Chapter, the recent accumulation of the $0^+ \rightarrow 4^+$ form factor data for a number of 2p-1f shell nuclei implies, in a somewhat indirect manner, the availability of the heretofore unmeasured E4 transition probabilities, $B(E4; 0^+ \rightarrow 4^+)$, since the latter can be looked upon as the appropriate $q \rightarrow 0$ limits of the $|F|^2 (0^+ \rightarrow 4^+)$ values. In this context one is tempted to enquire if the equation (IV.1) could also be used for relating the E4 reduced transition probabilities and the hexadecupole moments of the intrinsic states.

In this section we present explicit calculations to show that, whereas the zeroth-order approximation implicit

in the derivation of eq. (IV.1) in the Peierls-Yoccoz projection formalism[13] is qualitatively as well as, to a good extent, quantitatively quite reliable in the case of the quadrupole operator, it breaks down completely in the case of the hexadecupole operator, irrespective of the value of $\langle J^2 \rangle$. It is pointed out that the validity of various orders of approximation depends primarily on the similarities between a pure quadrupole field and the (one-body) self-consistent HF field resulting from the effective interaction and not so much on the magnitude of the $\langle J^2 \rangle$ value. The anomalous nature of the results for the hexadecupole operator in the 2p-1f shell can be traced back to the significant differences between the energy sequence as well as the structure of the eigenstates of the $Q_o^2$ and $Q_o^4$ fields in the shell.

We have listed in Table IV.2 the intrinsic quadrupole as well as hexadecupole moments of the axially symmetric HFB states (resulting from the MWH interaction) for the nuclei $^{48,50,52}Ti$, $^{50,52,54}Cr$ and $^{52,54}Fe$. We have also presented the reduced E2 and E4 transition probabilities resulting from explicit angular momentum projection, as well as their estimates resulting from the BM prescription (eq. (IV.1)).

A graphical presentation of the results (see Figure IV.6) shows that the rotor model predictions are in excellent qualitative agreement with the PHFB results for the

TABLE IV.2

The intrinsic multipole moments as well as the reduced transition probabilities involving the quadrupole and the hexadecupole operators for some doubly even 2p-1f shell nuclei. The reduced transition probabilities resulting from explicit angular momentum projection on the HFB intrinsic states have been compared with the rotor model predictions. The intrinsic $2^L$-pole moments have been given in units of $b^L$, where $b = (\hbar/m\omega)^{1/2}$ is the oscillator parameter. The reduced transition probabilities $B(E2; 0^+ \rightarrow 2^+)$ and $B(E4; 0^+ \rightarrow 4^+)$ have been given in units of $e^2.10^{-50}$ $cm^4$ and $e^2.10^{-102}$ $cm^8$, respectively

| Nucleus | $\langle Q_o^2 \rangle$ | $B(E2; 0^+ \rightarrow 2^+)$ | | $\langle Q_o^4 \rangle$ | $B(E4; 0^+ \rightarrow 4^+)$ | |
|---|---|---|---|---|---|---|
| | | Projected HFB | Rotor Model | | Projected HFB | Rotor Model |
| $^{48}Ti$ | 16.4 | 4.7 | 3.7 | 21.3 | 9.6 | 156.0 |
| $^{50}Ti$ | -9.4 | 2.5 | 1.2 | 18.9 | 25.6 | 79.2 |
| $^{52}Ti$ | 15.7 | 4.9 | 3.6 | 20.0 | 14.9 | 150.4 |
| $^{50}Cr$ | 26.3 | 10.7 | 9.7 | 23.2 | 5.2 | 192.2 |
| $^{52}Cr$ | 11.4 | 3.7 | 1.9 | 15.7 | 13.7 | 92.6 |
| $^{54}Cr$ | 26.7 | 12.5 | 10.6 | 33.7 | 18.8 | 449.2 |
| $^{52}Fe$ | 20.8 | 8.0 | 6.2 | -19.3 | 13.1 | 140.5 |
| $^{54}Fe$ | 9.0 | 3.0 | 1.2 | -7.5 | 14.1 | 22.3 |

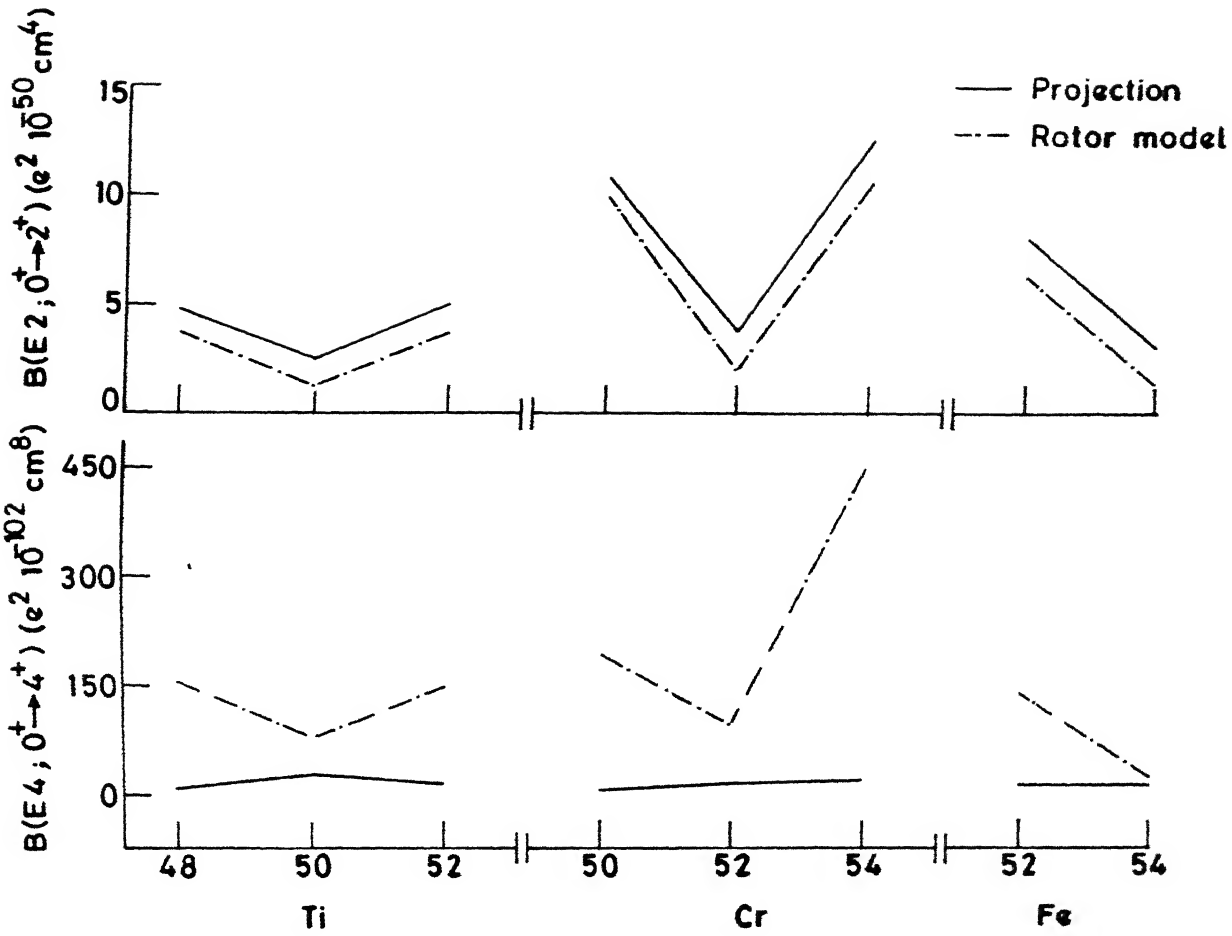


FIG. IV.6 COMPARISON OF THE REDUCED TRANSITION PROBABILITIES RESULTING FROM THE PHFB AS WELL AS THE ROTOR MODELS.

$B(E2;\ 0^+ \rightarrow 2^+)$ values. In fact, for the $N \neq 28$ nuclei, even the quantitative agreement between the rotor model and the PHFB estimates is quite good; the maximum discrepancy is only about 27 percent of the latter. Since the nuclei with $N \neq 28$ also possess significantly larger intrinsic quadrupole moment — and consequently larger $\langle J^2 \rangle$ values — compared to the nuclei with $N = 28$, the results obtained here are consistent with our à priori expectation concerning the general validity of the rotor model.

In sharp contrast to the situation vis-à-vis the $B(E2;\ 0^+ \rightarrow 2^+)$ values, we observe (see Figure IV.6) dramatic failure — both in the quantitative as well as qualitative sense — of the BM prescription as applied to the $Q_o^4$ operator. In fact the rotor model estimates are larger by an order of magnitude than the PHFB estimates in most of the cases.

In what follows we make an attempt to examine qualitatively the reasons for the inadequacy of the rotor model prescription as applied to the hexadecupole operator. In the framework of the rotor model, the state of angular momentum J and projection M (in the laboratory frame) is given by

$$|\Psi^J_{MO}\rangle = [(2J+1)/16\pi^2]^{1/2}\ D^J_{MO}(\Omega)\,|\Phi_{K=0}\rangle. \quad (IV.2)$$

Using these wave functions the matrix elements of the $Q_o^L$ operator between $J_i^\pi = 0^+$ and $J_f^\pi = L^+$ state becomes

$$< \Psi^{L}_{oo} \mid Q^{L}_{o} \mid \Psi^{o}_{oo} > = \begin{bmatrix} L & L & O \\ O & O & O \end{bmatrix} < \Phi_{o} \mid Q^{L}_{o} \mid \Phi_{o} > \qquad (IV.3)$$

We next employ the angular momentum projected states given by equation (II.128). As shown by Ripka[14], the matrix elements of the $Q^{L}_{o}$ operator between projected states are given by

$$< \Psi^{L}_{oo} \mid Q^{L}_{o} \mid \Psi^{o}_{oo} > = \frac{1}{2} [a_{o}\, a_{L}]^{-1/2} \sum_{\mu} \int_{o}^{\pi} d\beta \; \mathrm{Sin}\beta \; d^{L}_{o\mu}(\beta) < \Phi_{o} \mid e^{-i\beta J_{y}} \; Q^{L}_{\mu} \mid \Phi_{o} > \qquad (IV.4)$$

where

$$a_{L} = \frac{(2L+1)}{2} \int_{o}^{\pi} d\beta \; \mathrm{Sin}\beta \; d^{L}_{oo}(\beta) \; < \Phi_{o} \mid e^{-i\beta J_{y}} \mid \Phi_{o} > . \qquad (IV.5)$$

A comparison of equations (IV.3) and (IV.4) shows that they are expected to yield nearly the same results in the zeroth-order approximation — and this involves the usual assumption that the integrals give nonvanishing contribution only for $\beta \sim 0$ — provided the intrinsic states $\mid \Phi_{o} >$ are eigenstates (or near-eigenstates) of the operator $Q^{L}_{o}$. (Note that in the zeroth-order approximation the $\mu$-summation is also automatically restricted to just the $\mu = 0$ term). In Table IV.3 we have displayed the structure of the single-particle states in the quadrupole and hexadecupole fields in the 2p-1f shell. It is seen that the eigenstates of the $Q^{4}_{o}$

TABLE IV.3

Structure of single-particle states in pure quadrupole and hexadecupole fields in the 2p-1f shell. Here $k=\langle l_z \rangle$ is the expectation value of the component of the angular momentum along the symmetry axis and $\varepsilon_2(\varepsilon_4)$ is the eigenvalue of the intrinsic quadrupole (hexadecupole) moments in units of $b^2(b^4)$

| Quadrupole field | | | Hexadecupole field | | |
|---|---|---|---|---|---|
| k | $\varepsilon_2$ | $\Phi(k,\varepsilon_2)$ | k | $\varepsilon_4$ | $\Phi(k,\varepsilon_4)$ |
| 0 | 6.0 | $0.63f_0-0.77p_0$ | 0 | 19.9 | $0.80f_0-0.59p_0$ |
| $\pm1$ | 3.0 | $0.89f_{\pm1}-0.45p_{\pm1}$ | $\pm1$ | 9.8 | $0.74f_{\pm1}-0.68p_{\pm1}$ |
| $\pm2$ | 0.0 | $f_{\pm2}$ | $\pm3$ | 4.5 | $f_{\pm3}$ |
| 0 | 0.0 | $0.77f_0+0.63p_0$ | $\pm1$ | -8.3 | $0.68f_{\pm1}+0.74p_{\pm1}$ |
| $\pm1$ | -3.0 | $0.45f_{\pm1}+0.89p_{\pm1}$ | $\pm2$ | -10.5 | $f_{\pm2}$ |
| $\pm3$ | -3.0 | $f_{\pm3}$ | 0 | -10.9 | $0.59f_0+0.80p_0$ |

operator differ substantially from those of the $Q_o^2$ operator. Thus the intrinsic states $|\Phi_o\rangle$, which are near-eigenstates of the $Q_o^2$ operator due to the well-known quadrupole-quadrupole dominance[15] of the effective nuclear interactions, are not in general the eigenstates of the $Q_o^4$ operator. In other words, whereas the nature of the interaction facilitates the similarity between the rotor model and PHFB predictions for the quadrupole operator (by yielding intrinsic states that are close to the eigenstates of $Q_o^2$), the inherent differences in the 2p-1f shell eigenstates of $Q_o^2$ and $Q_o^4$ operator do not permit the recovery of the rotor limit from the expression (IV.4).

## IV.6 Conclusions

We have discussed in this Chapter the calculation of the form factors as well as the transition charge densities associated with the electroexcitation of the yrast $4^+$ levels in some doubly even 2p-1f shell nuclei. It turns out that the use of the $J^\pi = 0^+, 2^+, 4^+$ states projected from variational intrinsic states resulting from realistic 2p-1f shell interactions permits a reasonably satisfactory simultaneous description of both the $0^+ \rightarrow 2^+$ as well as $0^+ \rightarrow 4^+$ form factor data with nearly the same set of effective charges.

The present work has emphasized the necessity of providing an improved description of the large-q part of the $0^+ \rightarrow 4^+$ form factors in the nuclei $^{50,54}Cr$. In this context, the empirical transition charge densities are expected to provide valuable guidelines.

## REFERENCES


1. K. Hayakawa et al., Res. Rep. Nucl. Sc. (Tohoku University) 11, 1 (1978).

2. J.W. Lightbody, Jr., et al., Phys. Rev. C27, 113 (1983).

3. Y. Torizuka et al., Phys. Rev. 185, 1499 (1969).

4. R.B.M. Mooy and P.W.M. Glaudemans, Nucl. Phys. A438, 461 (1985).

5. G. Mukherjee and S.K. Sharma, Phys. Rev. C29, 2101 (1984); C31, 689 (1985).

6. A. Christy and O. Häusser, Nucl. Data Tables 11, 281 (1972).

7. W. Kutschera, in Proceedings of the EPS International Conference Florence (Italy), 1977, edited by P. Blasi and R.A. Ricci (Editrice Compositori, Bologna, 1978), p. 120.

8. M.J. Levine, E.K. Warburton and D. Schwalm, Phys. Rev. C23, 244 (1984).

9. T. Iwamoto, H. Horie and A. Yokoyama, Phys. Rev. C25, 658 (1982).

10. A. Bohr and B.R. Mottelson, Nuclear Structure, Vol. II (W.A. Benjamin, Reading, Mass., 1985).

11. F. Villars, International School of Physics "Enrico Fermi", Course 36, (Academic Press, New York and London), p. 14.

12. S.K. Sharma and K.H. Bhatt, Phys. Rev. Letters 30, 620 (1973).

13. R.E. Peierls and J. Yoccoz, Proc. Phys. Soc. (London) A70, 381 (1957).

14. G. Ripka, in Advances in Nuclear Physics, eds. M. Baranger and E. Vogt (Plenum Press, New York-London, 1968) Vol. I, p. 183.

15. M. Harvey, in Advances in Nuclear Physics, eds. M. Baranger and E. Vogt (Plenum Press, New York-London, 1968) Vol. I, p. 67.

# CHAPTER V

## CONCLUSIONS

In recent years the experimental studies involving electroexcitation of nuclear levels have provided extremely valuable information about several heretofore unexamined aspects of the nuclear structure of medium-mass nuclei. In contrast to the conventional experimental studies involving $\gamma$-transitions, the momentum-transfer dependence of the matrix element (extracted from the measured cross sections) yields detailed information vis-à-vis the spatial structure of the nuclear states participating in the transition.

Several earlier theoretical investigations have involved a comparison of the observed data with the predictions of nuclear collective models. The collective model analyses have sought to reproduce electroexcitation form factors by postulating general functional forms of the nuclear charge densities. While condensing the experimental data into concise parametrizations, such analyses provide us with only a qualitative characterization of the nuclear excitations; they do not permit us to interpret and correlate the data from the point of view of a wider perspective involving other microscopic features of nuclear structure.

In this thesis we have attempted an assessment of the capability of the projected HFB technique vis-à-vis the

interpretation of such fundamental results as those embodied in the data on electroexcitation transition charge densities as well as form factors involving several 2p-1f shell nuclei. It turns out that the available form factor data out to about 2.5 $fm^{-1}$ can be reproduced in most of the cases in a fairly satisfactory manner in terms of reasonable values of nearly mass-independent effective charges. The calculations presented in this thesis have also brought out the decisive role that the empirical transition charge densities in the Ni and Zn isotopes, extracted from the data via the Fourier-Bessel analysis, play vis-à-vis the choice of a model of core-polarization contributions.

The results presented in this thesis have revealed significant discrepancies in some cases between the observed and the calculated form factors for the large-q regions. These discrepancies seem to warrant a careful study of the role played by an explicit inclusion of the $^{40}Ca$ core-excitations as well as the configurations involving the $1g_{9/2}$ orbit. Further, it appears worthwhile to attempt a systematic renormalization of the transition charge density operator in terms of various core-excitation graphs. Apart from obviating the dependence on the existing 'models' for the core-polarization transition density, such a study is expected to reveal the relative importance of various core-excitation processes vis-à-vis the detailed coordinate-space structure of the transition charge densities.

## APPENDIX A

## THE ($1f_{7/2}$, $2p_{3/2}$, $2p_{1/2}$, $1f_{5/2}$) MATRIX ELEMENTS OF THE KB AS WELL AS THE MWH INTERACTIONS

The matrix elements <abJT|V|cdJT> of the Kuo-Brown (KB) interaction are tabulated. The columns labelled by (a,b,c,d) contain twice the j-value of the various shell model orbits.

| T | a | b | c | d | J | <\|V\|> | J | <\|V\|> | J | <\|V\|> |
|---|---|---|---|---|---|---|---|---|---|---|
| 1 | 7 | 7 | 7 | 7 | 0 | -1.807 | 2 | -0.785 | 4 | -0.087 |
| | | | | | 6 | 0.226 | | | | |
| 1 | 7 | 7 | 7 | 5 | 2 | 0.000 | 4 | -0.406 | 6 | -0.716 |
| 1 | 7 | 7 | 7 | 3 | 2 | -0.502 | 4 | -0.307 | | |
| 1 | 7 | 7 | 7 | 1 | 4 | -0.293 | | | | |
| 1 | 7 | 7 | 5 | 5 | 0 | -2.788 | 2 | -0.638 | 4 | -0.400 |
| 1 | 7 | 7 | 5 | 3 | 2 | 0.305 | 4 | 0.305 | | |
| 1 | 7 | 7 | 5 | 1 | 2 | -0.470 | | | | |
| 1 | 7 | 7 | 3 | 3 | 0 | -0.783 | 2 | -0.269 | | |
| 1 | 7 | 7 | 3 | 1 | 2 | -0.250 | | | | |
| 1 | 7 | 7 | 1 | 1 | 0 | -0.714 | | | | |
| 1 | 7 | 5 | 7 | 5 | 1 | -0.287 | 2 | -0.096 | 3 | 0.022 |
| | | | | | 4 | 0.031 | 5 | 0.156 | 6 | -0.894 |
| 1 | 7 | 5 | 7 | 3 | 2 | 0.014 | 3 | -0.118 | 4 | -0.114 |
| | | | | | 5 | -0.010 | | | | |
| 1 | 7 | 5 | 7 | 1 | 3 | -0.012 | 4 | -0.093 | | |

| T | a | b | c | d | J | <IVI> | J | <IVI> | J | <IVI> |
|---|---|---|---|---|---|---|---|---|---|---|
| 1 | 7 | 5 | 5 | 5 | 2 | -0.631 | 4 | -0.468 | | |
| 1 | 7 | 5 | 5 | 3 | 1 | -0.035 | 2 | 0.295 | 3 | -0.132 |
| | | | | | 4 | 0.493 | | | | |
| 1 | 7 | 5 | 5 | 1 | 2 | -0.342 | 3 | 0.080 | | |
| 1 | 7 | 5 | 3 | 3 | 2 | -0.018 | | | | |
| 1 | 7 | 5 | 3 | 1 | 1 | -0.079 | 2 | -0.150 | | |
| 1 | 7 | 3 | 7 | 3 | 2 | -0.861 | 3 | -0.027 | 4 | -0.047 |
| | | | | | 5 | 0.145 | | | | |
| 1 | 7 | 3 | 7 | 1 | 3 | 0.078 | 4 | -0.502 | | |
| 1 | 7 | 3 | 5 | 5 | 2 | -0.446 | 4 | -0.156 | | |
| 1 | 7 | 3 | 5 | 3 | 2 | 0.402 | 3 | 0.026 | 4 | 0.619 |
| 1 | 7 | 3 | 5 | 1 | 2 | -0.966 | 3 | -0.059 | | |
| 1 | 7 | 3 | 3 | 3 | 2 | -0.325 | | | | |
| 1 | 7 | 3 | 3 | 1 | 2 | -0.319 | | | | |
| 1 | 7 | 1 | 7 | 1 | 3 | 0.029 | 4 | -0.274 | | |
| 1 | 7 | 1 | 5 | 5 | 4 | -0.252 | | | | |
| 1 | 7 | 1 | 5 | 3 | 3 | 0.140 | 4 | 0.531 | | |
| 1 | 7 | 1 | 5 | 1 | 3 | -0.078 | | | | |
| 1 | 5 | 5 | 5 | 5 | 0 | -0.860 | 2 | -0.218 | 4 | 0.298 |
| 1 | 5 | 5 | 5 | 3 | 2 | 0.023 | 4 | 0.102 | | |
| 1 | 5 | 5 | 5 | 1 | 2 | -0.186 | | | | |
| 1 | 5 | 5 | 3 | 3 | 0 | -0.777 | 2 | -0.128 | | |
| 1 | 5 | 5 | 3 | 1 | 2 | -0.256 | | | | |
| 1 | 5 | 5 | 1 | 1 | 0 | -0.392 | | | | |

| T | a | b | c | d | J | <\|V\|> | J | <\|V\|> | J | <\|V\|> |
|---|---|---|---|---|---|---|---|---|---|---|
| 1 | 5 | 3 | 5 | 3 | 1<br>4 | -0.032<br>-0.243 | 2 | 0.215 | 3 | 0.120 |
| 1 | 5 | 3 | 5 | 1 | 2 | 0.389 | 3 | 0.007 | | |
| 1 | 5 | 3 | 3 | 3 | 2 | 0.068 | | | | |
| 1 | 5 | 3 | 3 | 1 | 1 | -0.058 | 2 | 0.159 | | |
| 1 | 5 | 1 | 5 | 1 | 2 | -0.135 | 3 | 0.205 | | |
| 1 | 5 | 1 | 3 | 3 | 2 | -0.047 | | | | |
| 1 | 5 | 1 | 3 | 1 | 2 | -0.241 | | | | |
| 1 | 3 | 3 | 3 | 3 | 0 | -1.206 | 2 | -0.380 | | |
| 1 | 3 | 3 | 3 | 1 | 2 | -0.601 | | | | |
| 1 | 3 | 3 | 1 | 1 | 0 | -1.465 | | | | |
| 1 | 3 | 1 | 3 | 1 | 1 | 0.152 | 2 | -0.688 | | |
| 1 | 1 | 1 | 1 | 1 | 0 | -0.249 | | | | |
| 0 | 7 | 7 | 7 | 7 | 1<br>7 | -0.525<br>-2.199 | 3 | -0.208 | 5 | -0.502 |
| 0 | 7 | 7 | 7 | 5 | 1 | 1.894 | 3 | 1.005 | 5 | 0.901 |
| 0 | 7 | 7 | 7 | 3 | 3 | -0.482 | 5 | -0.816 | | |
| 0 | 7 | 7 | 7 | 1 | 3 | 0.640 | | | | |
| 0 | 7 | 7 | 5 | 5 | 1 | 1.071 | 3 | 0.517 | 5 | 0.170 |
| 0 | 7 | 7 | 5 | 3 | 1 | 0.227 | 3 | -0.087 | | |
| 0 | 7 | 7 | 5 | 1 | 3 | 0.033 | | | | |
| 0 | 7 | 7 | 3 | 3 | 1 | -0.279 | 3 | -0.296 | | |
| 0 | 7 | 7 | 3 | 1 | 1 | 0.392 | | | | |
| 0 | 7 | 7 | 1 | 1 | 1 | 0.184 | | | | |

| T | a | b | c | d | J | <IVI> | J | <IVI> | J | <IVI> |
|---|---|---|---|---|---|---|---|---|---|---|
| 0 | 7 | 5 | 7 | 5 | 1 | -3.621 | 2 | -2.731 | 3 | -0.985 |
| | | | | | 4 | -1.886 | 5 | -0.112 | 6 | -2.217 |
| 0 | 7 | 5 | 7 | 3 | 2 | -0.735 | 3 | 0.328 | 4 | -0.039 |
| | | | | | 5 | 0.405 | | | | |
| 0 | 7 | 5 | 7 | 1 | 3 | -0.440 | 4 | -0.674 | | |
| 0 | 7 | 5 | 5 | 5 | 1 | -0.416 | 3 | 0.675 | 5 | 1.138 |
| 0 | 7 | 5 | 5 | 3 | 1 | 0.953 | 2 | -0.705 | 3 | 0.628 |
| | | | | | 4 | -0.544 | | | | |
| 0 | 7 | 5 | 5 | 1 | 2 | 0.427 | 3 | 0.539 | | |
| 0 | 7 | 5 | 3 | 3 | 1 | 0.871 | 3 | 0.538 | | |
| 0 | 7 | 5 | 3 | 1 | 1 | -1.449 | 2 | -0.659 | | |
| 0 | 7 | 5 | 1 | 1 | 1 | 0.168 | | | | |
| 0 | 7 | 3 | 7 | 3 | 2 | -0.293 | 3 | -0.604 | 4 | -0.164 |
| | | | | | 5 | -2.165 | | | | |
| 0 | 7 | 3 | 7 | 1 | 3 | 1.295 | 4 | 0.108 | | |
| 0 | 7 | 3 | 5 | 5 | 3 | 0.158 | 5 | 0.048 | | |
| 0 | 7 | 3 | 5 | 3 | 2 | -1.123 | 3 | -0.408 | 4 | -0.514 |
| 0 | 7 | 3 | 5 | 1 | 2 | 0.838 | 3 | 0.518 | | |
| 0 | 7 | 3 | 3 | 3 | 3 | -0.511 | | | | |
| 0 | 7 | 3 | 3 | 1 | 2 | -0.481 | | | | |
| 0 | 7 | 1 | 7 | 1 | 3 | -1.484 | 4 | -0.746 | | |
| 0 | 7 | 1 | 5 | 5 | 3 | -0.270 | | | | |
| 0 | 7 | 1 | 5 | 3 | 3 | 0.139 | 4 | -1.188 | | |
| 0 | 7 | 1 | 5 | 1 | 3 | 0.400 | | | | |
| 0 | 7 | 1 | 3 | 3 | 3 | 0.461 | | | | |

| T | a | b | c | d | J | <\|V\|> | J | <\|V\|> | J | <\|V\|> |
|---|---|---|---|---|---|---|---|---|---|---|
| 0 | 5 | 5 | 5 | 5 | 1 | −0.012 | 3 | −0.196 | 5 | −1.687 |
| 0 | 5 | 5 | 5 | 3 | 1 | −0.292 | 3 | −0.327 | | |
| 0 | 5 | 5 | 5 | 1 | 3 | −0.391 | | | | |
| 0 | 5 | 5 | 3 | 3 | 1 | 0.040 | 3 | −0.182 | | |
| 0 | 5 | 5 | 3 | 1 | 1 | 0.159 | | | | |
| 0 | 5 | 5 | 1 | 1 | 1 | −0.084 | | | | |
| 0 | 5 | 3 | 5 | 3 | 1<br>4 | −2.164<br>−0.722 | 2 | −1.236 | 3 | −0.459 |
| 0 | 5 | 3 | 5 | 1 | 2 | 0.255 | 3 | −0.988 | | |
| 0 | 5 | 3 | 3 | 3 | 1 | −0.073 | 3 | −0.340 | | |
| 0 | 5 | 3 | 3 | 1 | 1 | 0.620 | 2 | −0.071 | | |
| 0 | 5 | 3 | 1 | 1 | 1 | −0.393 | | | | |
| 0 | 5 | 1 | 5 | 1 | 2 | −0.081 | 3 | −1.234 | | |
| 0 | 5 | 1 | 3 | 3 | 3 | −0.084 | | | | |
| 0 | 5 | 1 | 3 | 1 | 2 | 0.464 | | | | |
| 0 | 3 | 3 | 3 | 3 | 1 | −0.639 | 3 | −1.832 | | |
| 0 | 3 | 3 | 3 | 1 | 1 | 1.554 | | | | |
| 0 | 3 | 3 | 1 | 1 | 1 | 0.709 | | | | |
| 0 | 3 | 1 | 3 | 1 | 1 | −2.291 | 2 | −1.897 | | |
| 0 | 3 | 1 | 1 | 1 | 1 | 0.686 | | | | |
| 0 | 1 | 1 | 1 | 1 | 1 | −1.074 | | | | |

The MWH interaction referred to in the thesis is obtained from the KB interaction by substituting the following matrix elements in place of their counterparts:

| T | a | b | c | d | J | <\|V\|> | J | <\|V\|> | J | <\|V\|> |
|---|---|---|---|---|---|---|---|---|---|---|
| 1 | 7 | 7 | 7 | 7 | 0 | -2.107 | 2 | -1.115 | 4 | -0.097 |
| 1 | 7 | 5 | 7 | 5 | 1 | -0.037 | 2 | 0.154 | 3 | 0.272 |
| | | | | | 4 | 0.281 | 5 | 0.406 | 6 | -0.644 |
| 1 | 7 | 3 | 7 | 3 | 2 | -0.561 | 3 | 0.253 | 4 | 0.283 |
| | | | | | 5 | 0.485 | | | | |
| 1 | 7 | 1 | 7 | 1 | 3 | 0.279 | 4 | -0.024 | | |